

Air Force Institute of Technology

**AFIT Scholar**

---

Theses and Dissertations

Student Graduate Works

---

3-1997

## Automatic Digital Processing for Calibration Data of Open Skies Treaty Sensors

Donna D. Keating

Follow this and additional works at: <https://scholar.afit.edu/etd>



Part of the [Atmospheric Sciences Commons](#)

---

### Recommended Citation

Keating, Donna D., "Automatic Digital Processing for Calibration Data of Open Skies Treaty Sensors" (1997). *Theses and Dissertations*. 5964.

<https://scholar.afit.edu/etd/5964>

This Thesis is brought to you for free and open access by the Student Graduate Works at AFIT Scholar. It has been accepted for inclusion in Theses and Dissertations by an authorized administrator of AFIT Scholar. For more information, please contact [AFIT.ENWL.Repository@us.af.mil](mailto:AFIT.ENWL.Repository@us.af.mil).



AUTOMATIC DIGITAL PROCESSING  
FOR CALIBRATION DATA  
OF OPEN SKIES TREATY SENSORS

THESIS

Donna D.B. Keating, Captain, USAF

AFIT/GOR/ENP/97M-01

**DISTRIBUTION STATEMENT A**

Approved for public release;  
Distribution Unlimited

DEPARTMENT OF THE AIR FORCE  
AIR UNIVERSITY  
**AIR FORCE INSTITUTE OF TECHNOLOGY**

Wright-Patterson Air Force Base, Ohio DTIC QUALITY INSURED

AFIT/GOR/ENP/97M-01

AUTOMATIC DIGITAL PROCESSING  
FOR CALIBRATION DATA  
OF OPEN SKIES TREATY SENSORS

THESIS

Donna D.B. Keating, Captain, USAF

AFIT/GOR/ENP/97M-01

APPROVED FOR PUBLIC RELEASE; DISTRIBUTION UNLIMITED.

19970402 081

The views expressed in this thesis are those of the author and do not reflect the official policy or position of the Department of Defense or the U.S. Government.

AFIT/GOR/ENP/97M-01

AUTOMATIC DIGITAL PROCESSING FOR CALIBRATION DATA OF OPEN SKIES  
TREATY SENSORS

THESIS

Presented to the Faculty of the Graduate School of Engineering

Air Education and Training Command

In Partial Fulfillment of the

Requirements for the Degree of

Master of Science in Operational Analysis

Donna D.B. Keating, BS

Captain, USAF

March 1997

APPROVED FOR PUBLIC RELEASE; DISTRIBUTION UNLIMITED.

# Thesis Approval

**NAME:** Donna D.B. Keating, Captain, USAF  
**CLASS:** GOR-97M-01  
**THESIS TITLE:** Automatic Digital Processing for Calibration Data of Open Skies  
Treaty Sensors  
**DEFENSE DATE:** 3 March 1997

**COMMITTEE:**                      **NAME/TITLE/DEPARTMENT**                      **SIGNATURE**

---

Advisor                      Michael C. Roggemann  
Associate Professor of Engineering Physics  
Department of Engineering Physics  
Air Force Institute of Technology



Advisor                      Byron M. Welsh, PhD  
Associate Professor of Electrical Engineering  
Department of Electrical and Computer Engineering  
Air Force Institute of Technology



Advisor                      Kenneth W. Bauer, Jr., PhD  
Professor of Operational Sciences  
Department of Operational Sciences  
Air Force Institute of Technology



# TABLE OF CONTENTS

<b>I. INTRODUCTION .....</b>	<b>1</b>
1.1. OPEN SKIES TREATY .....	2
1.2. BACKGROUND .....	4
1.2.1. Calibration Targets .....	10
1.3. PROBLEM DEFINITION .....	12
1.4. SUMMARY OF KEY RESULTS .....	16
1.5. ORGANIZATION OF THESIS .....	20
<b>II. CURRENT METHODOLOGY .....</b>	<b>21</b>
2.1. THE BASIC PHYSICS OF OST IMAGE QUALITY .....	24
2.1.1. The system modulation transfer function .....	26
2.1.2. Modulation and Contrast Ratio Are Different Photogrammetric Values .....	29
2.1.3. Undersampling reduces the certainty of identifying individual bar groups .....	32
2.2. CURRENT PROCEDURES .....	33
2.2.1. Calibration Target Data Collection and Analysis .....	33
2.2.2. Bar Targets Intrinsicly Add Uncertainty to GRD Calculation .....	38
2.2.3. Optics distort GRD measurement, and surface roughness distorts target modulation measurement .....	48
2.3. CHAPTER SUMMARY .....	50
<b>III. THE ADAPTIVE DIGITAL METHOD (ADIM) .....</b>	<b>54</b>
3.1. TECHNIQUE OVERVIEW .....	55
3.1.1. Step by Step ADiM .....	57
3.1.1.1. Finding $L_2$ .....	60
3.1.1.2. Finding $K_2$ .....	70
3.2. DISCUSSION OF DATA SPECIFICS .....	74
3.2.1. Noise Effects in the Data .....	74
3.2.2. For smaller bars, poor choice in bar group location makes automatic peak and valley identification difficult .....	78
3.2.1. Photographic Film Usage .....	81
3.3. ADiM DEVELOPMENT FURTHER ELABORATION .....	84
<b>IV. RESULTS .....</b>	<b>86</b>
4.1. RESULT COMPARISON .....	88
<b>V. CONCLUSION .....</b>	<b>93</b>
<b>VI. BIBLIOGRAPHY .....</b>	<b>96</b>
<b>APPENDIX I: NUMERICAL RESULTS .....</b>	<b>98</b>
<b>APPENDIX II: MATLAB ADiM CODE .....</b>	<b>99</b>

## TABLE OF FIGURES

Figure 1, Aerial Photo of WPAFB Calibration Target with Annotated Features.....	11
Figure 2, Scatter plot of $H_{\min}$ values obtained by OSMPF and ADiM.....	17
Figure 3, Point by point comparison between calculated $H_{\min}$ values for OSMPF and ADiM.....	18
Figure 4, Linear Model Residuals (Error) plotted against OSMPF $H_{\min}$ .....	19
Figure 5, Sources of GRD Degradation .....	23
Figure 6, Triple Bar Group Diagram.....	24
Figure 7, Comparison of Modulation and Contrast for a Fixed Exposure Difference of 500 $\mu$ J.....	31
Figure 8, Hurter-Driffeld Curve For KODAK 3034 Film, with fitted line to the linear region.....	37
Figure 9, Demonstration of Averaging Direction to Calculate the Lateral Mean Cross-Section of a Bar Group Image.....	41
Figure 10, Grayscale Image Bar Group #2.....	42
Figure 11, Surface Plot of Bar Group #2.....	43
Figure 12, Mean Lateral Cross-Section Plot of Bar Group #2 and 10 <sup>th</sup> Order Polynomial Fit.....	44
Figure 13, Grayscale Image Bar Group #9.....	45
Figure 14, Surface Plot of Bar Group #9.....	45
Figure 15, Mean Lateral Cross-Section Plot of Bar Group #9 and 10 <sup>th</sup> Order Polynomial Fit.....	46
Figure 16, Grayscale Image Bar Group #10.....	47
Figure 17, Surface Plot of Bar Group #10.....	47
Figure 18, Mean Lateral Cross-Section Plot of Bar Group #10 and 10 <sup>th</sup> Order Polynomial Fit.....	48
Figure 19, Surface Plot of Brightness Panels for OS Mission 095-MOC-007 to Emphasize Surface Inconsistencies.....	49
Figure 20, Histogram of Brightness Panel to Show Value Variance.....	50
Figure 21, Flowchart of Adaptive Digital Method .....	56
Figure 22, Opening Screen to ADiM.....	59

Figure 23, Selected Bar Group #1 Using ADiM .....	61
Figure 24, Mask and Identified Bar Group Cross Section .....	63
Figure 25, Demonstration of x-range and y-range extent determination.....	65
Figure 26, 60th Percentile Row and Column Vector Formation.....	66
Figure 27, Mean Lateral Cross Section of Bar Group #1 and 10th Order Polynomial Fit .....	67
Figure 28, $K_2$ Value Summary Based on Each Bar Group for Resolved Bar Groups .....	70
Figure 29, Brightness Panel Selection For $K_2$ Analysis.....	71
Figure 30, Bimodal Histogram of Brightness Panel Samples .....	73
Figure 31, Target Gray Level Histogram .....	77
Figure 32, Histogram of Bar Group #9 .....	78
Figure 33, Example of the Effect of Decreasing Barwidth on Peak and Valley Amplitudes of Bar Group #9 (30 cm-ground bar width, no filtering) .....	79
Figure 34, Gray Level Intensity Image of Bar Group #1(75.6 cm-ground bar width).....	80
Figure 35, Log E vs. 21-Step Wedge Gray Level Curve Demonstration of the S-Shape and Linear Region.....	83
Figure 36, Graph demonstrating a linear correlation between OSMPF and ADiM measurements.....	89
Figure 37, Graph shows a relationship between OSMPF and ADiM $H_{min}$ measurements.....	90
Figure 38, Same data as Fig 33—except the values were sorted in ascending order .....	91
Figure 39, Linear Model Residuals (Error) plotted against OSMPF $H_{min}$ .....	92

## ABSTRACT

World leaders depend increasingly on remote sensing technologies to gather information required for objective decision making as technologies and historical events blur national boundaries. The Open Skies Treaty depends on remote sensing in the form of aerial photography to enforce its bylaws and further inspire trust and cooperation among the international signatories. The Open Skies Treaty provides guidelines allowing participants to fly in air space over other participants' countries to monitor strategic military placement and development. The treaty restricts the ground size of the smallest detail recorded by these aerial imaging systems to any size larger than 30 cm. This restriction is enforced by placing a lower limit on the altitude at which a participating aircraft can fly and it is computed as the value of  $H_{min}$ . Current techniques rely on human photographic interpreters to select the value of  $H_{min}$  for every calibration pass and is very resource intensive. The Open Skies participants are investigating machine based techniques to supplement the traditional human role in an effort to increase the objectiveness of the measurement.

This thesis presents a software tool called, ADiM, a man-in-the-loop, algorithm which manipulates image statistics to identify the orientation and width of individual target bar groups from digitized images of aerial photographs of Open Skies Treaty calibration triple bar target. ADiM  $H_{min}$  results achieved an 88.6 percent correlation with the Open Skies Media Processing Facility's  $H_{min}$  computations.

# Automatic Digital Processing for Calibration Data of Open Skies Treaty Sensors

## I. Introduction

NASA's Voyager Space Probes I and II possessed the ability to record visual imagery data of planets Jupiter, Uranus and their moons and to transmit this information back to Earth. The technologies involved in unmanned space exploration, such as the Voyagers, relied heavily on the application of *remote sensing*<sup>1</sup> systems [Wilhelms, 1984: 167; Merchant, 1996]. In earth orbit, satellites record information and transmit it to ground based receiving stations using the same remote sensing technology as Voyager. Governments and industry both benefit from these remote sensing satellites which are used to map weather systems for predicting weather, or to map large areas of land on Earth for land development use or environmental measurements [Merchant, 1996]. Similar technology can be used to collect imagery of Earth-based regions of interest by the United States and many other countries to assess the capability and intentions of potential adversaries. Remote sensing systems are placed on aircraft as well as in earth orbit and can yield similar types of information.

Aircraft or spacecraft mounted remote sensing systems also play important roles in international treaty verification [Merchant, 1996]. The usefulness of aerial imagery in the

---

<sup>1</sup> In the most general terms remote sensing is "the acquisition of information about an object without physical contact" [Simonett, 1983: 1].

international arena is accentuated by the United States' National Security Policy which defines nine fundamental roles for the United States Air Force (USAF). As one of these nine fundamental missions, Air Surveillance and Reconnaissance requires the collection and processing of information from airborne, orbital, and surface based systems to provide strategic and tactical intelligence during peace and war [AFM 1-1, 1984: 3-5]. Since 1969, following the initial Cold War Strategic Arms Limitations Talks (SALT I) and the Anti-Ballistic Missile Treaty (ABM Treaty) between the US and the former Union of Soviet Socialist Republics (USSR), remote sensing has been an internationally accepted method of treaty verification [Luttwak, 1996].

## **1.1. Open Skies Treaty**

In 1992, the United States of America became a signatory to the Open Skies Treaty (OST). OST is an international treaty whose provisions grant participating countries<sup>2</sup> the authority to collect an annual quota of aerial imagery over strategic areas within the boundaries of other signatory countries. The OST participants aspire to improve confidence between their respective countries [AF News Service, 1995]. The following text is an excerpt from the treaty and reflects its ideals and purpose.

*Treaty on Open Skies:*

*The States concluding this Treaty*

---

<sup>2</sup> This list of countries includes, but is not limited to: USA, Germany, Belarus, Belgium, Bulgaria, Canada, Denmark, Spain, France, Great Britain, Greece, Hungary, Iceland, Italy, Luxembourg, Norway, Netherlands, Poland, Portugal, Romania, Russia, the Czech and Slovak Republic, Turkey, Ukraine, and Georgia.

*Recalling the commitments they have made in the Conference on Security and Co-operation in Europe to promoting greater openness and transparency in their military activities and to enhancing security by means of confidence- and security-building measures,*

*Welcoming the historic events in Europe which have transformed the security situation from Vancouver to Vladivostok,*

*Wishing to contribute to the further development and strengthening of peace, stability and co-operative security in that area by the creation of an Open Skies regime for aerial observation,*

*Recognizing the potential contribution which an aerial observation regime of this type could make to security and stability in other regions as well,*

*Noting the possibility of employing such a regime to improve openness and transparency, to facilitate the monitoring of compliance with existing or future arms control agreements and to strengthen the capacity for conflict preventions and crisis management in the framework of the Conference on Security and Co-operation in Europe and in other relevant international institutions,*

*Envisaging the possible extension of the Open Skies regime into additional fields, such as the protection of the environment,*

*Seeking to establish agreed procedures to provide for aerial observation of all the territories of States Parties, with the intent of observing a single State Party or groups of States Parties, on the basis of equity and effectiveness while maintaining flight safety.*

*Have agreed as follows:*

*1. This treaty establishes the regime, to be known as the Open Skies regime, for the conduct of observation flights by States Parties over the territories of other States Parties, and sets forth the rights and obligations of the States Parties relating thereto.*

*2. Each of the Annexes and their related Appendices constitutes an integral part of this Treaty [Open Skies Treaty, 1992: 1-2].*

## **1.2. Background**

In the last three decades most academic and commercial arenas of remote sensing have adopted digital data processing as the standard paradigm of data analysis. Astronomers, geologists, and other natural scientists are trading their cameras and large format non-linear response<sup>3</sup> photographic plates for cameras with integrated electronic systems composed of

---

<sup>3</sup> Linear and non-linear sensor response refer to the relationship between the input and the output of the sensor. Linear sensors have outputs which have a constant change in output for a given change sensor input over the design range; the input can be predicted from a simple linear regression model as a function of the output. Non-linear sensors cannot be described as a simple linear functions of the input and output. The output of photographic film is nonlinear. Film consists of an acetate strip coated with silver nitrate grains bound in an emulsion. The film is the sensor in a photographic system, where the input is the irradiance to which it was exposed for a fixed amount of integration time and the output is the emulsion thickness. The optical density (OD) of the photographic negative increases as the emulsion thickness increase. This OD is used as the measure of the emulsion thickness and it is proportional to the logarithm of the exposure [Slater, 1983:253-263].

linear opto-electronic detectors, such as charge coupled device (CCD) arrays or photomultiplier tubes, and high powered digital computers to coordinate the data collection and analysis for both infrared (IR) and visible imagery data [Menzel, et al., 1970: 94-96, 102]. Data stored in digital format can be transferred across network or telephone communication lines, reproduced easily, damage resistant, and analyzed by multiple parties simultaneously. Conversely, film can be fragile and bulky, only reproduced with great expense or loss of information, and only examined by one group of analysts at a time. Even with the advantages provided by digital technology, many reasons exist for analysts to continue to use photographic film for aerial imagery.

Due to the fall of the Berlin Wall and the division of the USSR into multiple nation states, many countries now exist whose national budgets and available technologies reinforce the use of older tools to perform remote sensing tasks. Aerial cameras using high resolution photographic film are widely available technologies with which aerial reconnaissance imagery data has been collected reliably since the 1940's. One notable reason for this film-based view is the access many countries have to the photographic reconnaissance equipment from the Cold War.

Newer European sovereign powers need the same strategic information about their well established neighbors to enforce their nations' security as their neighbors need from them. It is in the best interest of the more technologically advanced countries to support this gathering of information through remote sensing [AF News Service, 1995]. This information increases the probability of long lasting stability for all countries by increasing the confidence among neighboring states that no hostile movements are being organized [OST, 1992: 1-2].

As stated in the treaty preface, this openness was the central intent behind the Open Skies effort, and led to the international Open Skies Treaty. Technological equivalency concerns led the signatory countries, or State Parties, to initially accept the use of intelligence-type cameras and high resolution photographic film, not digital technology.

The OST allows signatory countries to collect aerial imagery of strategic areas during flights over other State Parties' borders. For the ABM Treaty and SALT I, verification imagery was limited only by *national technical means*, which was interpreted by the US and the USSR to allow the use of any means of verification commanded by either country [Luttwak, 1996]. The US and the USSR possessed evenly matched technologies to extract information from aerial or orbital imagery. The level of technologies commanded by members of the Open Skies regime varies to such an extent that an equitable distribution of information could not be guaranteed without administering standard restrictions on the *image quality* each country could achieve. Consequently, to implement the OST, limitations on *image quality* were required. The difficulty in defining an actual image quality metric will be discussed in Chapter 2, but as the matter stands, the OST contains several Decisions defining limits on image quality as factors which obstruct the ability of an airborne observer to see ground objects with dimensions smaller than 30 cm in perfect detail. These factors are synthesized into a function of the flight altitude, the length of the smallest identifiable object and the target modulation [OST Decision 14]. This three factor combination is used to calculate the minimum altitude at which an OST participating aircraft can fly over an area of interest and its result is computed as  $H_{min}$ . Although the identified terms in  $H_{min}$  have not yet been defined, for reference it is shown in Equation (2.5), it reflects the value placed on the information

extractable from an image by limiting the amount of ground detail any one participant can achieve. The computation of  $H_{min}$  is not an optical performance measure, but it is a restriction on data collection which attempts to enforce the limits placed on the size of useful details in an image.

The Open Skies Sensor Working Sub-Group (OS SWSG) was formed as the technical arm of the Open Skies (OS) regime, and has as one of its responsibilities to determine acceptable methods of measuring image quality. The US representatives to the OS SWSG report directly to the Office of Arms Control Implementation and Compliance, Office of the Under Secretary of Defense for Acquisition and Technology. Along with representatives from other OST countries, they chose to use a historically sound photogrammetric approach to an image quality metric composed of two measured factors.

The first factor, the ground resolved distance (GRD), is the smallest characteristic length distinguishable within a given photographic image [Holst, 1995:216]. At a known altitude, the relationship between the length of the smallest image object identified on a photographic negative,  $\Delta x_i$ , and length of the actual object on the ground are related geometrically as shown in Equation (1.1).

$$GRD = H \frac{\Delta x}{f} \quad (1.1)$$

where,

$H$ , is the altitude or distance away from the object for a given image,

$f$ , is the effective focal length of the camera system.

GRD is a common measure of optical system performance [Holst, 1995: 218]. The GRD recorded through the optical system increases as the image quality degrades (i.e. with altitude or film granularity). The GRD for a given OST participating airborne optical system is estimated by photographing a ground based target consisting of light and dark bars of decreasing width and determining the width of the smallest discernible bar group. The value of this width is referred to as  $L_2$  in the OST documentation [OST Decision 14, 1994].  $L_2$  only estimates the GRD because it is a measurement using imperfect detectors. This estimate is only an upper bound on the GRD because the bar groups occur in discrete bar widths. If the true system GRD lies between two of these sets of decreasing width bar groups, the selection of  $L_2$  will always be greater than or equal to the actual GRD. This measurement technique will be discussed in depth in Chapter 2. GRD, however, as a performance measure of the optical system, is not a measure of true system resolution, but a measurement of the interaction of factors such as the system optical resolution, atmospheric effects, object contrast, and sensor sensitivity.

The second component to the OS SWSG image quality metric is the target modulation. Modulation is a measure of the range in exposure values, or color depth, contained within a single image. All details in an image are described on the sensor as changes in exposure [Holst, 1995: 216]. Exposure,  $E$ , is a measure of incident energy per unit area<sup>4</sup> across a given plane. Modulation can be expressed empirically in terms of the minimum and maximum exposure values within an image, and can be expressed as Equation (1.2),

---

<sup>4</sup> SI units of  $E$  are  $J/m^2$

$$\text{Modulation: } M = \frac{(E_{\max} - E_{\min})}{(E_{\max} + E_{\min})}, \quad (1.2)$$

where  $E_{\max}$  and  $E_{\min}$  are the maximum and minimum values of exposure within an image.

When using photographic film, the image exposure actually recorded on film is degraded not only by the amount of irradiance<sup>5</sup> lost by the optical train in diffraction, reflection, refraction, and absorption, but also by the ability of the film to respond to small variations in the exposure distribution<sup>6</sup>. The film response and the irradiance transmission through the optical system are components of the system sensitivity. Resolution and sensitivity are separate quantities. *Spatial resolution*<sup>7</sup> is a property of a system of optics and is not affected by noise, film response, or irradiance transmission through the system, it is only a function of the geometry of the optical path from the target object to the sensing element (i.e. the film).

The measured GRD and modulation for a series of photographs taken over a calibration target determines the altitude an Open Skies aircraft can fly over the designated regions of interest within another country. The OST regime has chosen to use ground based targets composed of painted rectangular panels and rectangular bars. An Open Skies

---

<sup>5</sup> Irradiance is the rate of change of exposure with time ( $W/m^2$ , in SI units).

<sup>6</sup> For example, if the smallest visible object an optical system can resolve has length  $10\mu\text{m}$ , with a change in exposure of  $1 \mu\text{J}/\text{m}^2$ , but the film can only record changes in the exposure distribution of  $10 \mu\text{J}/\text{m}^2$ , the GRD will not be equal to the optical system resolution, because the object's contrast is not great enough.

<sup>7</sup> Three other aspects of resolution can be described [Holst, 1995: 218]:

*temporal resolution* is the ability to separate events in time--not an issue with single frame photography;

*gray scale resolution* is a measure of the dynamic range (the discernible range of exposure and the smallest detectable change in exposure) of a digitizer for data storage or visualization device and is strongly affected by the analog to digital converter design and noise floor of the electronics;

*spectral resolution* is the range of the electromagnetic spectrum discernible by a system (UV, visible, IR, etc.) and the smallest change in wavelength it can detect.

calibration target can have many configurations, but all Open Skies calibration targets share the series of light and dark-colored bars of decreasing bar widths with separate sets in perpendicular orientations.

Figure 1 portrays the calibration target constructed at Wright-Patterson Air Force Base (WPAFB) for the US Open Skies airborne optical system.

### ***1.2.1. Calibration Targets***

As previously discussed, the by-laws of the OST restrict the smallest detail in an image any country can achieve with their airborne imagery equipment to 30 cm for an acceptable target modulation. If a system can discern an object with a GRD less than 30 cm within the accepted modulation range, the aircraft must fly at a higher altitude to reduce the ground resolution. Each optical system must be certified in each of its configurations to be used during an OST flight. The image quality requirement is enforced with aerial images taken of ground based calibration targets. These targets are located at many sites around the world.

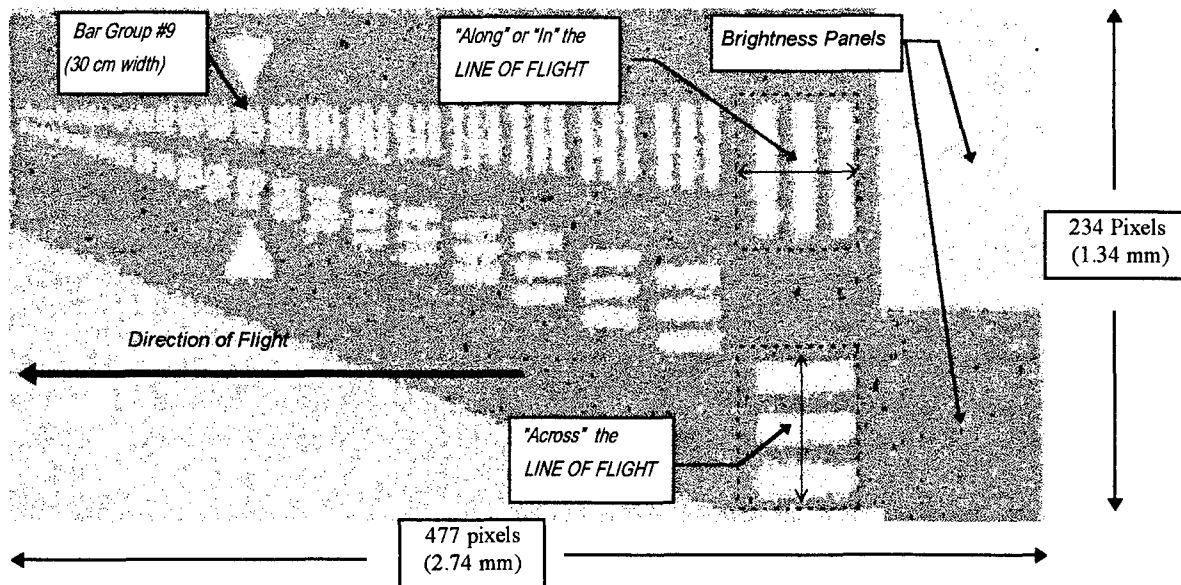


*Figure 1, Aerial Photo of WPAFB Calibration Target with Annotated Features (95-MOC-007 Mission, Altitude 1697m, KODAK 3404 Film) (Dimensions represent image size on film frame)*

An aerial image of the target constructed at Wright-Patterson AFB, OH, from OS Calibration Mission 95-MOC-007 is shown in Figure 1. The important features of the target are the orthogonal pairs of bar triads and the brightness panels and are indicated in Figure 1. Note the small size of the actual image digitized from the photographic film. This entire image could be drawn on an average sized fingernail. The small size of the image explains a majority of the challenges involved with the development of an automated calibration tool. Enough samples across the digitized image did not exist to use common image identification tools such as Fourier analysis or matched filter techniques.

The paint used to create the light panel and the light bars has the same reflectance, and a lower reflectance paint is used to construct the dark panel and dark bars with equal reflectance. The reflected light energy from across the panels is used to measure modulation. The bars are constructed with decreasing widths and separations to measure the GRD of aerial

photographic systems. These types of ground based calibration targets degrade over time due to fading of the paint and accumulation of environmental pollutants. This degradation decreases target contrast and is not regularly monitored in accordance with the OST.

The largest bar group set has a width of 120 cm and is not used as a bar group for certification purposes, but is used as a reference width in this thesis. The next smaller bar group is called Bar Group #1 and is a factor of  $(\sqrt[6]{2})^3$ , or 1.26, smaller than the largest bar group. The remaining bar groups are numbered Bar Group #2 through Bar Group #23 and decrease in width by a  $\sqrt[6]{2}$ , or 1.12, progression. Bar Group #9 is the 30 cm wide group and is marked with triangular fiducials. Both orientations of the bar triads are used to determine the smallest GRD and the brightness panels are used to find the modulation. The brightness panels and bar groups are both required to have a modulation between 0.66 and 0.82 [OST, Decision 14 1994:5].

### **1.3. Problem Definition**

Two overwhelming factors motivate the development of automated calibration techniques for the OST effort. The first reason supports the large quantity of work involved in calibrating each sensor, in each position for an OST mission. At any time, an OST country may call for a certification flight for the aircraft mounted optical systems [Open Skies Treaty, Decision 14]. Multiple photographic interpreters (PI) from each signatory country are responsible for determining the smallest identifiable bar widths by viewing dozens of magnified photographic negatives of the images of the calibration targets. The sheer quantity of images which must be used in order to obtain the values defined in the treaty must not be

over looked. Ten or more observers from participating countries could be employed to critique ten or more bar target images for each different camera system to be flown. Each country is permitted several dozen flights each year over any OST nation. The sheer quantity of work is enough to justify some automated simplification. The criteria they use will be discussed in Chapter Two.

The second motivating factor for developing an automated calibration tool involves the reduction of uncertainty found in many common calibration techniques. The qualitative calibration method currently employed by the OST signatories is influenced by human factors such as experience, fatigue, and ambient light level [Slater, 1983: 241]. As the Open Skies project continues, there is a need to improve consistency in the data processing arena ensuring no one country gains inequitable advantages over others. The perception of an unfair advantage could cause conflict among OST signatories and this conflict would defeat the purpose of the treaty and its philosophy of openness. Quantitative calibration techniques would reduce uncertainty. Hence, the creation of an objective measurement could increase the probability of trust.

Although automated computational methods of measuring imaging system capabilities are being created in Russia and other countries, personal computer power and digital imagery are not widely available to all of the Open Skies participants, and as such, many different methods need to be studied and debated in detail to increase confidence in this paradigm shift. The SWSG has been directed to explore automated digital methods for calibration in search of one which can be readily accepted and understood by all Open Skies members.

This thesis supports the certification automation efforts of the SWSG. Ease of use is required for any viable technique. It should compute valid detection parameters given only the information available in the current Open Skies data collection system. All algorithms must run on widely available computer equipment and use commercially available software.

Using only the information available in the OSMPF calibration method in use at the time of this study reduces the number of analytical procedures available. This restrictive analysis preference constrains the problem solution to techniques which only depend on the knowledge of the camera geometry, the sensor response, the flight altitude, the physical dimensions of the target, and the characteristics of the digitizing scanner employed. No physical transmission model of the optical system was created and atmospheric effects were not considered directly. Consequently, no knowledge of the expected signal levels is available at the time of processing is available.

The central issue in this thesis is to automatically and consistently determine which bar triad represents the smallest set resolved for all photographic images of the calibration target. More than one method to satisfy the requirement for a consistent and objective digital image processing algorithm was pursued in this thesis. The method developed determines the GRD, the target modulation, and the minimum altitude at which an OS aircraft can fly,  $H_{min}$ . These three factors were calculated and compared to OSMPF results to obtain measures of merit for the algorithms written for this study.

In the method used in this thesis, the user must first digitize the small region of the photographic film negative<sup>8</sup> containing the target region. Digitizing the photograph creates a very large bitmapped file which contains some irrelevant data. Cropping is an additional manual step which is useful since it reduces the computation time of the analysis. The user then applies the software from this thesis to the target image and extracts each bar group from the largest to the smallest widths as subimages. The software processes these subimages and collects the bar group statistics. The order statistics<sup>9</sup> of the digitized image gray levels, the gradients of the data, and the knowledge of the target layout and altitude are used to determine the GRD. The modulation is determined with an estimate of the gray level values from the light and dark brightness panels, which are converted to units of illuminance (Lumens) using calibrated film strips of known exposure. The calibrated film strips of known exposure are referred to as 21 Step Exposure Wedges which are film strips produced at the beginning (header) and end (tail) of each roll of film used for OST flights. The 21 Step Exposure Wedges are exposed with known exposure using Nation Bureau of Standards calibrated light sources.

---

<sup>8</sup>The image of the calibration target is a very small region of a very large film frame; for example, in the Kodak 3404 film type, the frame is 4.5" square, but the region containing the calibration target is less than 0.5" square. Digitizing the target region can require over 1 MB of 8-bit data, so even with many megabytes of RAM on a computer, it is best to extract the target region from each frame first.

<sup>9</sup>Order statistics are used in this thesis because the distribution of the bar group data is not normal, nor are the residual values from the estimated model of the bar groups used to calculate bar widths [Kreyszig, 1983: 981].

## 1.4. Summary of Key Results

Several methods for evaluating Open Skies imagery were developed in this study and tested on actual data. Due to an undersampling of the smaller bar groups and a significant amount of noise, Fourier filtering techniques proved to be unsatisfactory. An adaptive digital technique, however, works well and could form the basis for automated calibration of Open Skies Treaty systems. This method matches the GRD prediction from OSMPF human observers for some cases. For all data analyzed in this thesis, the GRD determined by ADiM was smaller than or equal to the GRD result from the OSMPF. This interactive technique is adaptable to individual bar group image gray level amplitudes and is based on the order statistics of the data and gradient search methods. The Adaptive Digital Method (ADiM) is implemented within a graphical user interface built from The MathWorks MatLab<sup>®</sup> programming language [MatLab<sup>®</sup> Users Guide]. Preliminary results suggest a reasonable match with human observers. Figure 2 and Figure 3 demonstrate the correlation between the OSMPF and ADiM computed values for  $H_{min}$ .

Figure 2 shows a scatter plot of  $H_{min}$  values determined by the OSMPF (horizontal axis) and the  $H_{min}$  values determined by ADiM (vertical axis). Figure 2 supports the supposition that the results from both techniques are highly correlated. Creating a linear fit between the two sets of data, containing 25 data points, in the form of a simple linear model yields a correlation coefficient of 0.886. This means almost 89 percent of the variation in the OSMPF  $H_{min}$  value is explained by the variation in the ADiM value. This high degree of correlation shows that the compromises made in the adaptation of OSMPF methods to digital data can be used to produce results similar to the manual method.

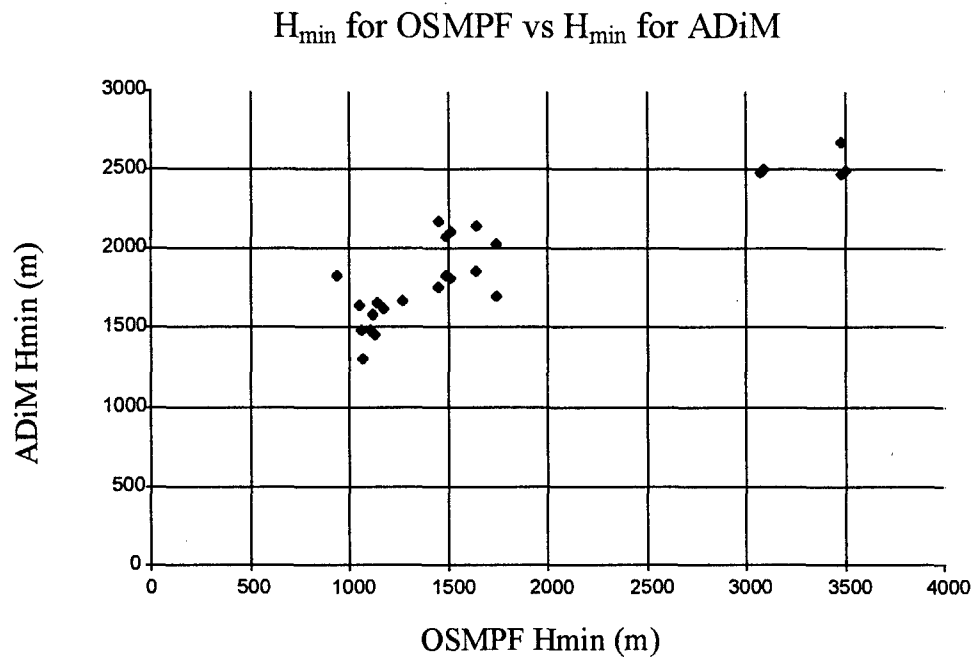


Figure 2. Scatter plot of  $H_{min}$  values obtained by OSMPF and ADiM

Explained variation does add to the credibility of the results, but a scatter plot of both OSMPF and ADiM computed results of  $H_{min}$  in Figure 3 shows that none of the ADiM results exactly matched the OSMPF values for  $H_{min}$ . The data points are arranged by the type of film used for data collection. Some systematic differences in the two methods exist. This difference in results can be traced most often to different values of the calculated film exposure modulation values between the two measurements.

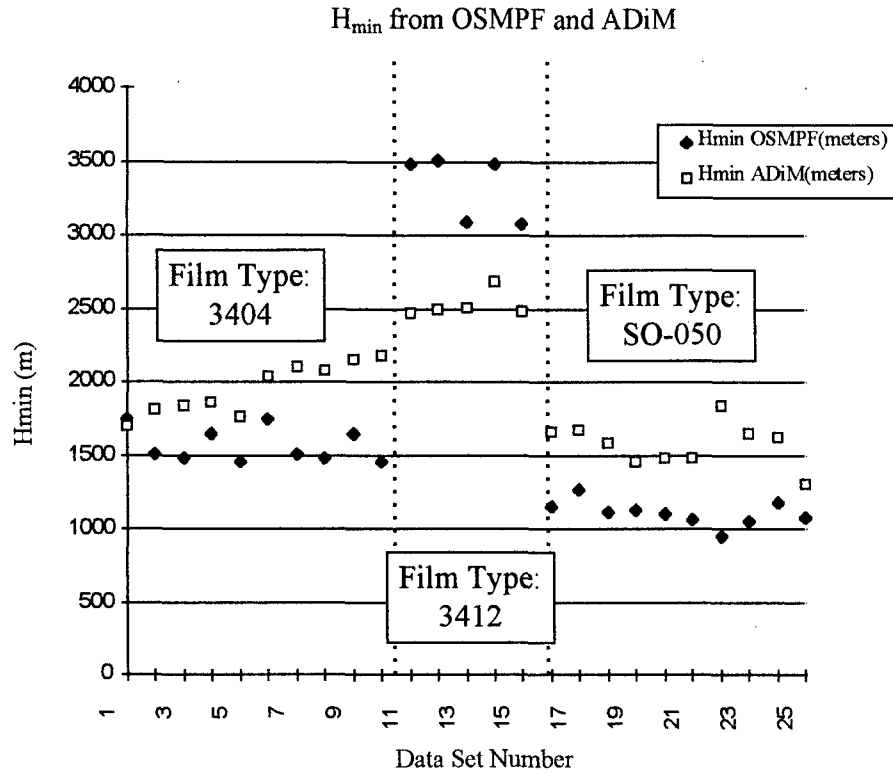


Figure 3, Point by point comparison between calculated  $H_{min}$  values for OSMPF and ADiM

A reason for this discrepancy could be that for the OSMPF results used a 10 by 10 sample set of data obtained by scanning the film with a Perkin-Elmer Digital Scanner (PDS) to calculate the brightness panel modulation, while the ADiM method used data digitized with the KODAK 5057 image scanner for averages of hundreds of samples all over the brightness panels.

A simple linear model was built with the least squares method to determine the correlation between the ADiM and OSMPF  $H_{min}$  results. In order to assess the value of a simple linear model, a diagnostic plot of the residuals, the difference between the estimated values of  $H_{min}$  from the model and the actual  $H_{min}$  values calculated by the OSMPF, versus the calculated OSMPF  $H_{min}$  values shown in Figure 4 [Neter, Wasserman, Kunter 1990:117]. The

abscissa of Figure 4 represents the difference between the linear model and the OSMPF  $H_{min}$  results. The three different symbol demarcate the three different film types analyzed. Note how the types of film group the residuals into three distinct regions. This structure could imply that higher order terms are needed in the linear model to explain additional variance in the OSMPF results with the ADiM results.

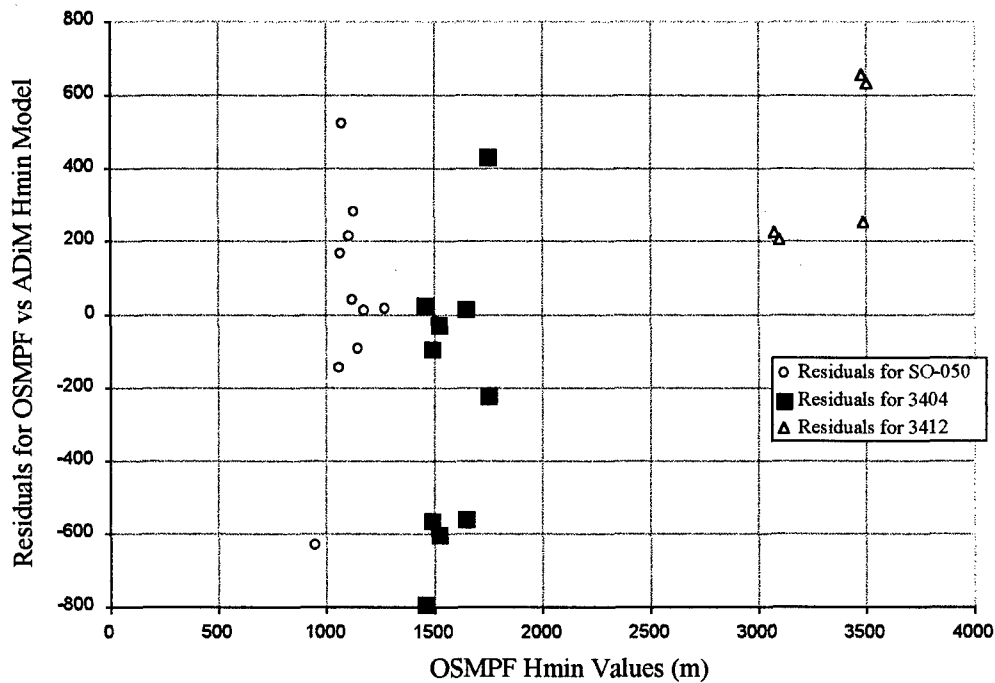


Figure 4, Linear Model Residuals (Error) plotted against OSMPF  $H_{min}$

Figure 4 demonstrates the possibility that different films affect the residuals between measured and modeled values. If it were important to convert ADiM  $H_{min}$  values to OSMPF  $H_{min}$  values, it may be useful to include a variable representing film type. This is not a requirement and will not be discussed further.

This structure in the residual plot could also imply that improper calibration data was used to compute  $K_2$ , since a sample of each type of film must be used in order to compute the modulation and translate the digitized values into measures of luminance. Further study is

required to fully understand the contribution to the errors made by the film types. However, the correlation of 88.6% between ADiM and OSMPF does support that the software methods developed in this thesis could be applied to the OST calibration problem.

## **1.5. Organization of Thesis**

The remainder of this thesis is organized as follows. Chapter Two reviews the elements of optical science required to discuss the issues of image quality and what the measurements of the OSMPF actually represent. The details of the existing methods used by the OS SWSG to determine the minimum altitude,  $H_{min}$ , are covered. Chapter Three describes the details of the solution method and the Adaptive Digital Method (ADiM) algorithm developed for the OSMPF and its validity. Tabulated results and discussion concerning the results are contained in Chapter Four, followed by conclusions and suggestions for additional work in Chapter Five. *MatLab*<sup>®</sup> code listings are contained in appendices.

## II. Current Methodology

This thesis develops a computer-based digital calibration method to determine which bar triad has the smallest discernible width in a digitized photographic imagery of an OS calibration target. This proposed digital method is derived from the current system calibration method employed by the signatory countries to the OST, which was developed from the need to assure all OS participants received the same detail of information. They have agreed to a level of *image quality* based on two quantities: the ground resolved distance (GRD) and the target modulation, defined in Equation (1.2) [OS Decision 14, 1994]. The OS calibration technique and their *image quality* criteria are discussed in the following pages and the details of the digital method, ADiM, will be the focus of the next chapter.

The OST and the appended Decisions do not refer to the selected criteria as measures of *image quality*. In spite of this omission, the two factors identified by the OST used as a standard for image information content regulation actually do constitute a true image quality metric and restrict the information recorded in an image by defining the lowest altitude at which an OST participant can record image data over another OST country. Much more will be discussed about this in Section 2.2.1. Image quality is a judgment on the inherent value of the information content in an image, and  $H_{min}$  restricts the level of detail recordable by an airborne remote sensing system. The process of this information extraction is called *image analysis*, whose principles encompass the methods for “detecting, identifying, and measuring objects of interest from the aerial perspective,” according to the Manual of Remote Sensing [Estes, et al., 1983:987].

The first factor in the OST image quality equation is the smallest width discernible in an aerial image taken of a ground target, at a known altitude, and it is represented by a measure of the minimum GRD, called  $L_2$ . The second factor is the film incident image exposure modulation, called  $K_2$ . Although the OST has no formal definition of an image quality metric, in using these factors to limit the flight altitude of the data collection aircraft, the OS regime has implicitly created a metric. However, the GRD is not an independent component of image quality, but a function of the target contrast as well as the width of the target on the ground and the geometric resolution of the camera optics.

GRD performance is measured for each aerial imaging system in use by the Open Skies participants, in each of the mounting locations and configurations to be certified for a data collection flight. GRD is called *resolution* in the OST; however, in this thesis, the ground width of the smallest set of bars deemed distinguishable will be called the GRD. The term *resolution* can refer to four different physical performance properties of an image acquisition system as discussed in Section 2.2. The measurement of GRD is affected by many environmental factors and the strongest parameters are illustrated in Figure 5. The GRD increases as the light reflecting off of the passive target is transmitted through the atmosphere. This increase is caused by the loss of light due to an unfavorable incident light angle with the sun as the day passes and the seasons change, image smearing due to imperfect camera shutter speed timing, imperfections in the bar target surface paint, atmospheric temperature changes which distort the reflected image as it propagates through to the sensor, and finally sensor imperfections. Smearing of the images in the direction of motion of the aircraft also occurs due to finite exposure time of the film.

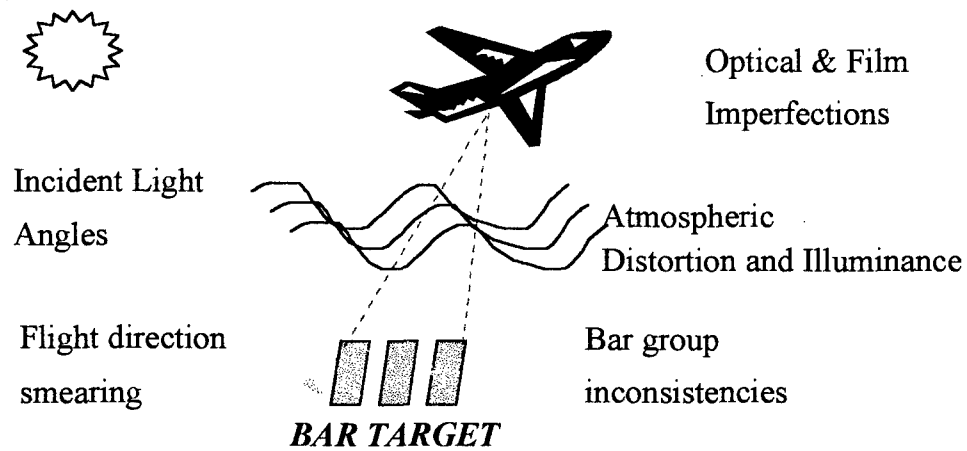
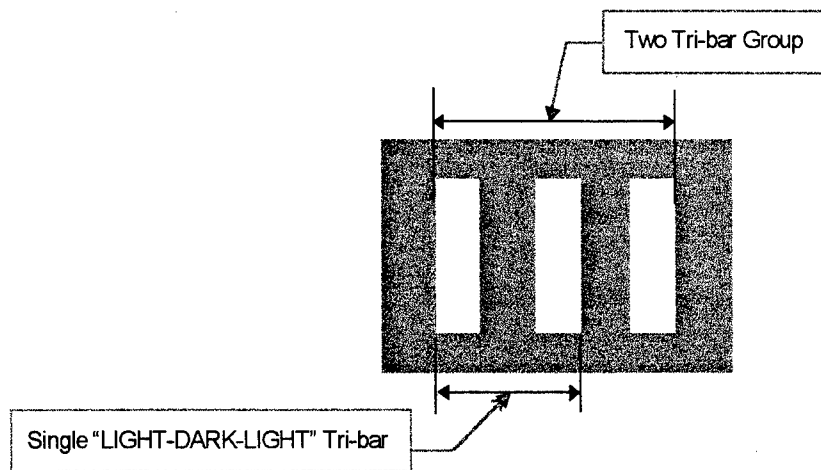


Figure 5, Sources of GRD Degradation<sup>10</sup>

The terms *distinguishable* and *resolved* are interpreted in the OST to mean the smallest bar group on which both *dark* bars are differentiable from their adjacent *light* bars, along their entire length. Figure 6 portrays the details of each bar to be distinguished. By definition in the OST, a bar group is defined as a pair of light bars separated by a dark bar of the same size. Hence, in Figure 6 the three light bars depicted represent two triple bar groups where the left most light bar, the center light bar, and the dark area between them represent the left most triple bar group. The dark area between them is considered the dark bar. The center bar and the right most bar group define the outside bars of the right most triple bar group. The bar length of both light and dark bars is five times longer than the bar width. The use of this target will be discussed in more detail later in this chapter. This standard for distinguishability will be relaxed for the digital method discussed in Chapter Three, because true edges in the image are difficult to define in the presence of noise and the digitized data has additional noise that could make a group of bars appear indistinguishable when the information content of each bar is actually resolvable.

<sup>10</sup>The GRD of the bar triad reflected irradiance can never increase as it propagates along the optical path to the receiving sensor.



*Figure 6, Triple Bar Group Diagram*

GRD for a photographic camera system is a function of the resolution of the system, the response of the film to light, the irradiance incident on the ground from the sun, the particulate content of the air, and the modulation of the calibration target, to name a few [Holst, 1995: 241]. Hence, using the GRD as part of the image quality criteria considers the interaction of the of all of these quantities for the given data run, not any of the individual factors directly. In order to further discuss the strengths and weaknesses of the OST approach, the concepts introduced above, resolution, sensitivity, and modulation must be established.

## **2.1. The Basic Physics of OST Image Quality**

For all studies which require an accurate and reproducible measurement of image quality, the actual definition of an image quality criterion is difficult [Holst, 1995: 239]. Defining the overall goal of the data collection should drive the details of this metric. A large variety of measures exist to describe the information content of a recorded image, and for the most part these criteria are not interchangeable among different sensors and may not

correspond to engineering or scientific measures of spatial resolution, dynamic range, or spectral resolution [Holst, 1995: 239]. For instance, the metric for observing a tan, camouflaged truck in the tan, brush-covered desert under a Saudi Arabian summer sun at a distance of two kilometers, is not the same system performance needed for seeing a black truck on the Siberian tundra driving across the snow white tundra from an airplane at noon.

The important distinction between the two scenarios is that the former is mostly an issue of detector sensitivity and the latter is mostly one of system resolution. It is also important to recognize, as will be discussed, the effects of sensitivity and resolution are complimentary. They are easily confused in determining image quality because the eye has difficulty distinguishing between a loss of sensitivity or a loss of resolution. Both effects can cause a loss in image detail to a detector or a human observer.

Before it is an image recorded on some type of receiver, such as film or electronic detectors, a light source has created a signal which has been reflected off or transmitted through several different types of media. The ground, the atmosphere, lenses, and mirrors can absorb and distort portions of this image forming light reducing the strength and warping the geometry of the original signal. The film or electronic detectors have ranges of signal strength sensitivity over which they can react and record incident light to form an image recognizable to a human observer. If the incident signal is too weak or the optical path has absorbed too much of the signal, the detector can not react, and therefore it can not form the details of the image. If the signal is too strong, the detector becomes saturated and can no longer distinguish between incremental changes in the signal strength which would form the details of an image. These are the issues of sensitivity. Furthermore, not only the optics of an optical

system attenuate available signal strength. Film and electronic detectors also have signal degrading natures and act as attenuating and distortion filters as the transmitted image passes onto them. Film has image recording capabilities which depend on the size of the smallest grain of emulsion and on the smallest amount of light it takes to change the color intensity. Other factors affect the performance of film and Slater discusses them in detail, but they will not be discussed in this thesis. The film used for the OST can have a sample size near  $1\ \mu\text{m}$ , which represents a ground size of approximately 1 mm at a flight altitude of 2000m. The KODAK 5057 used in this thesis can have sample sizes near  $6\ \mu\text{m}$ .

The effective optical system aperture also acts as a detail reducing filter. These degrading filter effects further complicate the attempt to define an image quality parameter by the fact that all images can be considered to be composed of an infinite number of frequencies, but the optical system can only capture a small fraction of these frequencies. Sharp edges are composed of nearly infinite numbers of the highest frequencies, so for bar target based methods, the first details to be lost are the sharp edges along the perimeter of each bar in a bar group. In order gain a greater understanding of the effect an optical system can have on a reflected image, the system modulation transfer function must be discussed.

### ***2.1.1. The system modulation transfer function.***

To some extent, even physics works against the definition of a universal image quality metric. This especially affects passive<sup>11</sup> techniques using bar targets or other edge defining measurement methods. Not only do the bars of higher spatial frequency have less surface area to reflect incident light than their neighboring bars of larger widths (and lengths for the

---

<sup>11</sup> Passive imaging techniques have no source of lighting beyond the natural light provided by the sun.

WPAFB target), but the finite diameter optics further attenuate the narrow bars due to diffraction, resulting in the attenuation of higher spatial frequencies described by overall system spatial modulation transfer function (*MTF*) [Castleman, 1995:371-377]. The *MTF* measures the attenuation of spatial frequencies due to the physical geometry of the optics, but does not show any information about the sensitivity of the system or its detector [Holst, 1995: 237].

The spatial variations in a recorded image depend on the geometry of the object(s) in the image and the geometry of the data collection optical system. The shape and size of the optical system as a whole determines the smallest distance resolvable in the exposure distribution incident on the detector. The study of Fourier Optics [Goodman, 1988 (Reissued)] treats the subject of electro-magnetic radiation propagation through optical systems in depth. In his classic text, Goodman develops the basic concept of the *MTF* and the relationship between the object spectrum,  $O(f)$ , the image spectrum,  $I(f)$ , and *MTF* given by:

$$I(f) = MTF_{system}(f)O(f) \quad (2.1)$$

The system *MTF* is a useful performance measure. It represents the attenuation of spatial frequencies, which compose the details visible in an object, due to the system being analyzed. The *MTF* is measured using the image a point source of light with known signal strength. Because each element in along the optical path of an image contributes to the over all system *MTF* and can be modeled as series of linear systems such that the effect on the image by the atmosphere, the lens system, and the windows and mirrors encountered by the propagating image can be represented in the following fashion:

$$MTF_{system}(f) = MTF_{atmosphere}(f)MTF_{window}(f)MTF_{optics}(f)MTF_{film}(f) \quad (2.2)$$

where,  $MTF_{atmosphere}(f)$ , is the transfer function describing the attenuation of detail due to the atmosphere,  $MTF_{window}(f)$ , the transfer function for the aircraft window where the image enters the optical system,  $MTF_{optics}(f)$ , the transfer function for the optical path along which the image transmits, and,  $MTF_{film}(f)$ , the transfer function for the emulsion on the film.

The  $MTF$  of a data collection system is a filter function which determines how spectral components of the object are attenuated or boosted as they pass through the particular system of interest. If the  $MTF$  is thoroughly known, then all of the original object details could be completely reconstructed from the recorded image by dividing the  $MTF$  from both sides of Equation (2.1) and retrieving the details of the original object. Unfortunately, the OSMPF does not have the end-to-end  $MTF$  curves for their optical systems, and the atmospheric  $MTF$  would need to be measured for each different image in order to remove its effects.

Optical systems are only one category of systems for which a filter function describes the effect the system has on signals in the frequency domain. The human ear is also a sophisticated data collection system. Sound waves are attenuated by the human ear such that most humans cannot hear waves with frequencies higher than 20 kHz or lower than 100 Hz. For comparison of an ear to an optical system, such as a camera, different spatial frequencies are manifested in the sizes of the objects to be imaged. Higher spatial frequencies appear as small objects or fine detail in an image, lower spatial frequencies correspond to large objects.

The on-axis  $MTF$  for the US Open Skies KS-87 lens was measured by the Wright Laboratory's Metrology Lab and is close to the diffraction limit. This lens was used in the collection of all of the data analyzed in this thesis. However, no theoretical analysis of the total system  $MTF$  was performed due to a lack of information about the  $MTF$  of the film

digitizer. The lack of measured local atmospheric conditions also prevented an accurate theoretical analysis.

For most imaging tasks, the primary goal of collection is to gain or record useable information. No direct correlation exists between the information derived from an image and the shape of the acquisition system's modulation transfer function (*MTF*) [Holst, 1995: 239; Slater, 1983: 240-241]. Nonetheless, human appreciation of an image increases when the signal irradiance level is high, the fine details in the image exist, and the image graininess is low. Humans tend to judge an image of this nature to have better image quality than one of lower signal strength or higher noise [Holst, 1995: 239]. Systems with high *MTF* values at high spatial frequencies are capable of providing highly detailed images.

The *MTF* of the optical system does not hold the answer to the question of finding a single number to describe an image quality metric. It is only a tool to describe the effect of the optical system on the final image. Since, the exposure distribution of the resulting recorded image is reduced by the same proportional amount at each spatial frequency, the final value of an image is still a function of the original details it contained and the interpretation of the user.

### ***2.1.2. Modulation and Contrast Ratio Are Different Photogrammetric Values.***

The terms *contrast* and *modulation* are well defined photogrammetric quantities and both quantitatively compare measurements of the maximum and minimum exposure recorded on the film or other sensor. For the OST image analysis, the averaged digitized gray level values of the brightness panels, shown in Figure 5, are used to compute the maximum and

minimum logarithm of exposure used to compute the contrast and modulation. Contrast is shown in Equation (2.3) and modulation is defined in Equation (2.4) [Slater, 1983:241].

$$\text{Contrast Ratio: } C = \frac{E_{\max}}{E_{\min}} \quad (2.3)$$

where,  $E_{\max}$  is the maximum exposure value and  $E_{\min}$  is the minimum exposure value.

Modulation is a measurement of the difference between the maximum and minimum exposure level normalized by the sum of the two and contrast is simply the ratio between the two exposure extremes. The algebraic relationship between modulation and contrast is seen in (2.4).

$$\text{Modulation: } M = \frac{C-1}{C+1} \quad (2.4)$$

The value of modulation is bounded between zero and one. However, the contrast ratio is an unbounded quantity which only describes the ratio of exposures, the original exposure level is masked.

Figure 7 demonstrates the results of contrast and modulation for a signal with a maximum and minimum difference of  $500 \frac{\mu J}{m^2}$  at five different signal levels. Notice that a measure of exposure near zero causes the contrast ratio value to increase without bound, but the modulation simply approaches unity. The graph shows that the Modulation values are bounded between zero and unity, yet the Contrast Ratio is unbounded as the difference between the minimum and maximum exposure increases.

Table 1, Demonstration of Contrast and Modulation Values for a Fixed Exposure Difference

$E_{\max} (\frac{\mu J}{m^2})$	$E_{\min} (\frac{\mu J}{m^2})$	Contrast Ratio	Modulation
500	1	500	0.9960
1000	500	2.0000	0.3333
10,000	9500	1.0526	0.0256
100,000	99,500	1.0050	0.0025
1,000,000	999,500	1.001	0.0003

Demonstration of Boundedness of Modulation

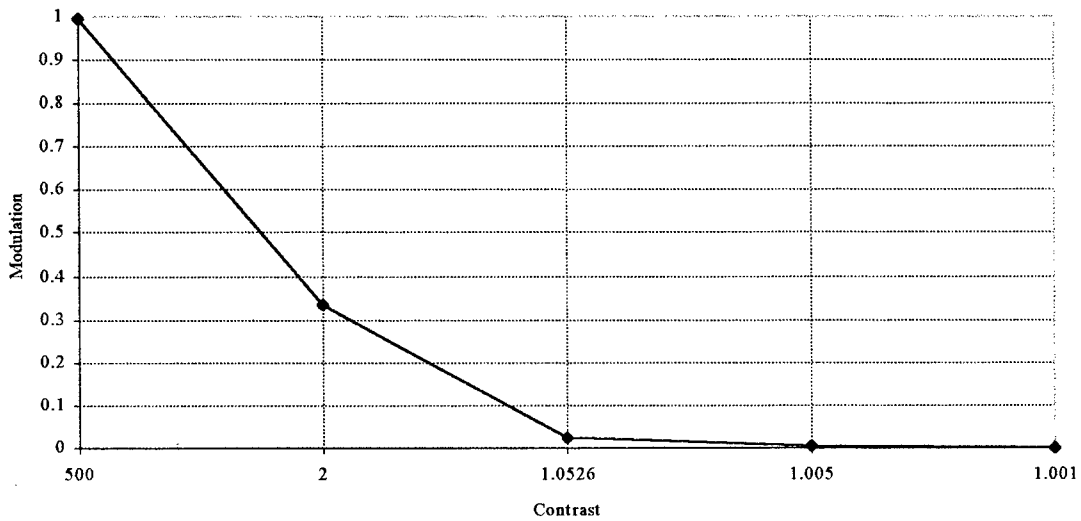


Figure 7, Comparison of Modulation and Contrast for a Fixed Exposure Difference of  $500\mu J$

The modulation calculated within an image and the actual modulation value in the *MTF* are not the same physical quantities. An important distinction between *M* in Equation (2.4) and the modulation value in the *MTF* is that *M* is defined from exposure differences within a single image, but the *MTF* values are defined as comparisons of exposure as a function of spatial frequency at the input and output of an optical system. Therefore, in this thesis the actual *MTF* cannot be calculated from the available data because no input irradiance measurements, across any band of spatial frequencies, were available for comparison.

### ***2.1.3. Undersampling reduces the certainty of identifying individual bar groups***

The undersampling in the digital image scanner which hinders the bar width measurement can be observed in Table 2. The sample size for the data set from the 95-MOC-007 mission was 30.98 microradians/pixel wide, which projects to 8.88 cm/pixel on the ground at an altitude of 2750m, using KODAK 3412 film. For bar groups 8, 9, 10, and 11, Table 2 shows that the width of each bar ranges from 2.7 to 3.8 samples wide. Distinguishing between them with only the estimated pixel widths could be difficult since they each are sampled with at most three full pixels for this sampling resolution. As discussed later, averaging improves the estimate of the bar widths and permits ADiM to effectively distinguish between bar groups 8 through 11. Bar groups 8 and 9 were not as differentiable as the other groups and this can be explained by noticing that the bar widths of bars 8 and 9 are only different by 0.4 pixels, both only 3 full pixels wide. Bar group 8 has a ground width of 3.8 and bar group 9 is 3.4 pixels wide, even using averaging, the variance of the data was too large to consistently differ between them.

The uncertainty due to undersampling does not affect the accuracy or usefulness of ADiM—it just demonstrates that the OS Treaty criteria applied to the data acquisition system in use at the writing of this thesis cannot be easily fully automated. Man in the loop analysis was required. Notice how small the bar group widths are on the film image. However, if the criteria and data acquisition were redesigned in order to eliminate the man in the loop, total computer automation could be possible. Potential designs are discussed in Chapters 4 and 5.

*Table 2, Comparative Number of Samples Across Bar Groups from One Target to Demonstrate Source of Uncertainty as the Number of Samples Across Each Bar Group Decrease*

Bar Group	Width on Film (cm)	Ground Width (cm-ground)	Angular Subtense @ 2750m	Samples
1	0.004877	75.6	275 (32.3)	8.5
2	0.00436	67.4	245	7.6
3	0.003873	60.0	218	6.75
4	0.003442	53.5	194.6	6.0
5	0.003098	47.6	173	5.4
6	0.002725	42.4	154	4.75
7	0.002433	37.8	137	4.24
8	0.00218	33.7	122.6	3.8
9	0.001951	30	109	3.4
10	0.001721	26.7	97.1	3.0
11	0.001549	23.8	86.6	2.7

## **2.2. Current Procedures**

The Open Skies Media Processing Facility, OSMPF, operated by the US Air Force National Air Intelligence Center (NAIC) at WPAFB, has among its many duties the task of data management for data taken from the US Open Skies aircraft and each of its sensors. To certify a single sensor in a particular configuration, they compile the PI recommended minimum resolvable bar widths, referred to as  $L_2$ , from several aerial passes over the ground-based calibration targets and calculate the minimum height at which an OS aircraft can fly with that sensor. They also work with other country's OS offices. This effort results in many redundant tasks, hundreds of rolls of film, and megabytes of data to manipulate and store.

### **2.2.1. Calibration Target Data Collection and Analysis**

Regardless of the calibration target configuration, the OS aircraft image acquisition system to be tested flies over the target, its optical systems record the target, the resulting images are processed, and the actual acetate film negatives are given to the PI for evaluation

on a light table under a microscope. The PI then determines which sets of bars are the smallest resolvable in each flight direction. This minimum bar width information along with the exposure modulation of the brightness panels is used to determine the minimum altitude the particular aircraft can fly for its image gathering mission discussed in later sections. Determination of the smallest bar groups and flight altitude is done by vote among the PI. The smallest bar width belongs to the bar group for which 80 percent of the PI involved voted to have the smallest resolved bar width. The value of  $L_2$  in the  $H_{min}$  equation is assigned the width meeting this *80 percent rule* criterion.

The treaty does not require a single standard configuration for a calibration target, but size and reflectance restrictions do exist. These specifications are discussed in section 1.2.1. According to the treaty, these targets will all consist of pairs of *light-dark-light* tri-bars, also referred to as *bar triads*, or *light-dark* bi-bars as discussed earlier and shown in Figure 6. The pair of bar triads or the bi-bars will be referred to as a bar group. The methods in this thesis only were tested on bar triad type targets and would require software updates to be used on other targets. With the proper digitization, there is no intrinsic reason the recording system must be an optical camera and film system. For example, the method developed in this thesis is based on the geometry of the bar target and adapts to the statistical nature of each target as will be discussed in Chapter 3. The sets of three light bars shown in Figure 6 actually comprise a *pair* of bar triads as the treaty specifications are stated. The two orientations of the bar triads record spatial frequency in directions *along* or *in* (parallel to) the aircraft line of flight and *across* (perpendicular to) the aircraft line of flight.

The data analyzed in this thesis is based on a target whose bar triad aspect ratio remains a constant of 5:1 (length to width). Figure 1 depicts an aerial photo of the actual target used, which is one of the USA's OS calibration targets, and is located on Wright-Patterson Air Force Base, in Ohio. In addition to the bar groups, the targets also include brightness panels of much larger dimension than even the largest bar triad, and have the same reflectance properties as the bars and will be discussed in detail later.

The participating PI view an image frame through a microscope on a light table. Both dark bars from each triad must be visible to deem a set of bars *resolved*. The decision process to select the accepted smallest bar set for a given pass leads to a collation of the chosen bar groups from each PI and then the choice is made based on the smallest set of bars on which at least 80 percent of the PI agree. Each PI votes on their preferred bar group set and the corresponding GRD. The smallest GRD with 80 percent of the total votes determines the final choice of resolved length. This *80 Percent Rule* generally yields reasonable results for  $H_{min}$ , but is not an analytical measure of optical system resolution and hence it is subjective.

The minimum altitude an aircraft can fly with a given optical system,  $H_{min}$ , is found with two pieces of information from the recorded ground-based target: 1) the smallest set of bar triads that can be visually separated, and 2) the exposure contrast between the light and dark brightness panels found on the target. The brightness panels of the target have the same reflectance as the bright and dark portions of the bar triads, and their average modulation is currently measured using a single machine which combines a Zeiss microdensitometer with a PDS (the machine is referred to as the *Micro-D*) to digitize the brightness panels<sup>12</sup>. Two

---

<sup>12</sup> A KODAK 5057 high resolution photographic scanner is currently being tested as an alternative to the PDS, but as of Jun '96, the PDS was still the primary source of brightness panel illuminance measurement.

calibration steps are required to go from the output of the PDS, or any scanner, to find the measurements in the terms needed to process the data.

As the first step, the PDS is used to digitize 21-Step wedges on processed film exposed by National Bureau of Standards (NBS) calibrated light sources to calibrate the PDS output values of analog-to-digital units (ADU) to optical density (OD). The PDS is operated in a mode such that the output ADU are linearly proportional to OD. A curve can then be interpolated resulting in a direct linear conversion of ADU to OD for the PDS. To confirm the film was exposed in valid exposure ranges and to do the altitude calculation, the next calibration step will convert the data into units of the light exposure incident on the film—so one more step is required. OSMPF has the capability to generate calibrated strips of film on which the exposure, really the logarithm of the exposure ( $\log E$ ) is known to high accuracy. These strips, called 21-step exposure wedges, are created on the beginning (head) and end (tail) of each roll of film processed.

The wedges are then scanned with the PDS, the head and tail results are averaged, and the resulting ADU versus  $\log E$  curve is transformed to a sigmoid shaped OD to  $\log E$ . The resulting curve is called the Hurter-Driffield (H-D) Curve, or the  $D \log E$  curve. A sample curve generated for the NBS and OSMPF wedges is shown below in Figure 8.

Hurter-Driffield Curve for Kodak 3412 Film Emulsion

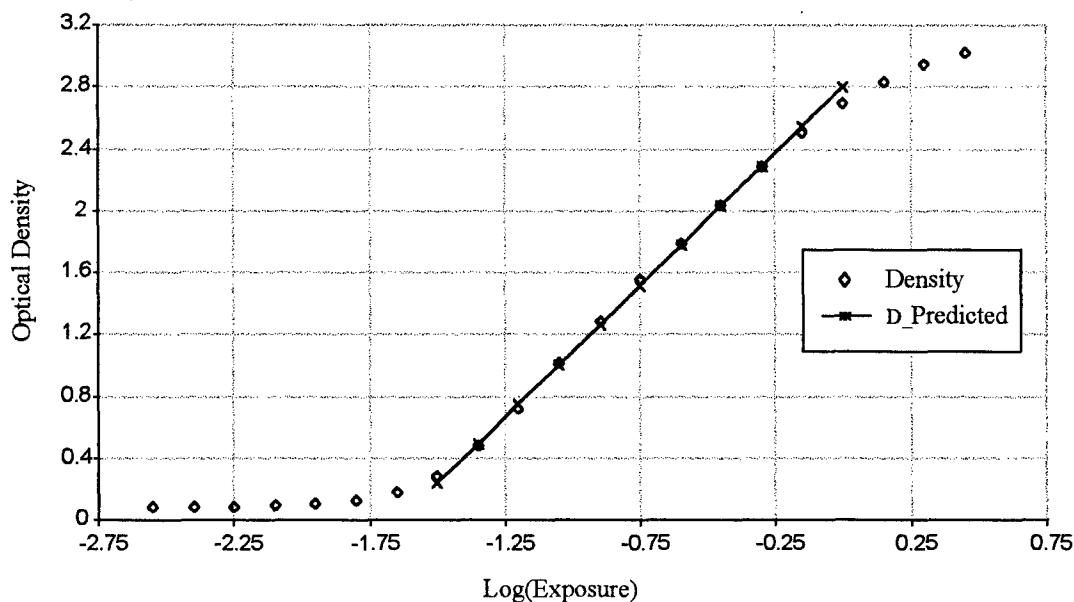


Figure 8, Hurter-Driffield Curve For KODAK 3034 Film, with fitted line to the linear region

The digitized portions of the brightness panels are then transformed into units of  $\log E$  and those points are plotted on the H-D curve to make sure they fall in the linear region of the curve. This linear region is demarcated by the least squares fit straight line in Figure 8 using "x" symbols to mark the predicted optical density. Currently, the points used to determine this linear fit are determined by the analyst.

As was mentioned in Chapter One, a different digitization method was used. Specifically, the data was scanned with a KODAK 5057 photographic film scanner. At the time of the writing of this document, the OST participants had not accepted the validity of the use of the KODAK 5057 scanner in the calibration mission procedures. The only difference in the two methods is the type of scanner used. The critical difference between the two instruments is that the PDS is an NBS accredited instrument accepted widely in the photometric community, and its linearity is calibrated with NBS instruments.

The image data is then used to calculate  $H_{min}$  with a Microsoft Excel<sup>®</sup> and VisualBASIC<sup>®</sup> macro/program called *K2.xls*. *K2.xls*, is used with the PI recommended minimum bar width, labeled  $L_2$ , in the  $H_{min}$  formula [OST, Decision 14]:

$$H_{min} = \frac{1}{n} \sum_{i=1}^n H_i \left[ \frac{30}{L_2} \right] \left[ \frac{0.40}{K_2} \right]^{0.45} \quad (2.5)$$

$$C = 10^{\Delta \log E} \quad (2.6)$$

$$K_2 = \frac{C-1}{C+1} \quad (2.7)$$

where,

$n$ , number of passes made over the target,

$H_i$ , the height above ground level at which the data was collected, in meters

$L_2$ , the ground separation of two adjacent bars in the minimum resolvable bar triad, in centimeters

$E$ , the exposure represented by the average density in emulsion over a brightness panel,

$\Delta \log E$ , the difference of the  $\log E$  value between the light and dark brightness panels.

$C$ , is the measurement of panel *contrast, units of exposure*.

The expression for  $K_2$  in Equation (2.7) is the OST label for the physical value of modulation,  $M$ , expressed previously in Equation (2.4). Hence, the modulation,  $M$ , will be referred to as  $K_2$ .

### **2.2.2. Bar Targets Intrinsicly Add Uncertainty to GRD Calculation**

The OSMPF approach to determining  $L_2$  is based on historically accepted methods for judging the quality of an aerial photographic camera system in the lab, under collimated, fully

illuminated conditions [Slater, pg 241]. Slater also notes that the original technique specified the use of a transparent slide of the bar target in transmission from the focal plane, not from reflectance as in the case of the ground based targets. He warns that even in these controlled conditions,

*The subjective and statistical nature of resolving power should not be overlooked, nor should the fact that the  $\sqrt[3]{2}$  increments in the size of the standard elements in a target correspond to a change of 12 percent in the spatial frequency. The reader may often be uncertain over a range of two or three target elements.*

Hence using this criterion on data collected under uncontrolled yield GRD determinations which are larger than the GRD which more accurately describes what level of detail an imaging system can record. Human factors such as fatigue or political agendas could further complicate this issue.

The selection of a bar group with width larger than the true system GRD underestimates the system's true performance and will produce an  $H_{min}$  altitude of at least 12 percent lower than it should be. This is due to the discrete  $\sqrt[3]{2}$  bar width progression multiplier<sup>13</sup> applied to the bar widths in the construction of OS bar targets and also due to the fact that  $H_{min}$  is linear in  $L_2$ . Once an automated digital technique is introduced as an acceptable data process, errors introduced in the digitization process will further complicate GRD determination by human observers. Degradation in the digitized image is called quantization error<sup>14</sup>, and the image will be further degraded due to noise introduced via the electronics required for digitization.

---

<sup>13</sup> (Note:  $\sqrt[3]{2} = 1.12246$ )

<sup>14</sup> Quantization error or noise is a result of taking a continuous signal and breaking it into discrete blocks of values. It is a form of aliasing which is using data taken with a sample size larger than the smallest detail in the original.

A key issue for both human and digital methods of GRD estimation is the determination of where the light and dark bars are separated. The OSMPF defines the two adjacent light and dark bars to be separated if there exists notable light and dark regions along the entire length two bars. Unfortunately, using a digital method this criteria is not adequate due to the *blurring* and noise corruption of boundaries. This blurring systemically occurs from the finite lens diameter and noise is introduced by the electronics and by the physics of the light detection process [Roggemann & Welsh, 1996]. However, in averaging within the same image, much of the random noise is attenuated leaving a picture of the bar group cross section which is easier to interpret. This averaging can be along the length of the bar group of a single image, as done in ADiM, or across multiple images of the target at the same altitude and within the same region of airspace. So, averaging can also increase the details available within an actual data run if enough frames in the same airspace are taken.

The next nine image are presented to demonstrate some of the imaging process affects on the bar group images as bar widths decrease. This presentation also alludes to the subject matter of the next chapter, which discusses the development of ADiM and the idiosyncrasies in the data which make ADiM challenging. The following bar group data are from OS Calibration Mission 095-MOC-007 (Pass 1, Frame 16). All of the following data was digitized from this mission taken over the WPAFB target at approximately 1700 meters above the target. The following figures depict three different bar groups in three different views. The presentation of these three sets of figures further demonstrates the ways in which a human observer could be convinced that information was not available within an image, when in fact, the important detail was in the photograph buried beneath the image noise.

The first figure in each set will be the gray scale image representation. The second figure displays the image as a surface plot so the smoothness of the edges of each bar group can be seen, and the third figure of each set contains two representations of the lateral mean cross section of each bar group and a 10<sup>th</sup> order polynomial fit of that cross sectional plot. Figure 9 defines the average of the lateral mean cross section of a bar group image. This is another way to represent digital imagery data and takes advantage of the statistical error reduction attributed to arithmetic averaging.

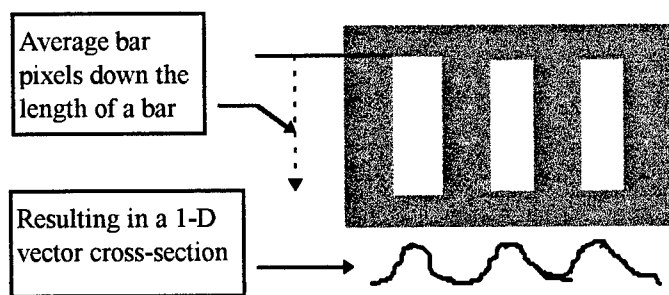
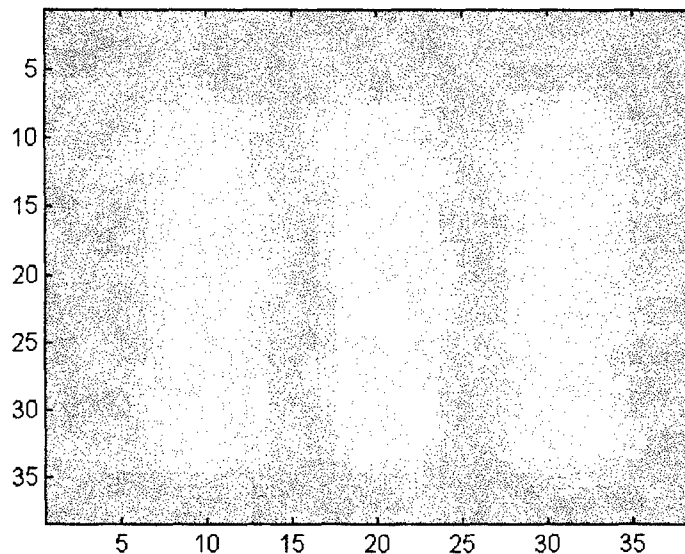


*Figure 9, Demonstration of Averaging Direction to Calculate the Lateral Mean Cross-Section of a Bar Group Image*

The imaging effects on the bar groups are caused by the optical system MTF and losses due to noise or other random effects. A few of these properties can be clearly observed in the following figures. Among these important properties are: the blurring of the bar edges, the diminishing peak bar group amplitude, and the assimilation of the dark bars by the spread of the light bars. These are the important effects of the system MTF on the images in providing digital tools to the OSMPF. Figures 10, 11, and 12 highlight the details of bar

group #2 (barwidth=67.35 cm-ground<sup>15</sup>) from this data set. The succeeding figures present bar groups 9 and 10.

Figure 10 is a gray scale image of bar group #2 and shows the light and dark bars with clearly defined edges, although those edges are not sharp. Each pixel represents a 6  $\mu\text{m}$  sample from the digitized film frame. The spread of the light bars already encompass much of the dark bar area notable in this image. Bar group #2 is the second largest bar group and the MTF is already making the task of edge detection difficult. Consequently, difficulty in edge detection translates into uncertainty in  $L_2$  determination.



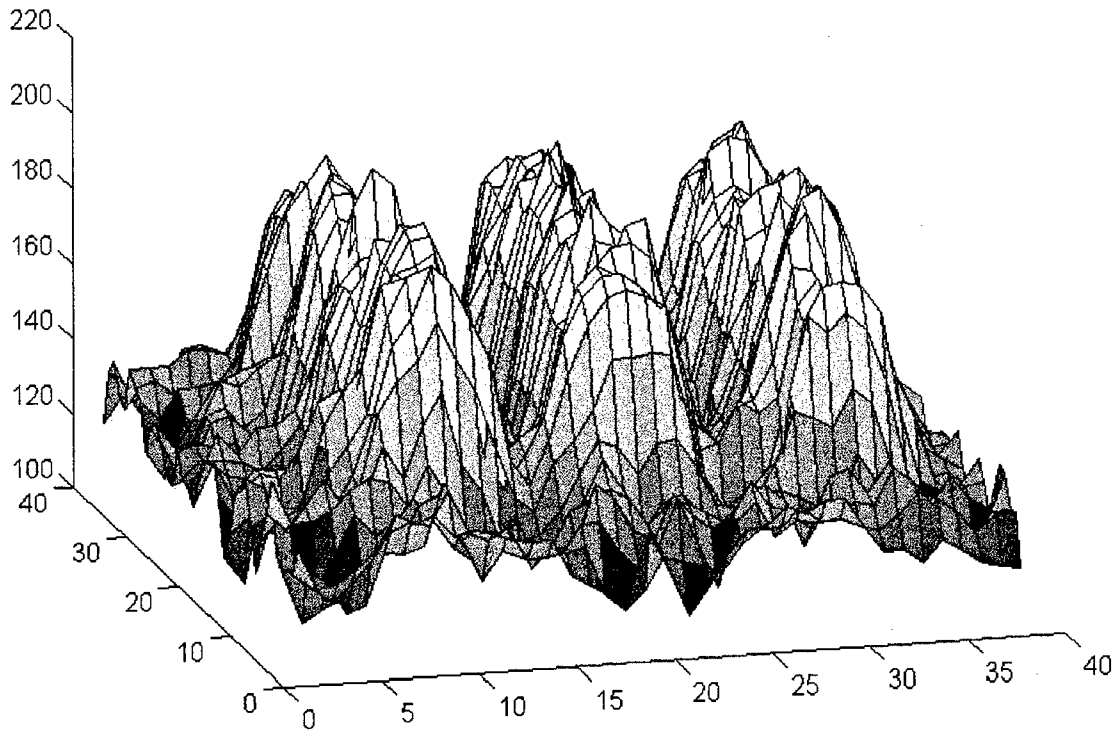
*Figure 10, Grayscale Image Bar Group #2*

Figure 11 is a surface plot of bar group #2 and confirms any suspicions that this bar group image is indeed that of a pair of resolved bar triads. The distinction between the light and the dark bars has been eroded, although it does still exist. The strength of the light bar signal is demonstrated for bar group #2. This surface plot of bar group #2 also shows the noise apparent in the data. The cause of the jagged peaks is not explained by this image, but

---

<sup>15</sup> Barwidth as measured on the ground target.

causes could stem from the atmospheric scintillation, imperfections in the paint surface across the bars, or any of the other systems involved in making this image.



*Figure 11, Surface Plot of Bar Group #2*

The next representation of bar group #2, in Figure 12, consists of two plots, a solid line connecting data points composing the average lateral cross-section of bar group #2 and the dashed line tracing the 10<sup>th</sup> order polynomial fit [MatLab<sup>®</sup> Reference Manual] found for these data points. Again, two distinct pair of bar triads are apparent. The asterisks present on the central peak represent the centroid of the cross section and the two points adjacent to it. These markers were used in ADiM to initiate a peak and valley identification search which will be discussed in Chapter 3.

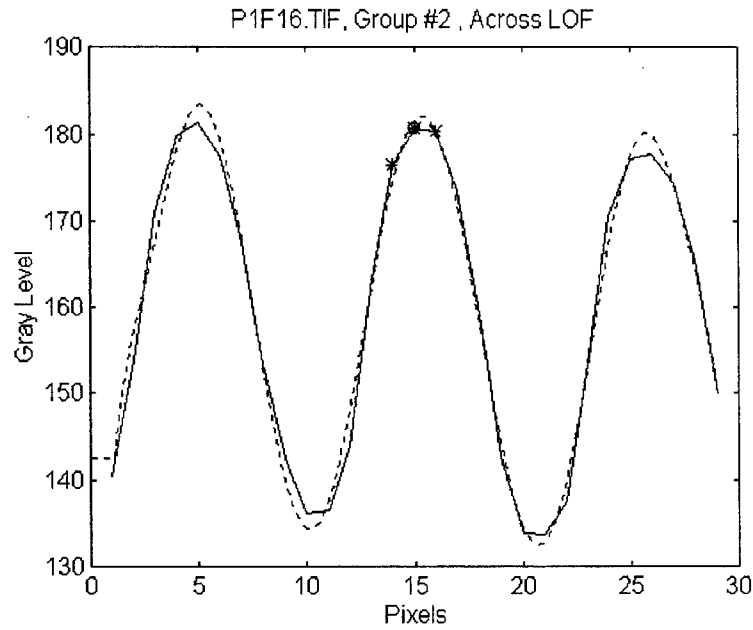


*Figure 12, Mean Lateral Cross-Section Plot of Bar Group #2 and 10<sup>th</sup> Order Polynomial Fit (Solid Line: Bar Group Data ; Dashed Line: 10<sup>th</sup> Order Polynomial Fit; Markers: the centroid and adjacent points)*

In the digitized image and surface plot of bar group #9 (Barwidth=30.00 cm-ground) in Figures 13 and 14, one cannot have complete confidence in distinguishing each edge along any bar edge in the gray scale image. The noise masks the information in the data.

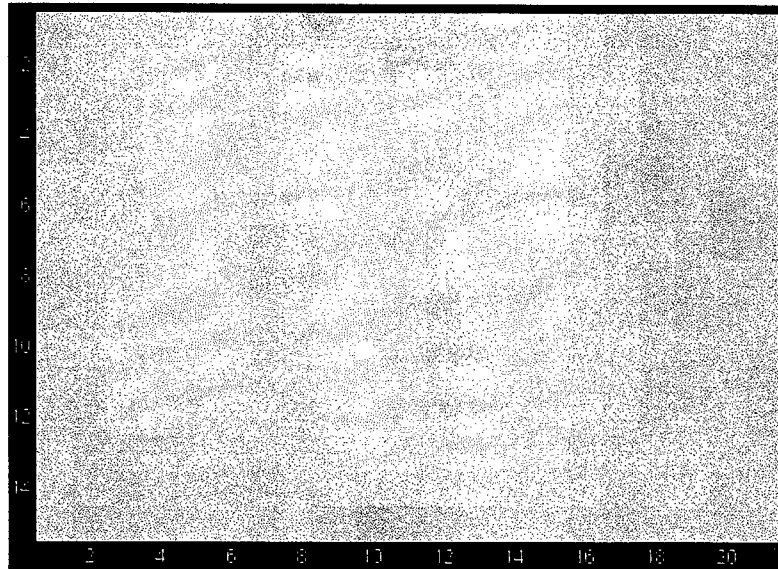


*Figure 13, Grayscale Image Bar Group #9*

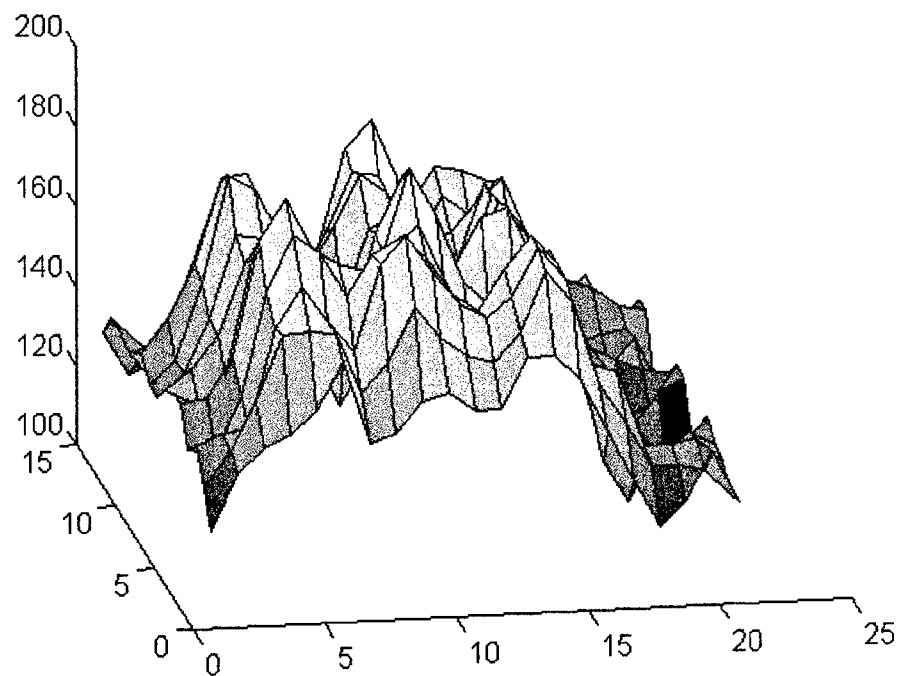


*Figure 14, Surface Plot of Bar Group #9*

However, by averaging along the rows, as shown in its mean lateral cross section in Figure 15; the light and dark bars are clearly distinguished and the polynomial fit further clarifies the distinction between the two bar triads. In the preceding Figure 11, bar group #2,

the dark bar amplitude values appear to be near the amplitude values of the background surrounding the bar group surface. But for bar group #9, the dark bar amplitudes are significantly higher than the peak amplitudes from the light bars. As the bar group widths decrease in the image, the light bars continue to spread until the dark bar amplitudes become difficult to discern. In Figure 15, the mean lateral cross section of bar group #9, it is evident that the dark bar amplitudes are significantly above the background amplitude level. Figure 9 demonstrates how this cross section is generated. This is an effect of the imaging system MTF on the reflected bar image and will be discussed in detail in the next section.

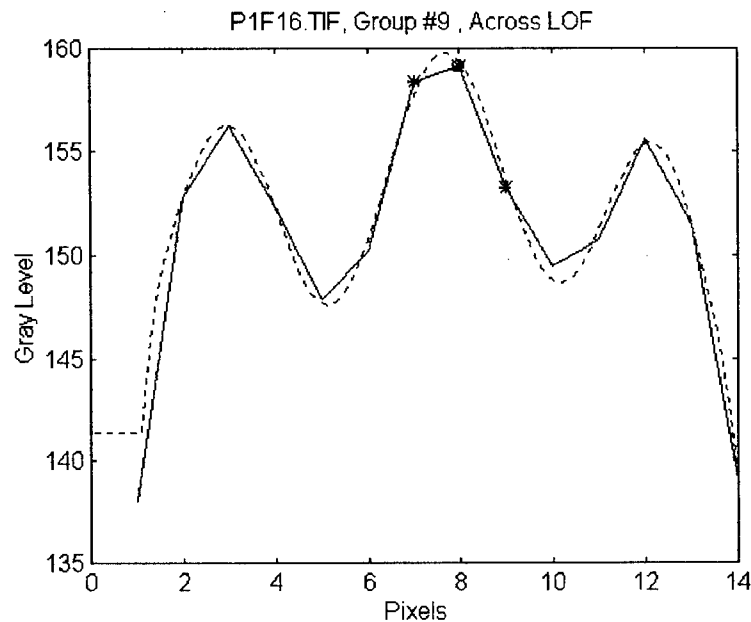


*Figure 15, Mean Lateral Cross-Section Plot of Bar Group #9 and 10<sup>th</sup> Order Polynomial Fit (Solid Line: Bar Group Data ; Dashed Line: 10<sup>th</sup> Order Polynomial Fit; Markers: the centroid and adjacent points)*

For the next smaller bar group, bar group # 10 (barwidth=26 cm-ground), no definitive bar edges can be detected in the gray scale image shown in Figure 15, and again, no edges can be detected in the surface plot in Figure 17.

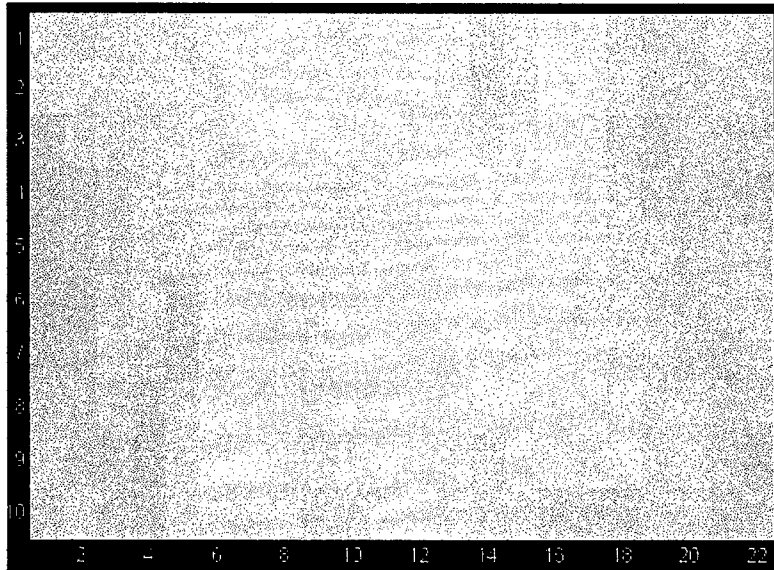


*Figure 16, Grayscale Image Bar Group #10*

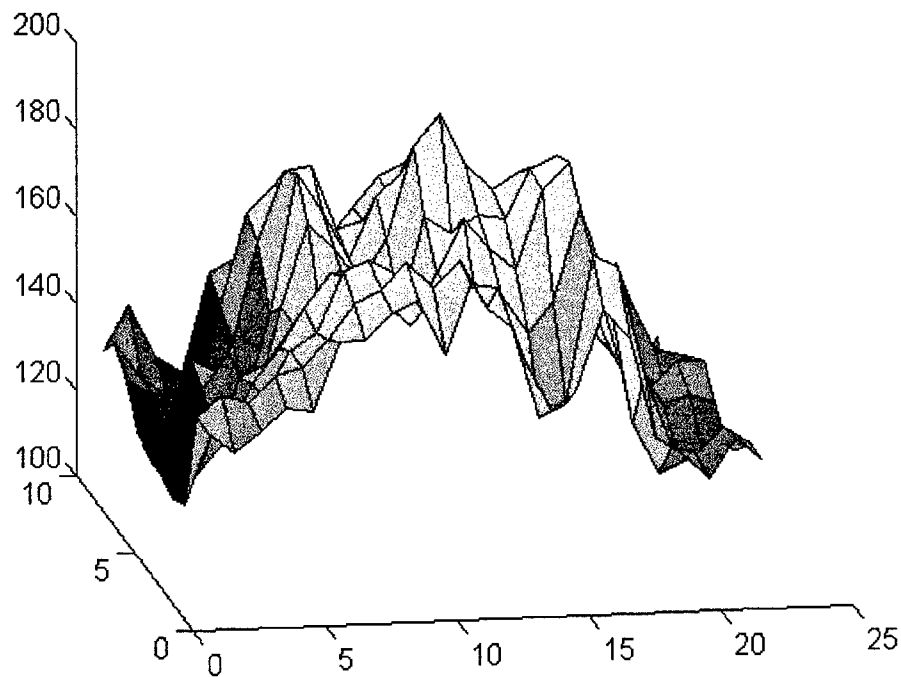


*Figure 17, Surface Plot of Bar Group #10*

As seen in the images for bar group #9, with the use of the noise reduction properties from averaging, clear separations between light and dark bars are easily distinguishable and

are demonstrated in Figure 18, despite the fact that this information was not available in either of the previous two plots for bar group #10.

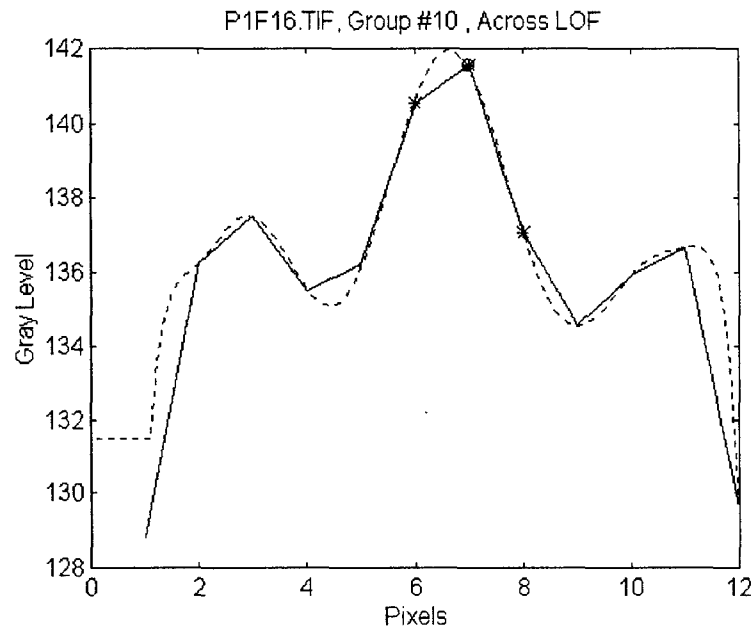
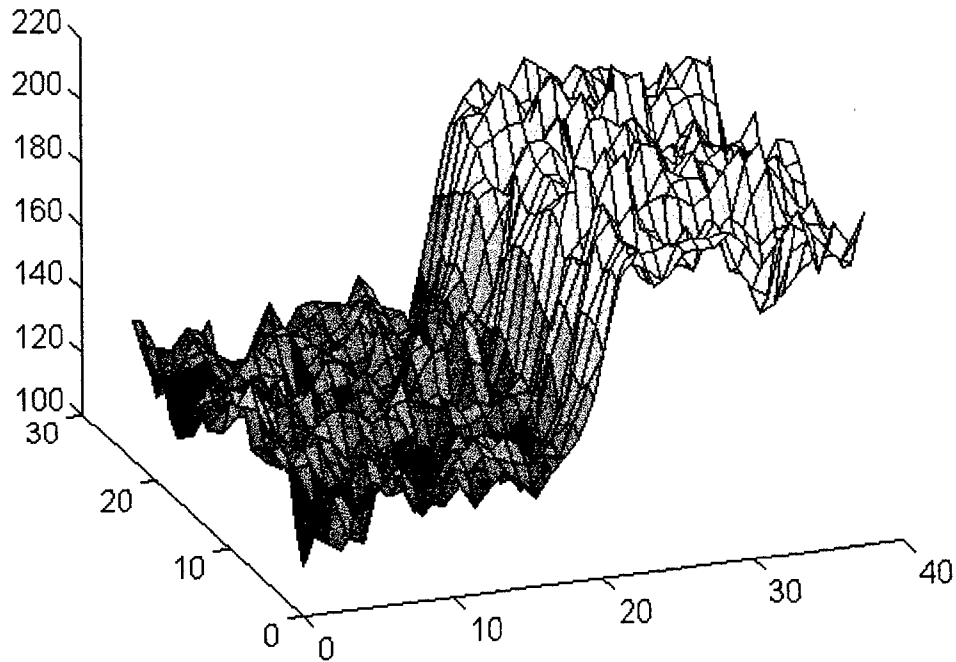


Figure 18, Mean Lateral Cross-Section Plot of Bar Group #10 & 10<sup>th</sup> Order Polynomial Fit (Solid Line: Bar Group Data ; Dashed Line: 10<sup>th</sup> Order Polynomial Fit Markers: the centroid and adjacent points)

### 2.2.3. Optics distort GRD measurement, and surface roughness distorts target modulation measurement

Not only is the determination of the  $L_2$  measurement of the GRD estimation adversely affected by measurement noise and target inconsistencies, the target modulation value,  $K_2$ , measurement is distorted as well. OSMPF computes the illuminance of the light and dark brightness panels by averaging a 10 pixel by 10 pixel region manually extracted from each panel. One hundred samples are produced and the average pixel value from each panel is converted to  $E_{max}$  and  $E_{min}$  and used to compute  $K_2$ .

Figure 19 shows a 30 pixel by 60 pixel subsection sample of the light and dark brightness panels and shows the inconsistency of the reflected surface and suggests the need for a larger sample set to calculate the actual modulation of a target.



*Figure 19, Surface Plot of Brightness Panels for OS Mission 095-MOC-007 to Emphasize Surface Inconsistencies*

Its light panel values range from 230 ADU to 160 ADU and its dark panel values range from 100 ADU to 150 ADU. The following histogram depicts the actual spread of the data values, for the entire brightness panel region.

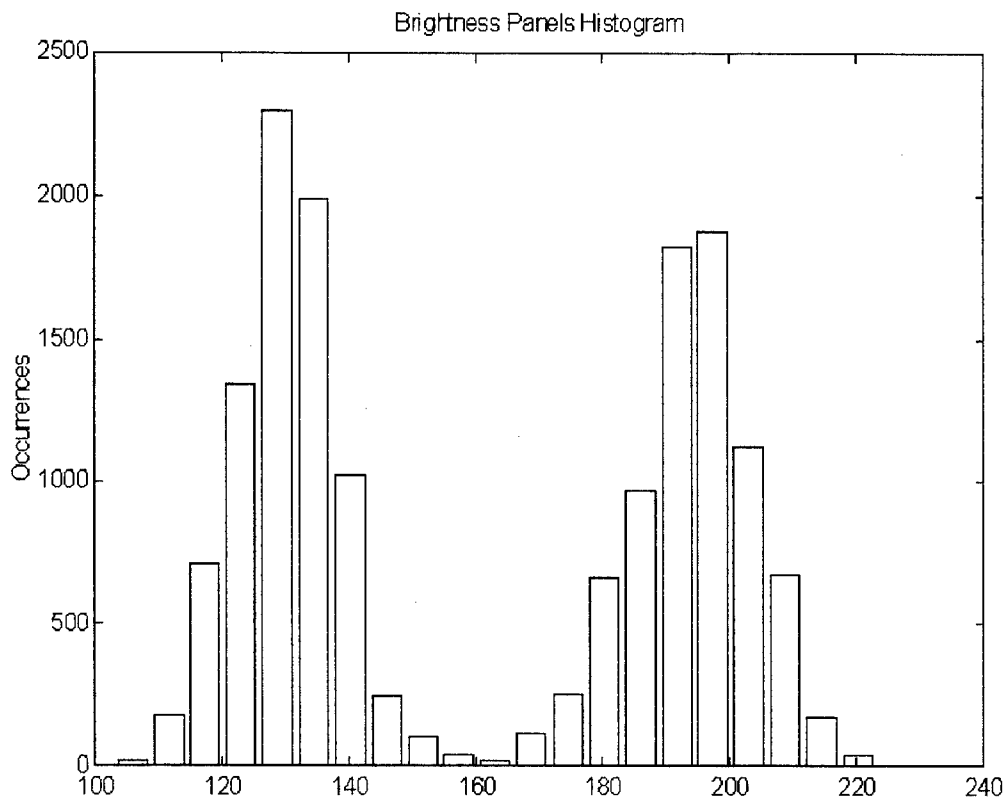


Figure 20, Histogram of Brightness Panel to Show Value Variance

Figures 19 and 20 suggest the need for a larger sample size than 10 pixels by 10 pixels, currently in use by the OSMPPF. In developing the ADiM software, fluctuations in the  $K_2$  value as much as 25 percent were noted by simply changing the size and location of the sample set across the brightness panels.

### 2.3. Chapter Summary

In order to construct the OST and gain the consensus of each of the desired participants, limits were placed on the smallest details recordable by airborne optical systems. These limits defined acceptable sizes,  $L_2$ , and modulations,  $K_2$ , of details within an image and were used to calculate the minimum height an aircraft could fly to collect imagery under the hospices of the OST. Effectively, the OST participants defined quantities whose combination

was used to determine a measure of image quality. Image quality defines the value of the information contained within an image.

Image quality definitions are inherently subjective due to the complicated interactions between human perception, image transmission, and image detection. The OST image quality standard set limits on the smallest detail recordable and the largest range in exposure levels observable in a image of a bar target. Unfortunately, the smallest width observable within an image of the original ground target is a function of both sensitivity and resolution. Additionally, the modulation, or exposure range, within an image is also a function of both the sensitivity and resolution of the entire optical system.

For a real image, the sensitivity factor is a limitation if the irradiance level of the reflected light from the target transmitted through the optical path of the airborne system is not strong enough or the film is not sensitive enough to react to and record the exposure from the incident image. The resolution factor usually describes the attenuation rate of an optical system on incident image spatial frequency content. If the signal strength of the smallest spatial frequencies transmitted from the ground object and passing through the airborne optical system to the film is not strong enough to be detected by the film, no record of those details will be observable in the final image. In other words, if the MTF of the entire optical system has attenuated spatial frequencies available to the system, but reduced their exposure below the sensitivity of the film, the details described by those spatial frequencies will not be observable in the final image.

Therefore, the two parameters used to compute  $H_{min}$  are not independent. In fact, with a thorough characterization of the optical system and atmospheric measurements for each

image, the MTF for the total system could be reproduced and removed from the digitized image. This new image reproduces the ground object almost perfectly. This could cause future problems for countries whose technology does not allow them the ability to make these post-processing corrections and would deny them details that more technologically advanced countries could record from them.

The correlated OST criteria, the discontinuous construction of the bar targets, and the coarseness of the digitization of the bar target images lead to a measure of image quality which is difficult to automate. The inconsistent surfaces of the bar target and the unknown background noise level make the development of a fully automated bar group finder very difficult, because the image on the film frame is very small and the orientation of the bar target is not consistent from frame to frame. The inability to find edges around the smaller bars due to noise, the physical rounding effects of the imaging process, and the insufficient numbers of samples across bar widths around 30 cm-ground and smaller makes the implementation of the OST bar resolution standard impossible to implement.

Even with a perfectly automated method, with the current technique of data acquisition and digitization, limitations on the confidence in the measurement of the GRD and modulation are unavoidable. The fact that the bar targets are constructed with decreasing discrete bar widths reduces confidence in the GRD measurement, because the actual value of the GRD will almost always exist between two bar groups. The analyst is only able to say the system GRD is no larger than a given bar group width, but can never bound the GRD result with tolerances smaller than the difference between two sets of bar groups.

The digital method developed in this thesis uses a set of criteria which is based on the spirit of the OST standards of image quality, but does not replicate their technique.

### III. The Adaptive Digital Method (ADiM)

As discussed previously, the optical system performance criteria used by the OS regime depends on two components: the target illuminance modulation,  $K_2$ , and the target GRD,  $L_2$ . These parameters determine the minimum altitude,  $H_{min}$ , at which an Open Skies aircraft can fly.  $K_2$  is measured directly from the brightness panels on the target in all calibration methods. Any value of  $K_2$  greater than 0.4 is penalized by increasing  $H_{min}$ , this can be observed in the  $K_2$  definition in the previous chapter.  $L_2$  is measured subjectively according to criteria concerning the geometry of the bar triads, and the OS regime agreed value for  $L_2$  is 30 cm [OST, Decision 14]. Chapter 2 contains the discussion of the  $H_{min}$  component calculation details.

This tool, the Adaptive Digital Method (ADiM), allows the user to extract the target image features required to estimate signal strength, contrast, and location against the target background environment. The accuracy of these estimates will determine the validity of the calculated values for  $L_2$  and  $K_2$ . Because these limits are placed on the values for  $K_2$  and  $L_2$  to accomplish the goals of the OST by its participants, the inferred quantity,  $H_{min}$ , represents a value judgment on the information content of the image. Hence,  $H_{min}$  is a measure of image quality. Holst has taken great pains to emphasize the subjective nature of image quality [Holst, pg 239]. In fact, with calibration targets such as the WPAFB target, all subjectivity in the OS certification process cannot be removed [Slater, pg 246]. The intent of ADiM is to offer the OS another tool with which to manage large quantities of data and increase the certainty held for the  $H_{min}$  computation.

### 3.1. Technique Overview

ADiM applies standard digital processing techniques to digitized files created from photographic negatives to determine the orientation and amplitude modulation of individual bar groups. First and second order difference functions are used in ADiM for gradient search techniques and edge detection. The flow chart in Figure 21 describes the steps in the ADiM process. Bar target analysis with ADiM is iterative and requires human interaction. No consideration is made in the current version of ADiM for rotational transformations, so the user must ensure that the rows and columns of the digital image lay parallel or perpendicular to the orientations of the bar groups of interest.

ADiM operation is simple and can be summarized in four easy steps: setup, select, analyze, and repeat as needed. The user selects a bar group, in either orientation. If the software can determine the orientation of the selection, and guess the bar group number, with its corresponding width, of the selection within one or two bar widths, the bar group is considered resolved. ADiM is then inactive until the next bar group is selected. This routine is followed until the software can no longer recognize the orientation of the bar group. In development, it was observed that if the orientation was not detected correctly, then the bar width was also reported incorrectly.

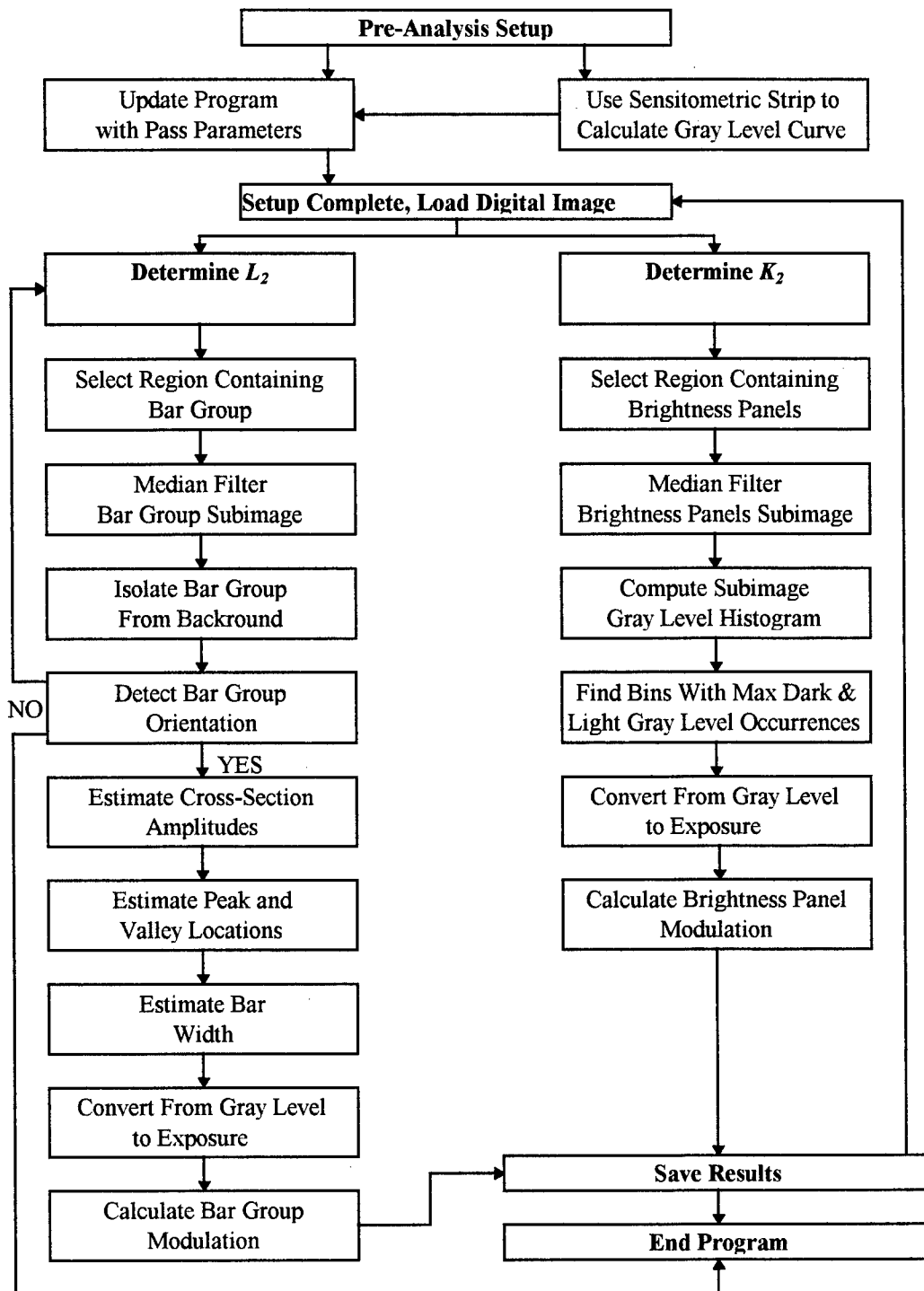


Figure 21, Flowchart of Adaptive Digital Method

### 3.1.1. Step by Step ADiM

A data run begins in ADiM the same way it begins in the OSMPF technique. Both ADiM and the OSMPF digitize the 21-Step Exposure Wedges, also known as sensitometric strips, and store the digitizer output, in ADU values, to a computer file. The output files of the sensitometric strip data are regressed against their known Exposure values, using a simple linear model. From the results of this computation, the conversion factors from ADU values to units of Exposure are estimated, and used without error analysis. A more detailed description of this calibration and the use of photographic film is discussed later in this chapter. The conversion equation coefficients are recorded and this completes the block diagram step, *Use Sensitometric Strip to Calibrate Gray Level Curve*. ADiM then requires the digitization of the bar target region under analysis. The region containing the bar target is scanned with the smallest sample size available on the digitizer.

Before launching the ADiM software, the user must update the *MatLab*<sup>®</sup> routines with the results of the gray level to logarithm of exposure calibration, the flight altitude, the effective focal length of the optical system, and the sampling size at which the data was digitized. The user must also enter the name used to identify the data run. This completes the *Update Program with Pass Parameters* step of the block diagram.

ADiM assumes the target images are available as digitized image files in tagged image file format (TIFF). In the current version of the software, these parameters must be entered directly into the *MatLab*<sup>®</sup> code. In future versions, this information should be placed directly in the header of the TIFF image as part of the data storage process. This procedure completes the *Setup Complete, Load Digital Image* stage of the ADiM block diagram.

ADiM does not model the physics or optics of the image acquisition system nor does it take into account the effects of image transmission through the atmosphere. This technical data is not readily available and would require alterations in the current OST data acquisition technique. For that reason, the solution presented here uses only knowledge of the target geometry and the stochastic properties of the digitized image data, which is readily available from the OSMPF.

The user now starts *MatLab*<sup>®</sup> and then launches the ADiM macros. The ensuing description follows the *Determine  $L_2$*  branch of the block diagram. ADiM enables the user to determine a target GRD,  $L_2$ , in each of the two perpendicular bar group orientations. The GRD is defined as the width of the smallest bar group for which the software can identify the bar group orientation<sup>16</sup> and calculate a valid estimate of the bar group width and geometry. After the ADiM routines have been launched, two dialog boxes appear enabling the use to use a previous file or select a new one. If a new file is being examined, a standard MS Windows dialog box appears to enable the user to browse the computer file system to find the correct file. The user selects the filename of the bar target to be analyzed. If the file selected is new or was previously analyzed, the user sees the screen shown in Figure 22.

---

<sup>16</sup> This criterion is the same as that used by Professor Beloglazov in his 1993 discussion of applying least squares indicators to the OS problem. The methods to determine the orientation and bar width in this thesis are unique to the best knowledge of the author [Beloglazov, 1993].

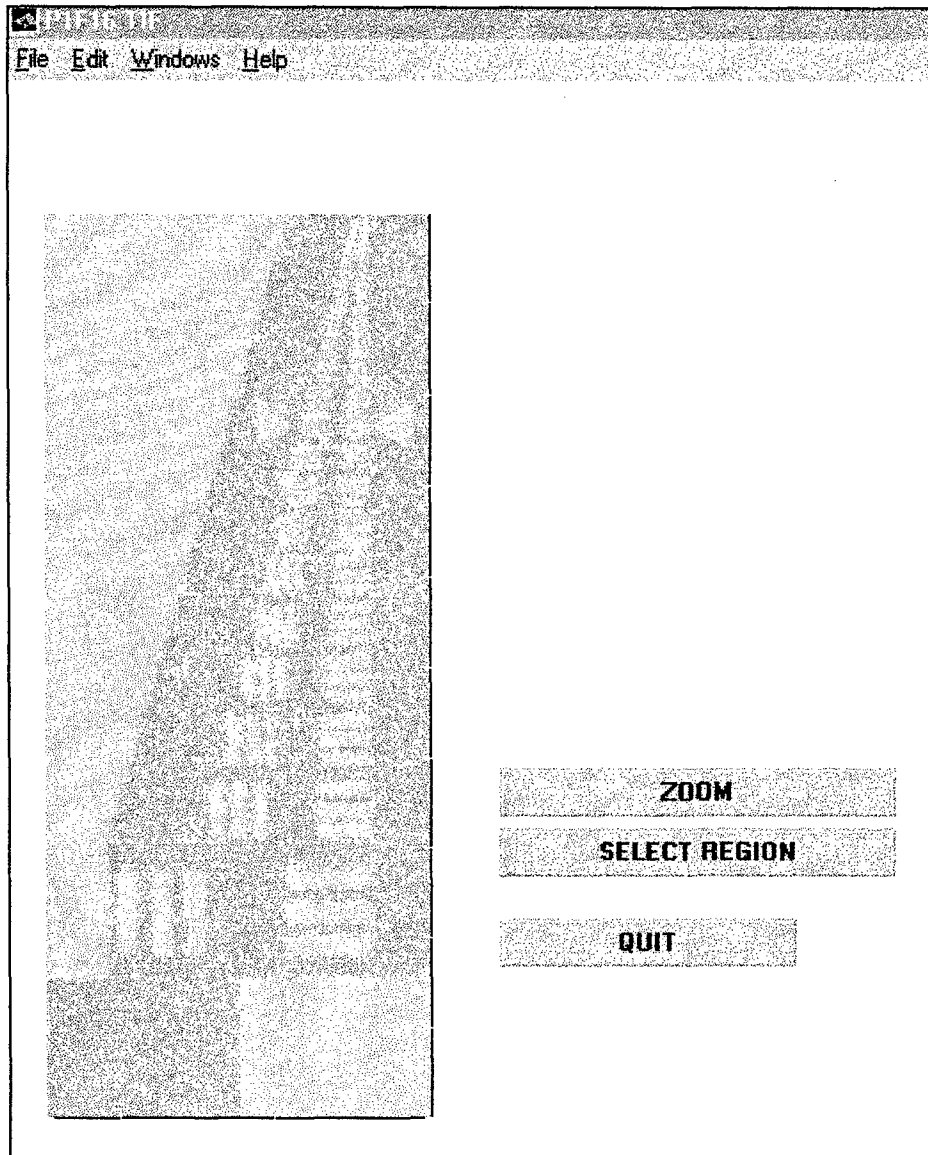


*Figure 22, Opening Screen to ADiM*

In the opening screen there are five important features. The most prominent feature is the image of the entire bar target along the left side of the window. The remaining features consist of the upper menu bar across the top of the window and the three control buttons on the lower left half of the window. The upper menu bar allows the user to exit and print the current window. The use of the control button icon is necessary to engage the processing

algorithms of ADiM. The *ZOOM* button allows the user to enlarge regions of the bar target image using point and drag mouse actions to make region selection easier. After the area of interest is in view, the *ZOOM* button is pressed again to disable the zoom feature (the button toggles the zoom function on and off). The *SELECT REGION* button allows the user to select the region of interest (ROI) containing the bar group and to launch the ADiM routines for analysis. For a typical data iteration, the user would use the *ZOOM* control to enlarge the area containing the ROI, toggle off the zoom function, and press the *SELECT REGION* control to select the ROI.

ADiM then captures the selected region and presents it to the user for verification shown in Figure 23. A pop-up window appears and queries the user as to the status of the presented selection. If the image is the intended ROI, the user selects *OK*, the processing begins, and the results are shown. If the image is not the intended ROI, he/she rejects the query, and the selection process starts again. This is an iterative process, especially for the smaller bar groups.

#### **3.1.1.1. Finding $L_2$**

The process to determine  $L_2$  is started by selecting the *Select Region* option and dragging a rubber-band box around the region containing the bar group or brightness panel to be analyzed. Figure 23 displays the result of the selection of bar group #1, for the 25 Aug 95 mission.

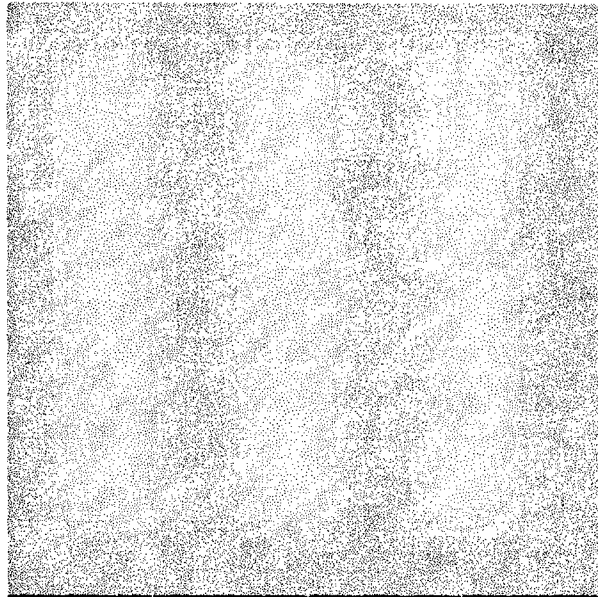


*Figure 23, Selected Bar Group #1 Using ADiM*

This ends the block diagram step, *Select Region Containing Bar Group*.

The next two steps along the block diagram denote progress toward extracting the bar group of interest from the ROI. These steps are labeled: *Median Filter Bar Group Subimage* and *Isolate Bar Group from Background*. The initial ROI is surrounded by unnecessary background data which adds uncertainty to the parameters to be estimated. It is useful to isolate the bar group pixels from those containing background data. The group perimeter, or a defined boundary around the outside of the bar group must be found to isolate the bar group from the background. Two *MatLab*<sup>®</sup> IPT functions are used to find this perimeter, *bwimg* and *perimeter*.

To find this group perimeter, a binary image is created. A binary image is an image consisting of only black and white pixels, these colors have gray level values of zero and 255, respectively. The *MatLab*<sup>®</sup> IPT *bwimg* function generates an array containing the binary image, but the user must define a threshold value for it to use. The threshold value is required

by *bwimg* to create a separate binary image from the subregion by assigning corresponding pixel gray level values in the subregion with greater than or equal value to the threshold value to one in the binary image, and those pixel values less than the threshold value to zero in the binary image. For all of the subregions analyzed in this thesis, the threshold value was set to the value of the 60<sup>th</sup> percentile of the gray level values in the subregion under analysis.

The *MatLab*<sup>®</sup> *IPT* perimeter function operates on the binary image. The perimeter function examines every pixel in the binary image and changes its value to a one or zero based on the following criteria. For every pixel in the binary image, the software examines its four nearest neighbors and when a pixel had at least two neighbors with the values of one and zero, the software function considered them to be part of the perimeter of the object.

This operation was effective, but as the bars became smaller and the bar group gray level values became closer to the background values, it was necessary to add one additional function to eliminate false detection of perimeter pixels. Another *MatLab*<sup>®</sup> *IPT* function was used. The majority filter function, called *majority*, examined every pixel in the binary image, similarly to the *perimeter* function. However, instead of looking for pairs of adjacent ones and zeros, it set each pixel value to the value of the most frequently occurring pixel among its four neighbors. This process is analogous to giving each pixel a vote, and the pixels whose vote represents the majority of the vote determines the value of the pixel under investigation. The majority filter was applied twice to the binary image.

The resulting binary image contains a mapping of the perimeter location from the bar group subregion and can be used as a template for use in the construction of a mask to separate the bar group from its background. The perimeter mask produces a result as shown

in Figure 24. Figure 24 also contains a plot of the bar group cross section which will be discussed later in this section.

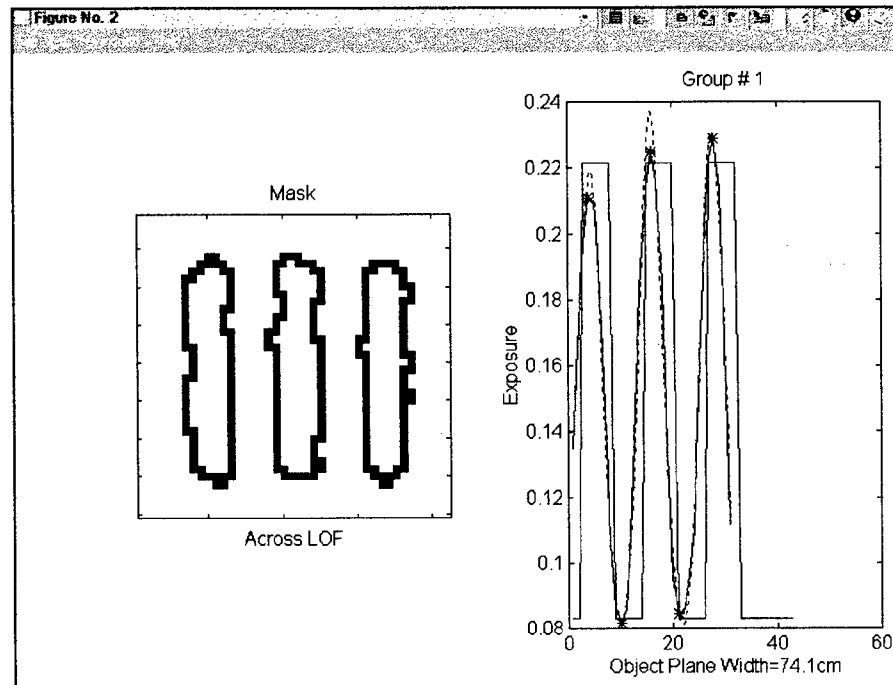


Figure 24, Mask and Identified Bar Group Cross Section

For smaller bars, the perimeter mask does not necessarily isolate all three light bars in a bar group, but the defined perimeter is still effective because the location of the bar group is still demarcated. This perimeter mask cannot be used to directly isolate the bar group pixels from the original image, however it can be used to construct the actual mask.

The actual mask is constructed directly from the binary image of the bar group perimeter. For this mask, the region inside the perimeter will have pixel values set to one and the region outside the perimeter contains pixel values set to zero. This type of mask is often called a *top-hat* filter, due to its value of zero outside the mask (or brim) and value of one inside the mask (as in the crown of the top-hat). This mask is to be used to isolate the bar

group from the rest of the selected region like a cookie cutter. It is the same size as the original bar group image, and the interior region corresponds in size and location to the region in the original image containing the bar group to be isolated.

However, a few pieces of information must be determined before the mask can be constructed. For instance, which pixels contain the top-hat crown and which contain the brim? Figure 25 demonstrates the method used to determine the inner and outer extent of the bar group isolating mask. This figure depicts the binary image containing the information on the location of the bar group perimeter, which is the top-hat crown location, within the selected subimage. A horizontal vector containing the nonzero pixel counts down each column of the binary image is created. This process is followed by the formation of a vertical vector containing all the nonzero pixel counts across each row of the binary image. These vectors mark the *x-range* and *y-range extents* of the binary mask perimeter. A search routine is used to find the *x-range* extent and *y-range* extent. The vector element locations are numbered from one to  $N$ , where  $N$  is the length of the vector. Within each row and column vector, it finds the vector element locations containing nonzero values<sup>17</sup>. The highest and lowest vector location values are determined with minimum value and maximum value searches, and these addresses are saved as the *x-range* extent and *y-range* extent of the mask perimeter.

---

<sup>17</sup> Due to noise, this criterion finds the vector locations with fewer than two pixel values.

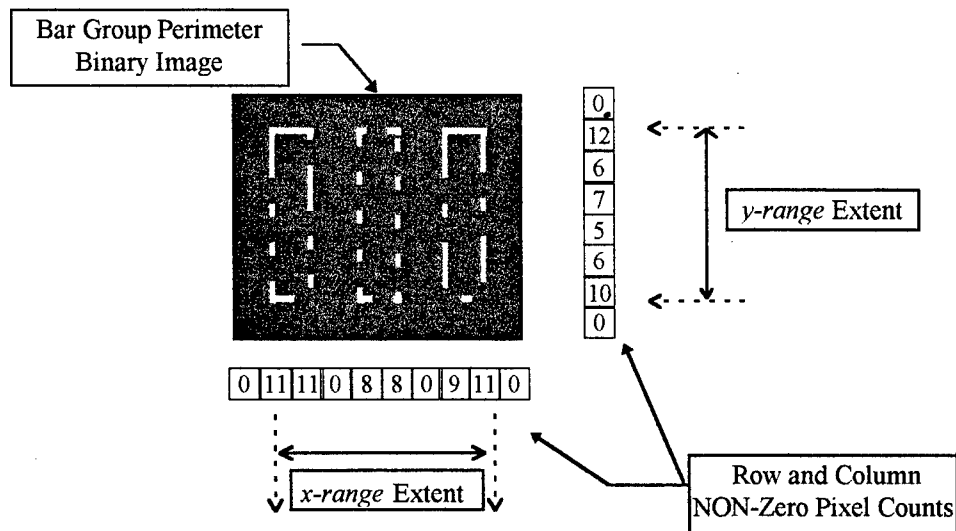
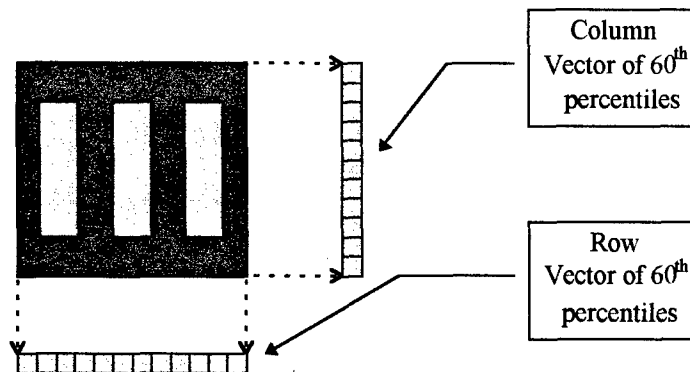


Figure 25, Demonstration of x-range and y-range extent determination

The original image is multiplied by this binary image, pixel by pixel, effectively removing the background from the original image. The resulting isolated bar group image is placed into a smaller matrix.

The next two steps of the block diagram, *Detect Bar Group Orientation* and *Estimate Cross-Section Amplitudes*, represent the crux of the  $L_2$  computation. The bar group orientation is determined by using the new isolated bar group image to form horizontal and vertical vectors of pixel values, as was done for the binary mask. Instead of containing the sums of pixel values, these new vectors contain the 60<sup>th</sup> percentile<sup>18</sup> values of the respective rows and columns. Figure 26 demonstrates the formation of these vectors.

<sup>18</sup> The 60<sup>th</sup> percentile is computed by finding the value within a set which is larger than 60 percent of the all of the values in the set; the 50<sup>th</sup> percentile is the median.



*Figure 26, 60th Percentile Row and Column Vector Formation*

After the application of an exponential smoothing filter [Makridakis, Wheelwright, and McGee, 1983:86], a second order finite difference operation is performed on both vectors to remove constant bias or linear trends. The variance of both vectors is then taken. The cross sections of the bar groups are actually composed of three adjacent Bessel functions [Gaskill, 1978: 72]. Since the second derivative, or Laplacian, of a Bessel function is another type of Bessel function, the vector with the largest variance is the lateral cross-section vector and the orientation is defined accordingly. Now, a mean lateral cross-section vector can be generated to form an estimate of the actual bar group cross section. Figure 27 shows the resulting mean lateral cross section of the bar group #1 image selected earlier. It also displays the tenth order polynomial fit [MatLab<sup>®</sup> Reference Manual] created to identify the pixel values and location of the maxima and minima.

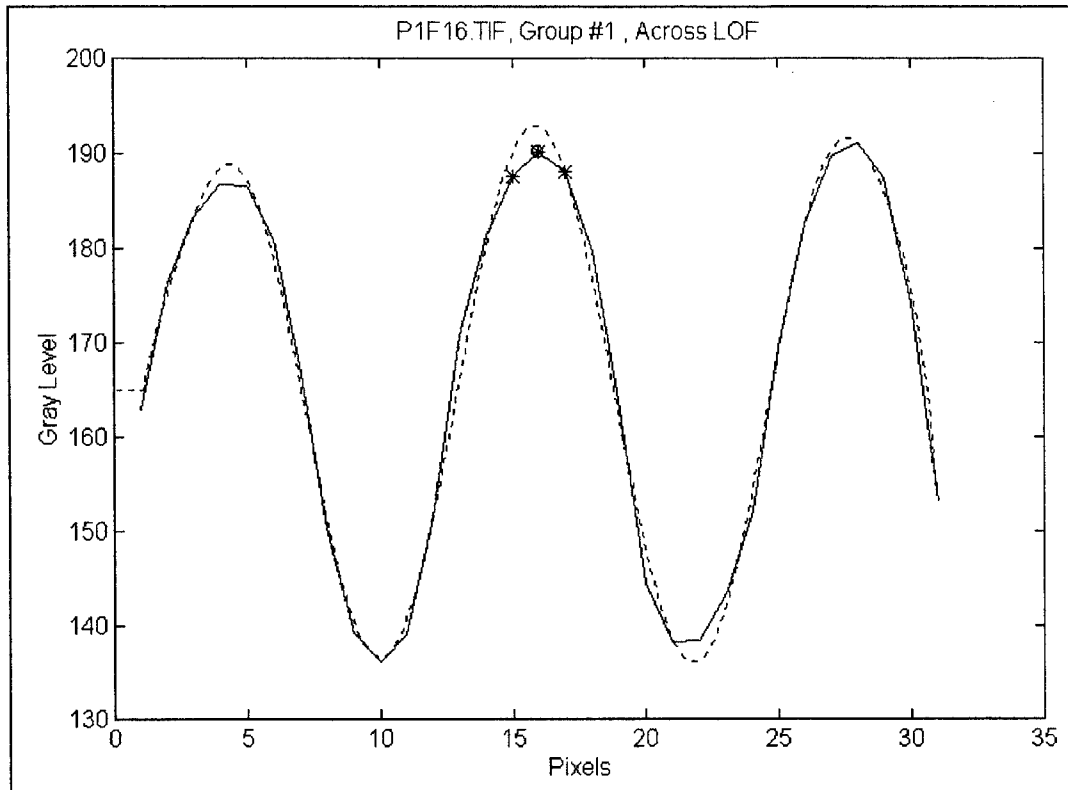


Figure 27, Mean Lateral Cross Section of Bar Group #1 and 10th Order Polynomial Fit

The  $L_2$  value is found by finding distances between each peak and valley location from the mean lateral cross section. Critical steps are described in the next two blocks of the flow diagram: *Estimate Peak and Valley Locations* and *Estimate Bar Width*. The mean lateral cross section is used to compute the  $L_2$  value. To start the search for the maxima and minima locations, the centroid,  $x^*$ , of the polynomial fit data is computed according to Equation (2.8). This centroid value, and two adjacent data points, are seen in Figure 27

$$x^* = \frac{\sum_{i=1}^N p_i \cdot x_i}{\sum_{i=1}^N p_i} \quad (2.8)$$

This three point comparison results in the starting point for the search. The starting point for the search is the vector element containing the maximum value in the polynomial fit data. The maximum value of three points are used to determine the centroid to compensate for centroid location error in the case of poor selection of the bar group subimage. The search algorithm is a gradient search technique and is specifically written to find the locations of three peaks and two valleys on the polynomial fit curve. After the search routine has found the three maxima and two minima, the bar widths are computed. So, the smooth polynomial fit is used to eliminate false extrema in the bar group cross section data due to noise, but the bar group cross section data is used to compute bar width and modulation. The bar width is estimated by finding the pixel differences in the locations of adjacent maxima and minima. This is justified because no edges exist to measure the width of the light and dark bars. The original bars have equal widths. By finding center to center differences between adjacent peak and valley pixel locations, the actual width of the bar group in pixels can be estimated. Averaging is used to reduce errors introduced by undersampling and the jagged edges due to the noise introduced by the imaging process. Equation (2.9) describes the estimate of the actual bar width in pixels,  $w_{pixel}$ , where the locations of the maxima in Figure 27 were labeled as  $p_1$ ,  $p_2$ , and  $p_3$  from left to right and the minima locations were labeled  $v_1$  and  $v_2$ ,

$$w_{pixel} = \frac{(v_1 - p_1) + (p_2 - v_1) + (v_2 - p_2) + (p_3 - v_2)}{4} \quad (2.9)$$

In order to compare the estimated width to the bar target, the width must be converted into units of ground length, or centimeters-ground (cm-ground). To make this conversion,

the sample size from the digitizer,  $s$  ( $\frac{\mu\text{m}}{\text{pixel}}$ ), the effective optical system focal length,  $f$ , and the flight altitude,  $h$  (m), are shown in Equation (2.10).

$$w_{bar} = w_{pixels} \cdot \frac{h \cdot s}{f} \quad (2.10)$$

This conversion from gray level to  $\log(E)$  units uses the calibration data provided by the user to ADiM during the setup stage. The next two steps described in the flow diagram, *Convert From Gray Level to Exposure* and *Calculate Bar Group Modulation*, were not used or required by the OSMPF to compute  $L_2$ . This determination of individual bar group modulations was an attempt to determine another image quality metric or reference and will be discussed later in this chapter. The method used to ensure a good estimate of the orientation and bar width also provided data to estimate the actual peak and valley amplitude values of each bar group. The amplitudes of the three identified peak values were averaged together to form the estimate of the bar group maximum amplitude. The two identified local minima, or valley amplitude values, were averaged to estimate the minimum amplitude for the bar group. The maximum and minimum gray level amplitudes were converted to  $\log(E)$  units.  $K_2$  was calculated according to Equation (2.5) and the result was stored for each bar group.

Figure 28 shows the results of computing  $K_2$  for every ADiM resolved bar in a bar target image, for both orientations. The figure also plots the average  $K_2$  for each bar width. This data is from the same image as from the full bar target shown earlier.

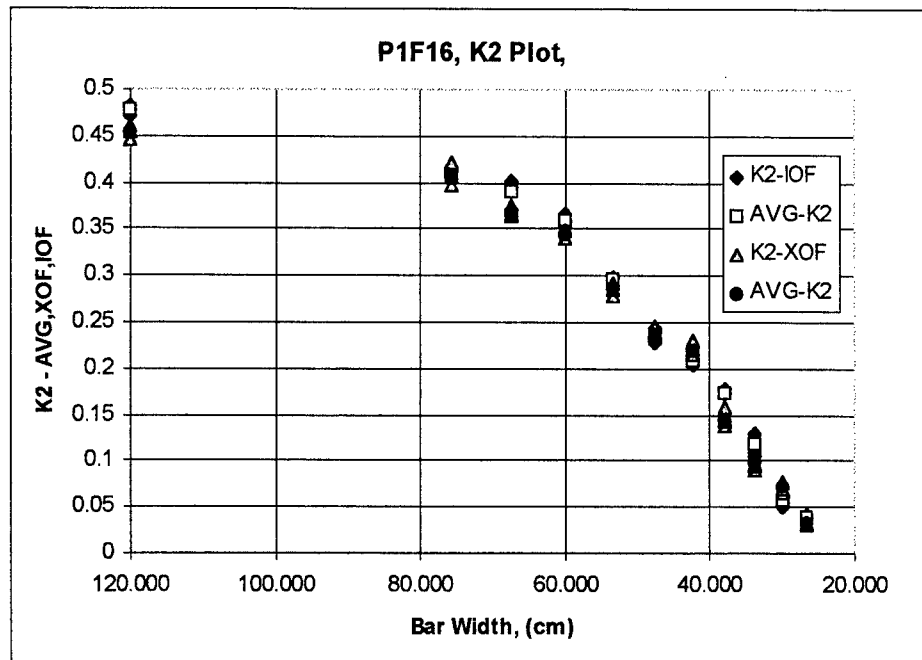


Figure 28,  $K_2$  Value Summary Based on Each Bar Group for Resolved Bar Groups

The legend in the upper right corner of this figure describes the markers denoting the four types of  $K_2$  which were computed to create this graph. Ten or more measures of  $K_2$  were made and recorded for each bar width and in each bar group orientation. Please refer to Figure 1, in Chapter 1, for a description of the bar group orientations. The  $K_2$  from the bar group measuring the *in-the-line-of-flight* characteristics is called K2-IOF, and the  $K_2$  from the bar group measuring the *across-the-line-of-flight* characteristics is called K2-XOF. The results of these measures were averaged and two more points were plotted at each bar group width. This chart was an attempt to demonstrate the mean and variance statistics. This graph also demonstrates the consistency of ADiM.

### 3.1.1.2. Finding $K_2$

The second parameter used to compute  $H_{min}$  is the modulation of the brightness panel exposure. The two blocks in the flow diagram, *Select Region Containing Brightness Panels*

and *Median Filter Brightness Panels Subimage*, begin the  $K_2$  measurement. ADiM parallels the OST method, using the average gray levels of the brightness panels. This value of  $K_2$  is used to find the ADiM value of  $H_{min}$ . The software assumes the user can select a sample of the bright and dark regions of the brightness panels within the same rectangular region. The following graphic, Figure 29, portrays a potential sample region for  $K_2$  analysis.

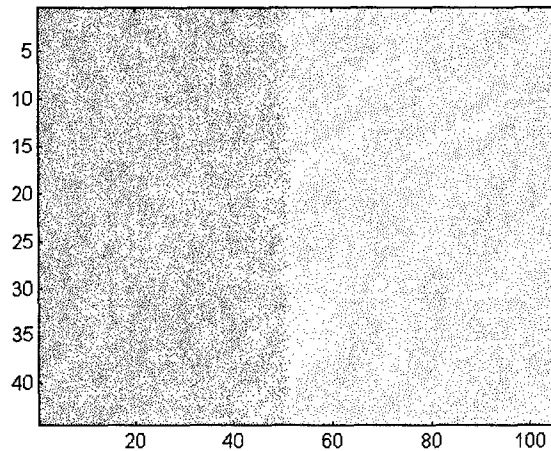


*Figure 29, Brightness Panel Selection For  $K_2$  Analysis*

ADiM only differs from the OSMPF by the method the dark and light sample regions are separated. The OSMPF separates the two regions by selecting two separate samples, one from the dark brightness panel and one from the light. The ADiM technique uses a single subimage containing both regions.

The user starts ADiM from the initial screen shown in Figure 22, and selects a region from the bar target containing the brightness panels. The rectangular area extracted must contain pixels from both the light and dark brightness panels. The selection is median filtered to filter extraneous data, because it is known that the brightness panels are supposed to approximate a Lambertian surface. Now, the subimage preparation moves to the next steps of

the flow diagram, *Convert from Gray Level to Exposure* and *Calculate the Modulation of the Brightness Panels*.

An estimate of gray level values for the light and dark brightness panels is needed to compute the image modulation,  $K_2$ . Inconsistencies in the images of the brightness panels gave the author cause to seek alternative ways to find an estimate of  $K_2$ . A histogram function was used to create a vector containing the number of occurrences, also called counts, of the gray levels. An example of this histogram is shown in the following figure. The consistent bimodal nature of the brightness panel data makes this type of measurement possible. Noise effects are present and can be observed in the wide variances around each of the distinct mean gray level values.

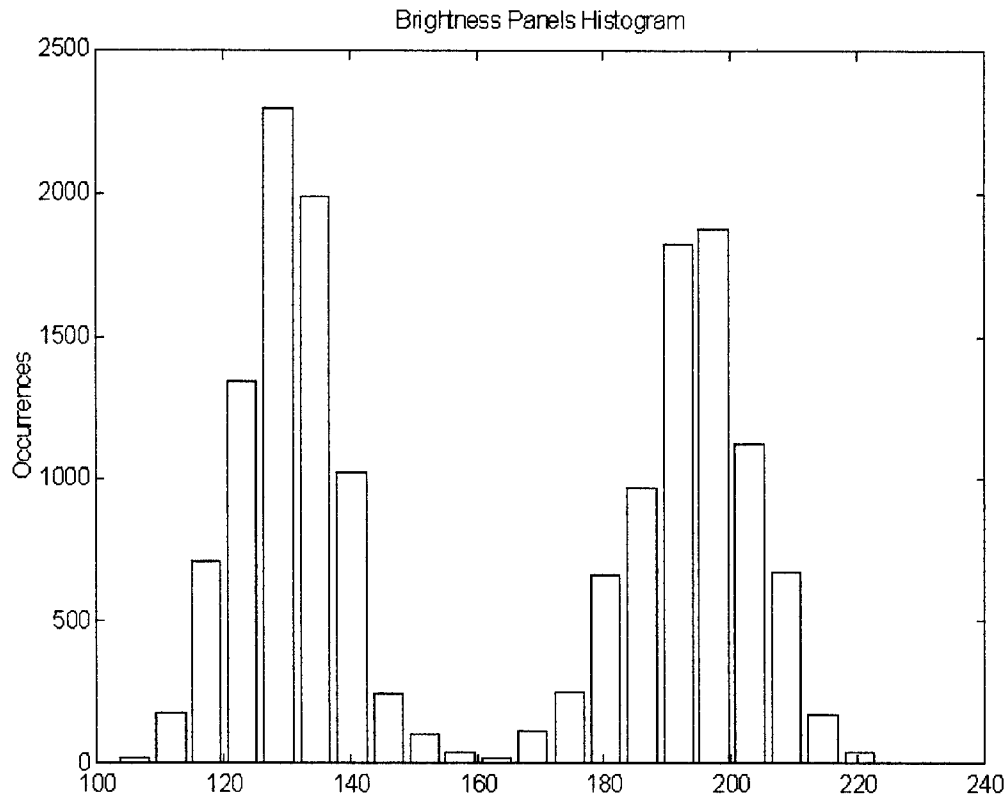


Figure 30, Bimodal Histogram of Brightness Panel Samples

The number of bins used to separate the data was dependent on the number of samples. In general, for large sample sizes, the number of bins in the histogram were computed as  $N = k \log(n)$ , where  $N$  is the number bins,  $k$  is a constant with values between 2 and 5, and  $n$  is the number of samples available. The MatLab<sup>®</sup> Histogram function, *hist*, returns two vectors, a vector containing the gray level counts for each bin and a vector containing the center value of each bin. The bins containing the greatest frequencies of gray level values are found for both the high (light) and the low (dark) gray level values. The values are then averaged, converted to  $\log(E)$  units, and used to calculate  $K_2$ .

## 3.2. Discussion of Data Specifics

The idiosyncrasies associated with the data drove the development of ADiM from the beginning. The high noise level and the undersampling present made creating an automatic solution to the processing needs of the OSMPF very difficult. Some of the adaptations made to ADiM to handle these properties have been described earlier, but in the next sections, additional topics will be covered.

Each system in the process to satisfy the OST calibration requirements introduced uncertainty. Film is a nonlinear detector and adds uncertainty to the process if it is not used properly. The digitization of the film data introduces other problems with sampling size. The effect of the imaging process on bar target edges has been shown, but additional information on finding thresholds to demarcate these objects is included below.

### 3.2.1. *Noise Effects in the Data*

In truth, a bar group is really not composed of light and dark bars. Each bar group effectively consists of white bars painted on a black background and so the set of contours around the artifacts with the strongest signal return from the ground target, and if the selection of the threshold value is suitable, the perimeter gray level will be larger than all of the background gray levels, such that only the bar group signal has gray level values which exceed the perimeter value.

To understand the importance and difficulty of finding a thresholding value, the stochastic nature of the data must be discussed. Although all of the images considered in this thesis have pixel values between 1 and 256, the variance and mean of the data is not predictable between different images; nor are the statistics of the gray level values consistent

within a given calibration target image from bar group to bar group. Few assumptions can be made about the distributions of the gray level values in any sample image, because the probabilistic distributions of gray levels in all images are asymmetric, bimodal, and therefore non-Gaussian [Kreyszig, 1983: 981].

At the end of Chapter 2 a discussion of the lack of homogeneity in the brightness panels demonstrated the inconsistency and roughness of the gray level values across larger surfaces on each target with apparently the same color of reflective paint. The variance in their surface gray level values appears to be normally distributed, but is very wide. If the bar group sampled from the target image contains too many samples from the surrounding area, the inconsistencies bias the ADiM calculations and the perimeter edges of the light and dark bars cannot be distinguished.

Figure 31 portrays a histogram of the gray levels from an image of the WPAFB target taken on 25 Aug 95. Notice the two distinct modes with local minima at the left, right, and center of the distribution. In many image processing applications, edges can be identified by choosing the threshold value based on the histogram minimum value [Castleman, 1996:247]. Using the histogram central minima present in the histogram, one could infer that the bar group edges are defined by the transition from dark to light values around the pixel gray level of 160. So, if each bar group had enough samples in respective subimages to form a meaningful histogram, and all of the bar groups appeared to have bimodal gray level distributions with the central minima occurring around the 160 gray level range, determining the edge locations among each of the bar triads would be trivial. The histogram of such a target would show how to threshold gray level values in order to differentiate signal from

noise; unfortunately, it does not work for the situation defined by the OS Treaty. The proportionally shrinking bar group dimensions on the OS target have correspondingly decreasing illuminance amplitudes. This decreasing amplitude is a decrease in signal level and it is the result of the convolution of the optical system MTF and the reflected ground image of the target. The physics of the effects of the optical system MTF were discussed in more detail in Chapter 2.

For now, the important fact is that the gray level values along the perimeters of the light and dark bars on the OS target decrease as the bar group width and length dimensions decrease, and the number of samples within each subimage decreases as each group gets smaller in order to reduce the introduction of noise from artifacts other than bar groups which are present in every OS target. Notice the 60<sup>th</sup> percentile of this data is near the gray level value of 160.

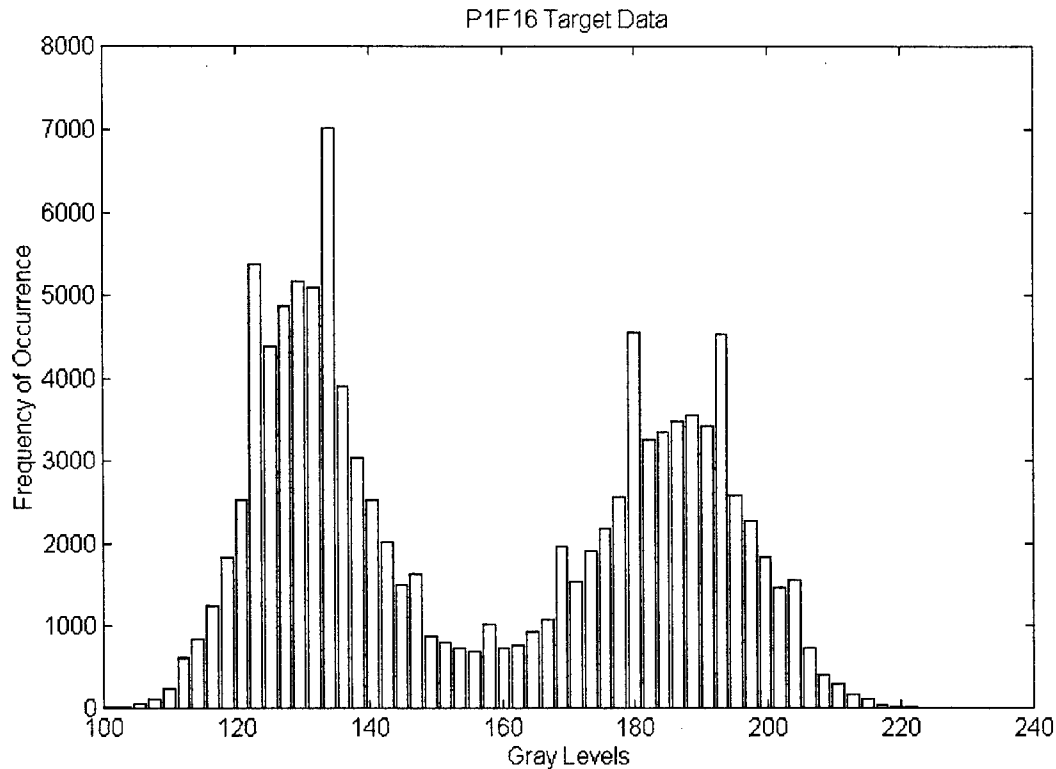


*Figure 31, Target Gray Level Histogram*

But in the case of the OS data, the bimodal nature of the data cannot be used because the distribution of gray levels changes and not enough samples exist in the smaller bar groups, as shown in Figure 32. Almost all of the analyzed target data sets in this thesis had GRD values less than 30 cm, which is the bar width of bar group #9. The details available in a histogram depend on the number of samples used in its computation; since the following figure represents the histogram computed from a resolved bar group, its lack of available structure proves the inappropriateness for use in finding a proper threshold value.

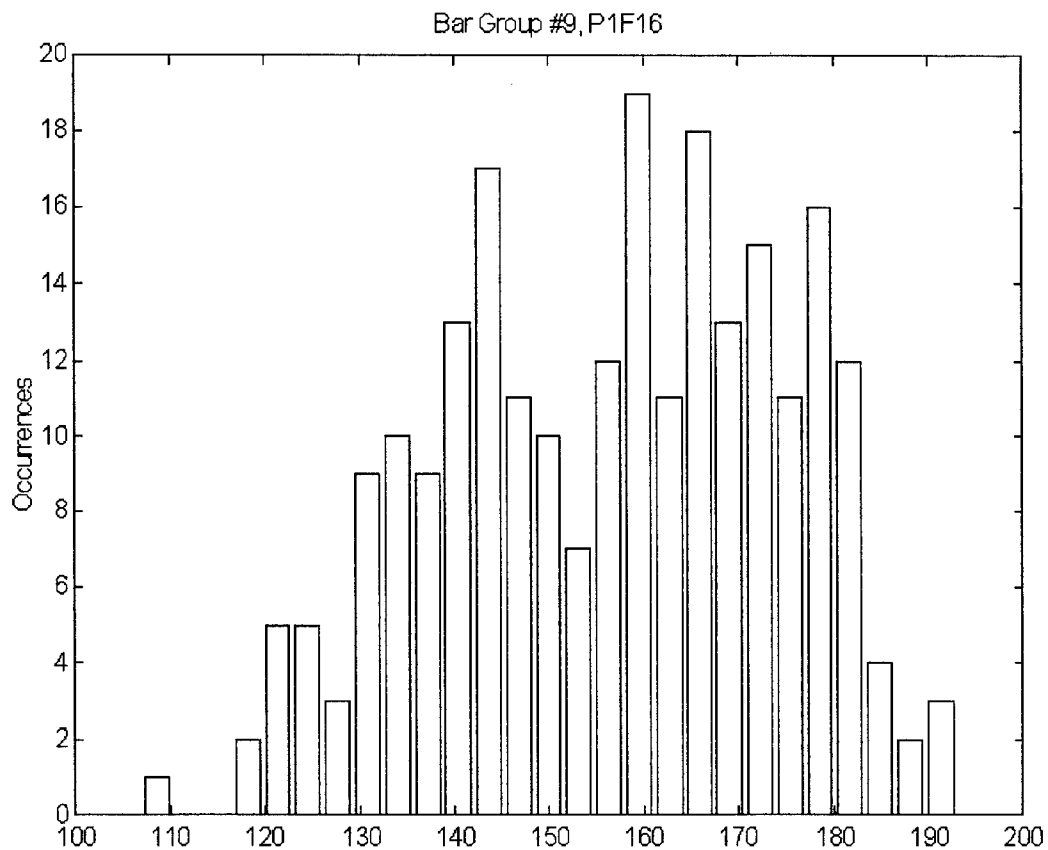


*Figure 32, Histogram of Bar Group #9*

***3.2.2. For smaller bars, poor choice in bar group location makes automatic peak and valley identification difficult***

As the bar widths narrow, the amplitudes of the peaks and valleys decrease, and the relative distances between the peaks and valleys also decrease. This is a result of the system MTF as discussed in Chapter 2. In other words, as the width of the bar groups get smaller, the peaks and valleys become more and more difficult to distinguish, until only a single peak remains. The smallest bar group for which the peaks and valleys are discernible should be the GRD, but it is possible for noise or atmospheric distortion to blur a bar group image beyond the true system GRD. The resulting GRD for the target could be greater than or less than the

noise free result. Bar group #9 is significantly smaller than bar group #1, and is shown below in Figure 33.

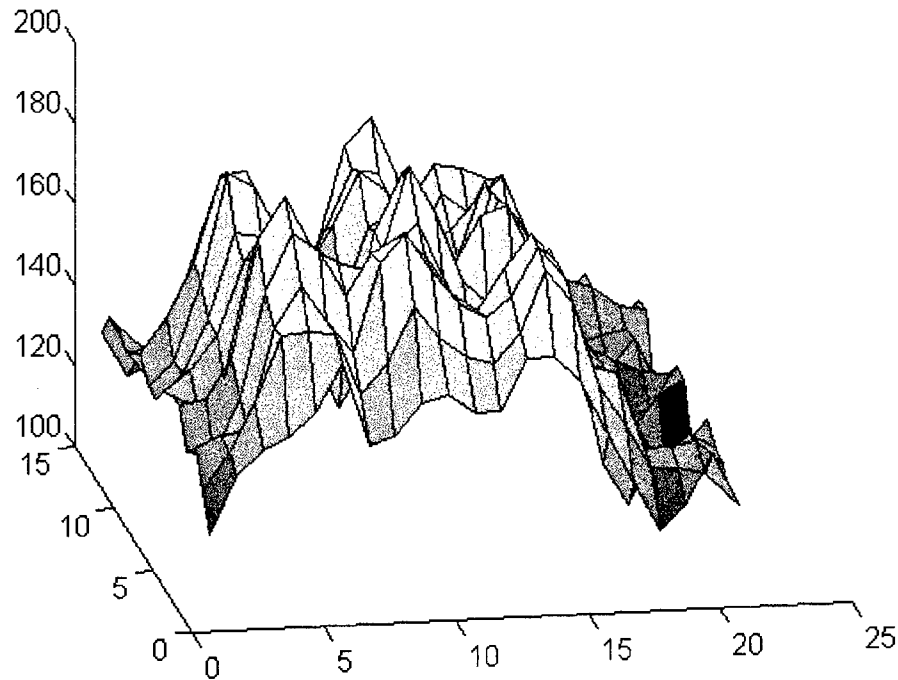


*Figure 33, Example of the Effect of Decreasing Barwidth on Peak and Valley Amplitudes of Bar Group #9 (30 cm-ground bar width, no filtering)*

The edges of the bar groups are rounded through the imaging process. For all bar groups, MTF and noise effects created jagged regions along each bar length in the group, but in a small bright bar these jagged regions represented amplitude changes which could be as large as the amplitude of the bar group itself. The 60<sup>th</sup> percentile threshold value allowed ADiM to define a legitimate contour around a group of interest and the *MatLab*<sup>®</sup> *IPT* functions provided a means to extract the most likely contours inside of the noisy data. For small bars, it was still often necessary to try several different subimage selections before ADiM successfully identified the bar group.

If the OSMPF had to calculate the  $K_2$  value from the bar group bounding the system GRD and not from the brightness panels, the issue of bar group edge selection would become a significant issue, because the  $K_2$  value calculated from the bar group varied up to 25% depending on the ROI selection. The  $K_2$  estimate is reduced by the imaging process edge smoothing, because it reduces the average maximum amplitude measured. Then the mean lateral cross section is computed, and the amplitudes of the maxima are underestimated. ADiM avoids this by cropping the pixels from the edges before computing the mean lateral cross section. The figure below shows the reduced peak amplitude at the narrow edge of the bar group image. By increasing the sample rate, without increasing the noise of the system, this sensitivity could be reduced by increasing the knowledge of the region around the smallest bar groups.

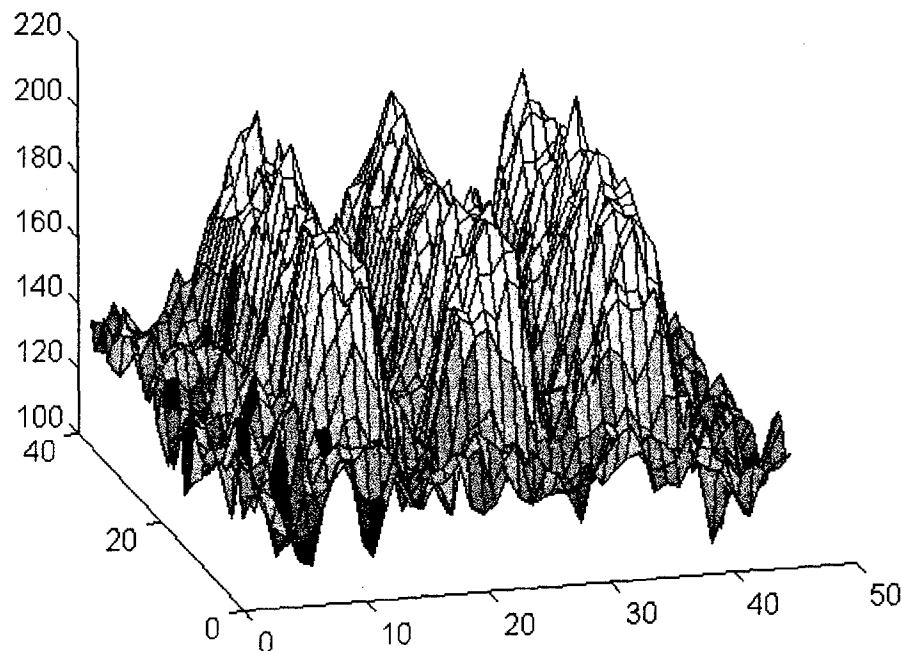


*Figure 34, Gray Level Intensity Image of Bar Group #1(75.6 cm-ground bar width)*

### ***3.2.1. Photographic Film Usage***

The use of photographic film is well documented [Slater, 1983]. Photographic film consists of two parts, the photosensitive emulsion which reacts to exposure to light and the acetate to which it is adhered. For black and white photography, this emulsion is a silver nitrate based compound. When the emulsion is exposed to light and put through the liquid chemical developing process, the parts of the emulsion exposed to light remain on the acetate in proportion to the amount of light to which it was exposed. At the end of the developing process the emulsion remaining on the film has an optical density which is linearly related to the logarithm of the exposure from the incident light. The image present in the incident light has its darker details recorded in thinner regions of emulsion and its brighter regions recorded in thicker regions. Lower values of optical density (OD) correspond to a thinner presence of emulsion, and higher exposure level to light. The plot of OD versus  $\log E$  is called the Hurter-Driffield (H-D) curve. Although not shown here, the curve is an increasing s-shaped curve and a similar curve is discussed below.

For the OST, if the film is exposed to too much light or not enough light, the information contained on the film will be seriously degraded or misinterpreted. The OSMPF have two sources of information to ensure the film is used in the proper range of exposure. NBS film strips of known optical density allow the OSMPF to calibrate their optical scanners from gray level values to optical density. They also have an instrument used on each roll of film used for an OS Treaty flight or practice flight which exposes the mission film beginning (head) and end (tail) to a series of know exposures, in order to convert the digital scanner output from gray levels to units of the logarithm of exposure,  $\log E$ . The  $\log E$  values from

the brightness panels are computed and plotted on the H-D curve for the film. As long as the plotted values reside in the linear region of this curve, the OSMPF considers the film properly exposed.

The data analyzed in this thesis had been analyzed by the OSMPF and was known to originate from properly exposed film, so there was no need to generate a calibration curve of optical density of the film at different light levels to the H-D curve. The conversion for the KODAK 5057 scanner output from gray level to  $\log E$  was made in ADiM. The shape of this curve is the same shape as the H-D curve, because the scanner gray level output is linearly proportional to the OD of the input photograph. A minimum sum of squares criterion is used to determine the data points to be used in the computation of the linear model to describe the gray level and  $\log(E)$  relationship. This model is used to predict the  $\log(E)$  values from the gray level values and fits to the central linear region of the elongated *s-shaped* curve [Neter, Wasserman, and Kunter, 1990:26].

For this criterion, the centroid of the region is found and pairs data points smaller and larger than the centroid are added to the model iteratively. With each pair of additional data points, the regression coefficients were computed, the mean square error (MSE) was computed between the data and the model prediction. To select the final model, the MSE values were compared for each. The model containing more than three points and the smallest MSE was used for the calibration curve. Figure 35 shows the linear region and the distinctive s-shape. A plot of the  $\log(E)$  versus the gray levels generated by the KODAK 5057 image scanner are shown below.

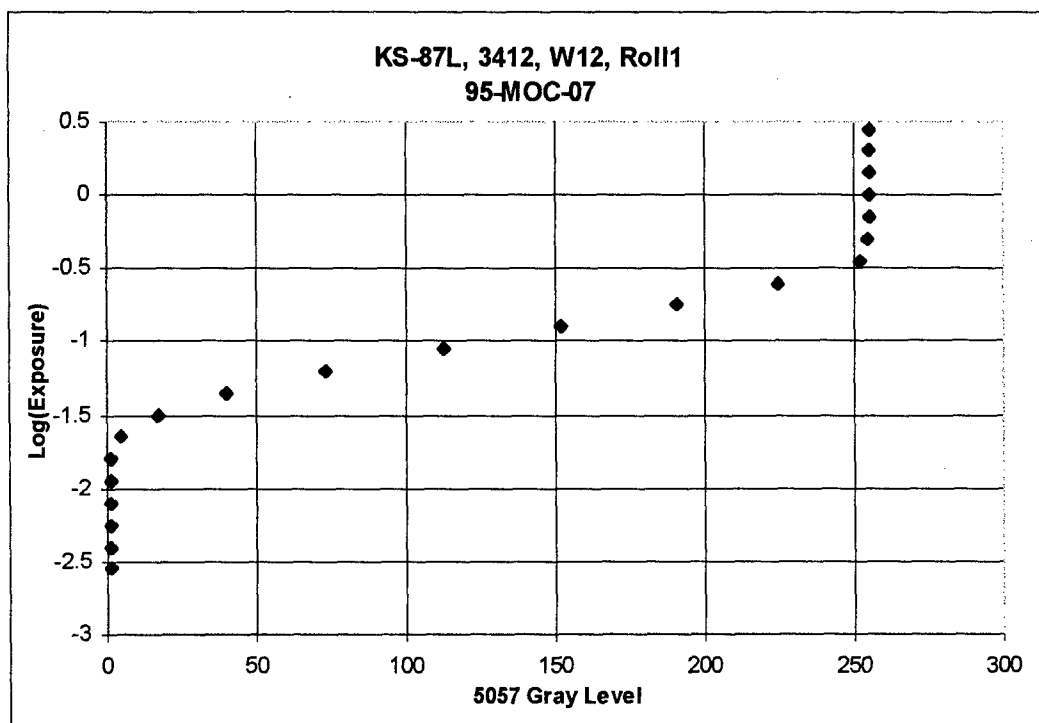


Figure 35, *Log E vs. 21-Step Wedge Gray Level Curve Demonstration of the S-Shape and Linear Region*

$K_2$  is determined with an estimate of the gray level values from the light and dark brightness panels, which are converted into values with units of exposure (Lumens \* integration time). The  $\log E$  values for the three maxima are averaged and the values for the two minima are averaged. The difference is taken and used in Equation (2.4) and then in Equation (2.5) in order to compute the actual value for  $K_2$  to be used in the calculation for  $H_{min}$ .

The complete data sets in this thesis were analyzed using data digitized by the KODAK 5057 scanner. One incomplete set of data from the Perkin-Elmer Digital Scanner was considered, and the ADiM software was able to resolve bar groups commensurate with OSMPF results.

### 3.3. ADiM Development Further Elaboration

ADiM does not re-implement the OS method for finding the GRD. In fact, it cannot due to the excessive variance and noise in the data, as well as, the undersampling of the smaller bar groups of interest. ADiM increases the confidence in estimates of the bar group signal amplitudes and locations in order to improve the estimates of  $L_2$  and  $K_2$ . To do this, ADiM, like most digital techniques, assumes symmetric error distributions between the pixel values and locations of the recorded bar group and those corresponding to them in the theoretical bar group image. As a result of this assumption, it can take advantage of the variance reduction achieved through averaging related values in the raw data. Averaging reduces the effects of symmetrically distributed, random, unbiased, noise.

In general, averaging is applied within a single data set or image or with an ensemble of repeated measurements of a data source such as series of images. The type of data currently taken for the OS regime does not lend itself to ensemble averaging techniques for several reasons. Since the frame rate is only fast enough to minimize blurring due to aircraft motion and the aircraft flies at different altitudes and attitudes for each pass over the target. In addition, the number of flights required for each configuration to generate a significant ensemble is too expensive. Hence, ADiM is applied to individual target subregions and uses row and column averaging to estimate the bar group width and amplitude.

Median filters and lowpass filters are widely used to reduce and smooth random noise effects in data and thereby improve the estimated values of signal amplitudes [Castleman, 1996: 207, 247]. Both filters are used by ADiM to calculate the two components of  $H_{min}$ . The first operation performed toward the determination of the GRD on the selected subregion

of the image is a median filter. Each pixel is replaced with the median, or 50<sup>th</sup> percentile, value among it and its eight adjacent neighbors. The median filter displaces “salt and pepper” type noise pixels toward the edges of the image. This noise is caused by pixels with gray level values significantly different from their surrounding neighbors. Since the calibration target is known not to have any intentional high or low reflective speckle associated with its surface, this median filter is not removing any useful information. It tends to sharpen edges, but is non-linear and non-reversible [Castleman, 1996:247, Thompson, 1995:79,83].

After the first binary image is formed, it produces a binary edge map image of the locations of the bar group perimeter pixels. The edges are assigned the value of one, and the remaining pixels are set to values of zero. The edges that are found are defined corresponding to the edge location in the actual image. The *MatLab*<sup>®</sup> *IPT* is used to eliminate the pixels which were spuriously assigned the value one. Each pixel is replaced by the value of the majority value of its four adjacent pixels, not including diagonally adjacent pixel location. Due to these *MatLab*<sup>®</sup> *IPT* functions and the median filter, very few single pixels will have the value of one outside the bar group perimeter in the binary edge map image.

## IV. Results

In this chapter, the results of the data processing are analyzed. With only one exception, the data comes from Open Skies Certification Mission 95-MOC-007, 25-27 August 1995. One set from another mission, 95-MOC-006 on 25 April 1995 is used. The former mission used the WPAFB target for calibration and the latter used the 51-51 Target at Eglin AFB, Florida. The data is catalogued first by the mission name and the sensor used to collect it, then by the film type used, followed by any filters used, and finally by the physical pass number over the target and the frame of film on which the data is recorded. All data was taken with the OS KS-87 sensor, which is a framing camera with an  $f/4.5$ , 76.2 mm focal length lens. The KS-87 is a single camera system and can be mounted in three separate positions on the OS OC-135 aircraft. With these positions it can record data looking vertically down to the ground, or out two different aircraft fuselage portals to cover the land areas along the left and right sides of the aircraft. The data analysis in this thesis only considers the data from the vertical and left looking positions. The MTF measurements of the KS-87 lens system are included in Appendix 2 for several incident angles and positions. On-axis performance is near the diffraction limit, but as the incident angle diverges from the center line, the performance degrades.

The data in this thesis was collected at altitudes which vary from 1460 m to 7010 m above ground level. The weather conditions were not considered to have a strong influence on the collection. Each configuration for sensor, position, filter, and film must be flown over the target of interest, as many times as is agreed to between the aerial imagery collectors and

the land area governors. In this thesis, five passes in four configurations are explored. An additional set of data from a separate mission over the Eglin AFB 5151 is included as an example of the effectiveness of the ADiM to find  $L_2$  for added scenarios. The single set of EAFB target data analyzed is exhibited without any information about the modulation or film characteristics needed to calculate  $H_{min}$ , but it is valuable in that it demonstrates the ADiM is stable for cases from different environments. Some analysis of simulated data is performed—not to calculate  $H_{min}$ , but to demonstrate that the success of the order statistics method used on actual target images is not by chance, but is an analytically sound method for estimating the values for the bar group image extrema. Each image from a physical pass over a target was recorded on a frame of film and then the target region was digitized as described previously and converted directly to a TIFF file. The scanner employed here is capable of producing images of several Megabytes in volume, so it is usually necessary to crop all of the surrounding area around the target and reduce the file size to hundreds of kilobytes.

In an ideal experiment, this TIFF file would contain a header containing useful information about the image and the binary representation of each sample pixel from the image. No processing or averaging would be done at this stage, but much of the unnecessary imagery information would be cropped from the area surrounding the target. Unfortunately, one of the four sets of data received from the OSMPF had accidentally been digitally resampled while using Adobe® *Photoshop*® software for cropping the data. The sampling size was decreased (the sampling rate was increased) within *Photoshop*® by interpolating between the raw image data pixels and adding additional points between each pair. This causes an averaging effect which is similar to low pass filtering. One of these interpolated sets of target

data was a duplication of a previously provided data set. It will be used to show the effect of the resampling of the data is minimal and will not prevent the use of this data for analysis in this thesis. This result should not be surprising because the nature of the method described here depends heavily on averaging.

Using the techniques of ADiM, the results that follow were found. In the first set of results, the OSMPF values for  $L_2$ ,  $K_2$ , and  $H_{min}$  are compared directly to the ADiM values. Due to a consistent residual between the OSMPF value for  $K_2$  and the value for  $K_2$  found in this thesis, the next results use the OSMPF values for  $K_2$  to calculate  $H_{min}$  for the  $L_2$  values from both techniques. Although more research and testing needs to be performed, this difference in  $K_2$  values is attributed to the lack of NBS calibration for the KODAK 5057 scanner. The Zeiss microdensitometer is regularly calibrated in accordance with NBS guidelines.

#### **4.1. Result Comparison**

Figure 36 shows a scatter plot of  $H_{min}$  values determined by the OSMPF (horizontal axis) and the  $H_{min}$  values determined by ADiM (vertical axis). It supports the supposition that the results from both techniques are related in a simple linear fashion. The result of this supposition is that each calculation can be predicted by knowing the other. Finding the linear fit for the two sets of data containing 25 data points in the form of a simple linear model yields a correlation coefficient of 0.886. This means almost 89 percent of the variation in the OSMPF  $H_{min}$  value is explained by the variation in the ADiM value. The *F-Statistic* for the model was 1.96E-08. The *p-values* for the estimated slope and intercept coefficients,  $\beta_0$  and  $\beta_1$ , were 0.21872 and 1.96E-08, respectively. Thus, the parameters and model are

statistically significant. This demonstrates that ADiM values are correlated to OSMPF, and the methods changed in order to adapt the OSMPF techniques to digital processing are consistent with the original method.

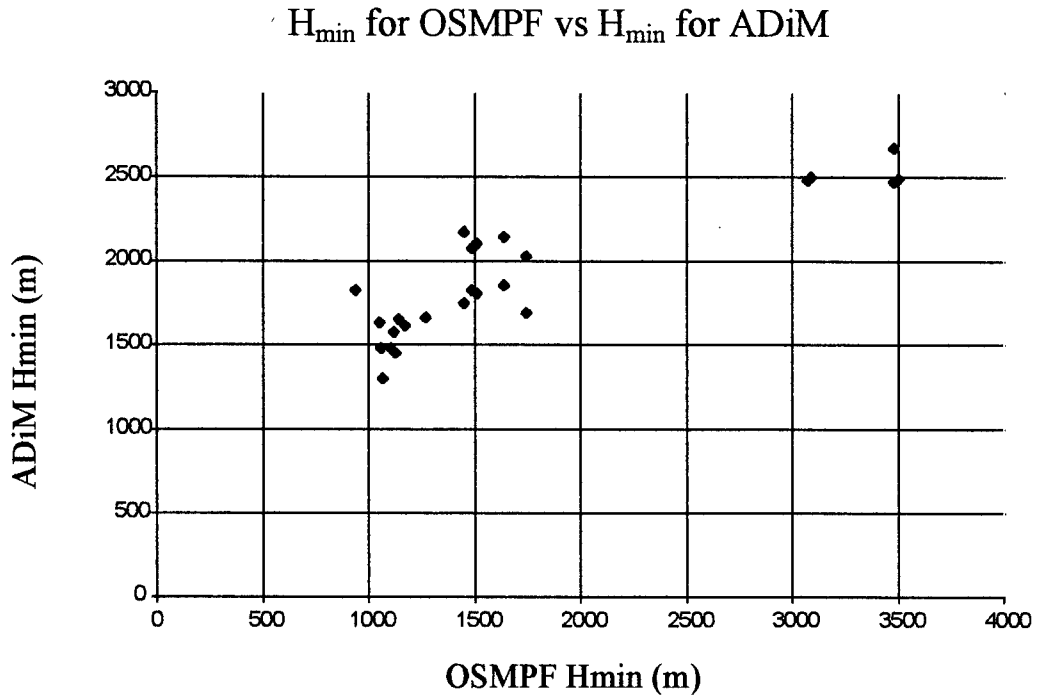


Figure 36, Graph demonstrating a linear correlation between OSMPF and ADiM measurements

Explained variation does add to the credibility of the results, but a scatter plot of both OSMPF and ADiM computed results of  $H_{min}$  in Figures 36 and 37 show that none of the ADiM results exactly matched the OSMPF values for  $H_{min}$ , so some systematic differences in the two methods exist. This difference in results can be traced most often to different values of the calculated film exposure modulation values between the two measurements.

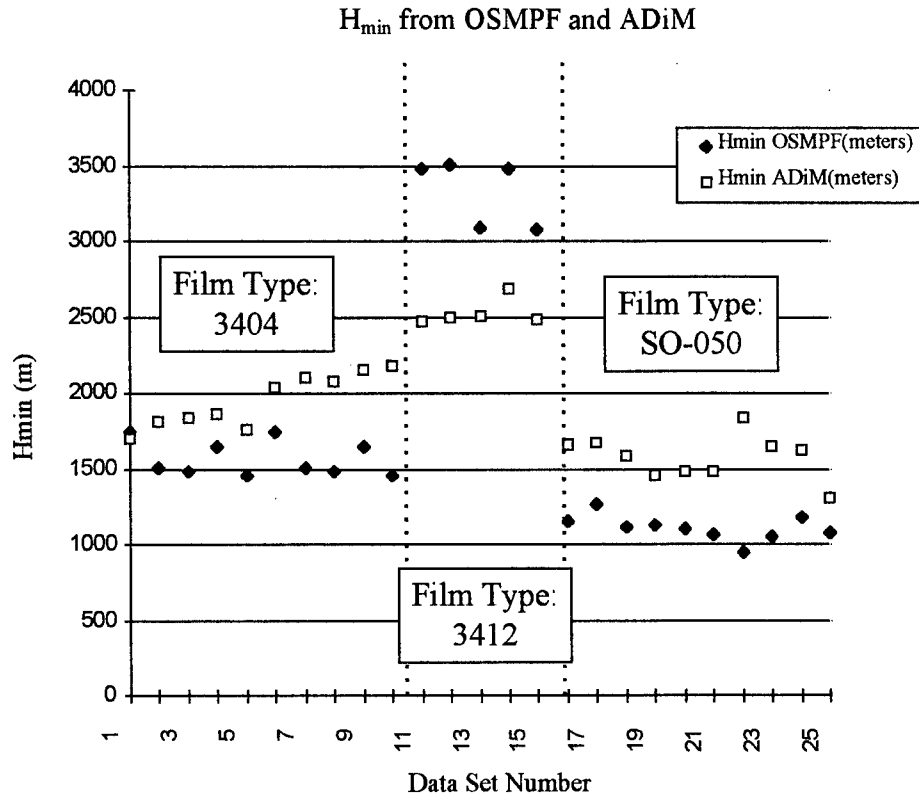


Figure 37, Graph shows a relationship between OSMPF and ADiM  $H_{min}$  measurements

Figure 38 displays the same data as Figure 37, but the order of the data points has been sorted by the increasing OSMPF  $H_{min}$  values. The oscillation of the ADiM results for data points numbered 10-20 could support the presence of some systematic error in ADiM. Although, it must be said that an difference in  $L_2$  value of even one bar could result in such discrepancies.

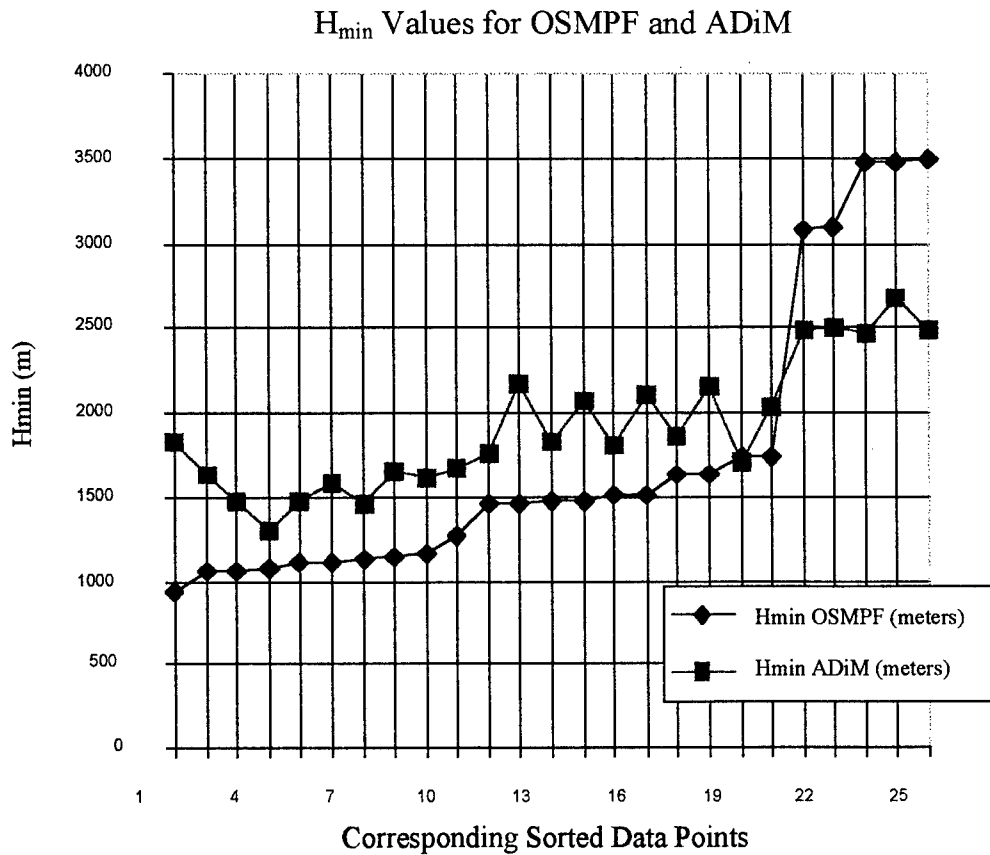


Figure 38, Same data as Fig 33—except the values were sorted in ascending order

A simple linear model was built with the least squares method to determine the correlation between the ADiM and OSMPF  $H_{min}$  results. In order to assess the value of a simple linear model, a diagnostic plot of the residuals, the difference between the estimated values of  $H_{min}$  from the model and the actual  $H_{min}$  values calculated by the OSMPF, versus the calculated OSMPF  $H_{min}$  values are shown in Figure 39 [Neter, Wasserman, Kunter 1990:117]. The left axis measures the aforementioned residuals between the model and the OSMPF values. The three symbol types correspond to three different film types used in the analysis. This structure could imply that higher order terms are needed in the linear model to explain

additional variance in the OSMPF results with the ADiM results. Note how the types of film group the residuals into three distinct regions.

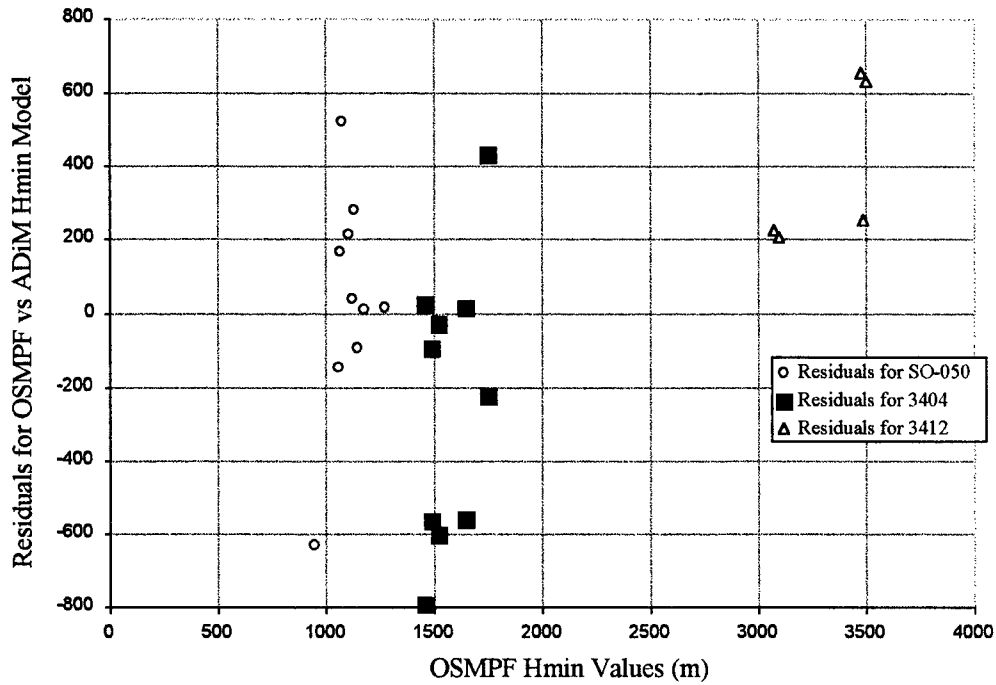


Figure 39, Linear Model Residuals (Error) plotted against OSMPF  $H_{min}$

Another parameter which varied within the data analyzed for this thesis was film type.

Figure 39 demonstrates the possibility that different films affect the residuals between measured and modeled values. This structure in the residual plot could also imply that improper calibration data was used to compute  $K_2$ , since a sample of each type of film must be used in order to compute the modulation and translate the digitized values into measures of luminance. Nevertheless, with linearity of Figure 36 and the similar trends between the ADiM and OSMPF values for all of the data runs, the simple linear model will be accepted as valid. The linearity of the comparison between the two sources of computed  $H_{min}$ , albeit under poor calibration conditions, supports the validity of the technique.

## V. Conclusion

Statistics and commercial image processing tools can be used to develop a less subjective method of determining the GRD and  $K_2$  of an OST ground target. The method developed in this thesis is not fully automated, and a human is used to select a region in which it is known a bar group exists. Undersampling of the bar groups made the creation of a fully automated technique too formidable.

In fact, the most promising option, in the opinion of the author, to automate the OSMPF process involved fitting a digital template over the digitized image and scanning these predefined areas region by region for bar groups and brightness panels to compute the GRD and  $K_2$ . This template concept could work with the current digitized resolution, but obtaining an accurate fit would be extremely difficult for the undersampled regions, whose widths are often representative of the GRD. This could be solved if the calibration flights were flown at lower altitudes, or a higher resolution digitizer could be used. Thus, it is possible the techniques developed in this thesis to locate and identify the bar group extent and orientation could be extended to remove the human in the loop, but this step is left for the next investigator to uncover.

The sample size of the OST target with the photographic film would have greatly simplified this task, because it was on the order of single micrometers, which translates to around 20 mm of ground dimension for the calibration runs flown under 2000 m. Unfortunately, the KODAK 5057 digitizer increased the sample size three times for the same data runs. Due to the large sample size introduced with the digitizer, the smaller bars within

each target were often only defined by two or three samples across their width, especially for the image data collected at altitudes over 1800 m. Undersampled images result in hard to quantify GRD, because the edges of the bar groups are difficult to isolate. However, the shape and location of the bars were known a priori and this knowledge made identification much easier.

In order to fully automate this technique, higher sample rates should be used. A higher sampling rate would provide more samples which could be used to generate clearly bimodal histograms. These histograms could be interpolated and used to determine the threshold values defining the transition from light to dark bars. The OST participants could experiment with flying calibration missions at lower altitudes to increase sample rate.

The specialized tool developed in this thesis is functional, but better results would be reaped from a change in data collection technique. The current technique assumes the participants will only use single frames of images of double or triple bar targets for calibration analysis, but with the cost of computing power decreasing, good confidence in the identification of details much smaller than those available on a single frame can be achieved. Faster frame rates allow ensemble averaging of the data and reduce the normally distributed error introduced to the images by atmospheric, optical, and electronic noise.

An even further change in the data collection paradigm involves a radical change in the ground target itself—to a configuration allowing a continuous comparison of identified bar edge distinctions with decreasing bar width dimension. A large black and white “spoke target” [Goodman, 1988:126] could work properly and the analysis would use the diameter

cross-sections for averaging to produce a graph depicting the smallest angular separation achieved in a given photograph.

Another improvement in the OSMPF method for calibration would be to increase the number of samples in the  $K_2$  computation. Currently, they use a 10 pixel by 10 pixel region. Due to the lack of homogeneity within the brightness panels, more samples are useful in increasing the confidence in this computation. This improvement could be enacted with very little change in current procedure.

## VI. Bibliography

- Beloglazov, I.N., "Methodology for Determining From Uncoordinated Experimental Data the Minimum Height Permissible Under the Treaty on Open Skies When Using Electro-Optical Means of Observation," Annex to Methodology Using IR Devices (Part of the International Open Skies Technical Discussions), 1993.
- Boreman, Glenn D. and Sidney Yang, "Modulation Transfer Function Measurement Using Three and Four-Bar Targets," Engineering Laboratory Notes,
- Building a Graphical User Interface (Fourth Printing), The MathWorks, Inc., December 1995
- Castleman, Kenneth R., Digital Image Processing, Englewood Cliffs, New Jersey. Prentice-Hall, Inc., 1996.
- Department of the Air Force. Doctrine. AFM 1-1. Washington
- Encarta '96® Encyclopedia, Microsoft® Corp, 1995
- Goodman, Joseph W., Introduction to Fourier Optics (Reissue), New York, McGraw-Hill Publishing Co., Inc. 1988.
- Kreyszig, Erwin, Advanced Engineering Mathematics (Fifth Edition), John Wiley and Sons, 1983: 980-983.
- Holst, Gerald C., Electro-Optical Imaging System Performance, SPIE Optical Engineering Press and JCD Publishing, 1995: 218-247.
- Luttwak, Edward N., "Strategic Arms Limitation Talks," Encarta '96® Encyclopedia, Microsoft® Corp., 1995
- MatLab® . Version 4.2C.1, IBM, Microsoft Windows® Ver 3.11, Computer software and programming language. The MathWorks®, Inc., Natick, Mass, 1994.
- The MatLab® Users Guide (Second Printing), The MathWorks®, Inc., Natick, Mass. November 1994.
- The MatLab® Reference Guide (Fifth Printing), The MathWorks®, Inc., April 1995.
- Menzel, Donald H., Fred Whipple, and Gerard deVaucouleurs, Survey of the Universe, Prentice-Hall, Inc., Englewood Cliffs, New Jersey, 1970: 60-102.

- Merchant, James W., "Remote Sensing," Encarta '96® Encyclopedia, Microsoft® Corp., 1995
- Makridakis, Spyros, Steven C. Wheelwright, and Victor E. McGee, *Forecasting: Methods and Applications*, John Wiley & Sons, Inc., Toronto, Canada, 1983
- Neter, John, William Wasserman, and Michael H. Kutner, *Applied Linear Models*, Richard D. Irwin, Inc. Burr Ridge, Illinois, 1990
- Roggemann, Michael C., Gradient Search Method, Feb 1996 in preparation for OS SWSG meeting.
- Roggemann, Michael C. and Byron Welsh, *Imaging Through Turbulence*, CRC Press, Boca Raton, FL 1996
- Slater, P. N., F. Doyle, N. Fritz, and R. Welch, "Photographic Systems for Remote Sensing," *Manual of Remote Sensing*, v. 1, American Society of Photogrammetry, 1983: 231-287.
- Thompson, Clay M. and Loren Shure, *Image Processing Toolbox: for Use with MatLab®*, The MathWorks, Inc., Natick, Mass, August 1993.
- "TU 154 Flies Surveillance," Air Force News Service [Off the World Wide Web], 27 June 1995.
- Wilhelms, Don E., "Moons," in *The Geology of the Terrestrial Planets*. NASA SP-469, Washington D.C.: US Government Printing Office, 1984.

## Appendix I Numerical Results

*Table 3, Numerical Results Comparing OSMPF Analysis to ADiM*

Target	Sensor	Film	Altitude (meters)	$K_2$ (cm) OSMPF	$K_2$ (cm) ADiM	$L_2$ (cm) OSMPF 80% rule	$L_2$ (cm) ADiM IOF/XOF	$H_{min}$ OSMPF (meters)	$H_{min}$ ADiM (meters)
EAFB	KS-87	3404	7010	na	na	#25/#21	#25/#21	na	na
WPAFB	KS-87V	3404	1697	0.627	0.5159	23.8	26.7/''	1747.4	1698.8
"	"	"	1666	0.641	0.5136	26.7	23.8/''	1512.3	1812.7
"	"	"	1630	0.634	0.5143	26.7	23.8/''	1486.95	1834.5
"	"	"	1610	0.641	0.4864	23.8	23.8/''	1640.7	1857.6
"	"	"	1608	0.648	0.4854	26.7	26.7/23.8	1452.5	1755.7
WPAFB	KS-87V	3404	1697	0.627	0.5113	21.2	23.8/''	1747.4	2032.8
"	"	"	1666	0.641	0.5135	21.2	21.2/''	1512.3	2106.9
"	"	"	1630	0.634	0.5054	23.81	21.2/''	1486.95	2076.2
"	"	"	1610	0.641	0.518	21.2	21.2/18.9	1640.7	2151.5
"	"	"	1608	0.648	0.5052	23.8	21.2/18.9	1452.5	2173.2
WPAFB	KS-87L	3412	2746	0.511	0.5063	21.2	30/''	3478.7	2469.7
"	"	"	2743	0.502	0.4944	21.2	30/''	3502.8	2493.6
"	"	"	2741	0.511	0.489	23.8	30/''	3093.2	2504.1
"	"	"	2746	0.519	0.4839	21.2	26.7/30	3481.2	2678.2
"	"	"	2741	0.519	0.4984	23.8	30/''	3071.6	2482.7
WBAFB	KS-87V	SO-050	1467	0.536	0.5039	33.7	23.9	1145.8	26.7
"	"	"	1470	0.552	0.4996	30.0	23.9	1271.7	23.9
"	"	"	1472	0.568	0.5670	33.7	23.9	1120.1	<b>21.2</b>
"	"	"	1469	0.56	0.5280	33.7	26.7	1125.0	<b>21.2</b>
"	"	"	1484	0.576	0.5186	33.7	26.7	1107.0	21.2
WPAFB	KS-87L	SO-050	1484	0.654	0.4003	33.7	30	1059.9	30
"	"	"	1469	0.641	0.3181	37.8	26.7	943.2	26.7
"	"	"	1469	0.646	0.4056	33.7	26.7	1054.9	26.7
"	"	"	1468	0.661	0.4159	30	26.7	1171.0	26.7
"	"	"	1470	0.627	0.4050	33.67	33.6	1069.9	33.6

## Appendix II MatLab ADiM Code

---

ADiM Source Code. Written in MatLab®

```
%%
%% EXTRACT.m
%%
%% Donna Keating,
%% version 24 Feb 96
%%          29 feb 96

function [G]=extract(m)

global hdl
global img_hdl
global imgax
global sym
global callorient

if (nargin == 0),
%----- START UP -----
lastone = menu('Most recent image or new one??','Most Recent','NEW');

if (lastone == 1),
    load lastdata;
else
    [filename,pathname]=uigetfile('*.*tif','IMAGE TOOL',40,40);

    if filename ~= 0
        [img,map]=tiffread([pathname,filename]);
    else
        error(['Error Reading ' filename]);
    end
end

end
save lastdata

[rows,cols]=size(img);

hdl = figure('Name',filename,'NumberTitle','off',...
            'Units','Pixels',...
            'Position',[75 10 max(600,200+cols) max(600,rows+20)],...
            'Interruptible','yes');

imgax = gca;
img_hdl = imshow(img,map);
if (isind(img)), img = ind2gray(img,map); end
set(hdl,'UserData'.filename);
```

```

rtside = 20+cols+10;
n = fix(cols/5);

xlims = [n 3*n 5*n];

set(gca, 'XLimMode','manual',...
        'XLim',[1 cols],...
        'YLim',[1 rows],...
        'XTick',xlims,...
        'Units','pixels',...
        'Position',[20 20 cols*1 rows*1],...
        'Interruptible','yes');

cropbutt = uicontrol(hdl,'Style','Pushbutton',...
                    'String','SELECT REGION',...
                    'Position',[rtside 140 200 25],...
                    'Interruptible','yes',...
                    'CallBack',...
                    'IMCROPII; extract(1) ');

zoombutt = uicontrol(hdl,'Style','Pushbutton',...
                    'String','ZOOM',...
                    'Position',[rtside 170 200 25],...
                    'Interruptible','yes',...
                    'CallBack',...
                    'IMZOOM; extract(1) ');

file = uimenu(hdl,'Label','FILE');

menu1 = uimenu(hdl,'Label','VIEW');

menu4 = uimenu(hdl,'Label','METRICS');
%
%-----
sym(1) = uicontrol(hdl,'Style','radio', ...
                  'Position',[rtside 275 150 25], ...
                  'String','Horizontal Bars', ...
                  'Value',1);

sym(2) = uicontrol(hdl,'Style','radio', ...
                  'Position',[rtside 300 150 25], ...
                  'String','Vertical Bars', ...
                  'Value',0);

for i=1:2, set(sym(i),'UserData',sym(:,[1:(i-1),(i+1):2])); end

callorient = ['me = get(gcf,"CurrentObject");',...
             'if(get(me,"Value") == 1),',...
             'set(get(me,"UserData"),"Value",0),',...
             'else,',...
             'set(me,"Value",1),',...
             'end'];

```

```

set(sym,'CallBack',callorient);
%-----
endbutton = uicontrol(hdl,'Style','Pushbutton',...
    'String','QUIT',...
    'Position',[rtside 95 150 25],...
    'CallBack','close all; clear all;');

newfile = uimenu(file,'Label','New',...
    'CallBack','cla; close; extract');

% -----END START UP -----

elseif (nargin == 1),

    if (m == 1),

        end

    end

end

acsl
return

```

---

```

function [bout,rect] = imcropii
%%
% IMCROPII   Crop image.
%% IMCROP, Changed by Donna Keating
%% Version   23 Feb 96
%%
%%          26 Feb 96, 0710 hrs
%%
%%          06 Mar 96, 0500 hrs

global hdl
global img_hdl
global imgax
global sidehdl

% Determine which IMAGE coordinate system is being used.
s = [version ' ']; k = find(s<46 & s>58);
if ~isempty(k), s = s(1:min(k)); end
[ver,count,msg,next] = sscanf(s,'%f',1);

if ver > 4.1,
    useNew = 1;
elseif ver < 4.1,
    useNew = 0;

```

```

else
  if s(next)>='a', useNew = 1; else useNew = 0; end
end

axes(imgax);
[x,y,a,hasimage] = getimage(imgax);

if ~hasimage,
  error('The current figure must contain an image to use IMCROP. ');
end

rect = getrect(hdl) % Get rect info from the user.
set(gca,'UserData',rect);

[m,n] = size(a);
xmin = min(min(x)); ymin = min(min(y));
xmax = max(max(x)); ymax = max(max(y));
if useNew,
  % Transform rectangle into row and column indices.
  kx = n-1; ky = m-1;
  i1 = max(ceil((rect(2)-ymin)/(ymax-ymin)*ky+1),1);
  j1 = max(ceil((rect(1)-xmin)/(xmax-xmin)*kx+1),1);
  i2 = min(floor((rect(2)+rect(4)-ymin)/(ymax-ymin)*ky+1),m);
  j2 = min(floor((rect(1)+rect(3)-xmin)/(xmax-xmin)*kx+1),n);
else
  % Transform rectangle into row and column indices. Fix-up coordinates
  % to deal with coordinates extending from pixel boundaries rather
  % than pixel centers.
  dx = max( (xmax-xmin)/size(a,2), eps );
  dy = max( (ymax-ymin)/size(a,1), eps );
  kx = (n-1+dx); ky = (m-1+dy);
  i1 = max(ceil((rect(2)-ymin)/(ymax-ymin)*ky+(1-dy/2)),1);
  j1 = max(ceil((rect(1)-xmin)/(xmax-xmin)*kx+(1-dx/2)),1);
  i2 = min(floor((rect(2)+rect(4)-ymin)/(ymax-ymin)*ky+(1-dy/2)),m);
  j2 = min(floor((rect(1)+rect(3)-xmin)/(xmax-xmin)*kx+(1-dx/2)),n);
end

bout = a(i1:i2,j1:j2);

save img bout

sidehdl = figure;
set(sidehdl,'Position',[310 200 400 400]);
imshow(bout);
colormap(gray(256))
filename = get(hdl,'UserData');
title(filename)

clear bout

task = menu('Bar Group OR Brightness Panels??','Bar Group','Bright. Panels');

```

```
if (task == 1), m = 'fit'; end
if (task == 2), m = 'bp' ; end
```

```
if (strcmp(m,'fit')),
    goon = menu('Analyze this bar group?','YES','NO');
    if (goon == 2),
        return
    else
        st=fit(1,0);
        return
    end
```

```
elseif (strcmp(m,'bp')),
    goon=menu('Analyze this pair of Brightness Panels?','YES','NO');
    if (goon == 2),
        return
    else
        st=fit(1,1);
        return
    end
```

```
else
    return;
end
```

---

```
% fit.m
%%
% Version 26 Feb 96, 0151
%%          12 mar 96 1615
%%          20 mar 96 0230
```

```
function [modulation] = fit(i,m)
```

```
global hdl
global img_hdl
global imgax
global sidehdl
global sym
global callorient
```

```
load img
```

```
outfile = mat2str(['Pass1top','.out']);
```

```
figure(sidehdl);
filename = get(hdl,'UserData');
colormap(gray(256))
```

```
img2 = zeros(size(bout));
img2 = medfilt2(bout);
```

```

clear bout

map = gray(256);

if (isgray(img2)),
    [imgf,map] = gray2ind(img2,256);
else
    imgf = img2;
end

clear img2

% Watch out for side effects here---am I really changing img, or is it pass by value?
if (m == 0),
%=====
imshow(imgf,gray(256));

title([filename ' Median Filtered'])

[M N] = size(imgf);
mask = zeros([M N]);
len = M*N;

%-----

thr1 = mean(prctile(imgf,60));
thr2 = mean(prctile(imgf,60));
thr = max(thr1,thr2);
%% This is the level I assume the "bar edge" is located (I hope its valid) (???)

imgbw = im2bw(imgf,thr);
imgbw = bwmorph(imgbw,'majority',2);
imgbw = bwmorph(imgbw,'hbreak',2);
subplot(1,2,1)
imgbw = bwperim(imgbw,8);
imshow(imgbw,2)
title('Mask')
% Use this mask to find the bar in the image, and
% as a first pass to approach a good estimate of the modulation

% Need this, 'cause imgbw could be a filled in square!
% Use imgbw to determine xrange and yrange
hold on

% Want to exclude rows or columns with fewer nnz pixels than "some limiting value" that I
% currently choose to be the mean col or row population. Think median will be too high...(??)

xrange = find(sum(imgbw) >= 2);
yrange = find(sum(imgbw')>= 2);

clear imgbw

xmax = max(xrange);

```

```

xmin = min(xrange);
ymax = max(yrange);
ymin = min(yrange);
xrange = [xmin:xmax];
yrange = [ymin:ymax];

mask(yrange,xrange) = ones([length(yrange),length(xrange)]);

imgff = imgf.*mask;

%% ----- END MASK -----

xx = prctile(imgff(yrange,xrange),60);
xy = prctile(imgff(yrange,xrange)',60);

xx = expsmth(xx); xx = expsmth(xx);
xy = expsmth(xy); xy = expsmth(xy);

%dx2 = del2(prctile(imgff(yrange,xrange),60));
dx2 = del2(xx);
%dy2 = del2(prctile(imgff(yrange,xrange)',60));
dy2 = del2(xy);

%vardx2 = var(del2(prctile(imgff(yrange,xrange),60)));
%vardy2 = var(del2(prctile(imgff(yrange,xrange)',60)));
vardx2 = var(del2(xx));
vardy2 = var(del2(xy));

%stddx2 = std(del2(prctile(imgff(yrange,xrange),60)));
%stdddy2 = std(del2(prctile(imgff(yrange,xrange)',60)));
stddx2 = std(del2(xx));
stdddy2 = std(del2(xy));

%% The DEL2 function takes the "Laplacian" and basically zeros out
%% constant or linear changes! Making it ideal to determine orientation
%% With out needing to know the exact location of the region of interest!

% Assume the orientation with largest variance is the width-wise direction.
% --->If this isn't true, I could fit a polynomial to the known bar cross-section
% and measure the error of what I have to what I expect...noise could make
% this unreliable too--especially normalizing the amplitudes and such.

clear imgff;
maskarea = bwarea(mask);
clear mask;
meaning = mean(mean(imgf(yrange,xrange)));

if (vardx2 > vardy2),
    orient = 1;
    grpwidth = maskarea/length(yrange);
    meanmat = (ones([length(yrange),length(xrange)]))*meaning;
    imgf = ((detrend(imgf(yrange,xrange)')) + meanmat)';
    set(sym,'Value',0);

```

```

set(sym,'CallBack',callorient);
elseif (vardx2 < varydy2),
    orient = -1;
    grpwidth = maskarea/length(xrange);
    meanmat = ones([length(yrange),length(xrange)])*meanimg;
    imgf = detrend(imgf(yrange,xrange)) + meanmat;
    set(sym,'Value',1);
    set(sym,'CallBack',callorient);
else
    error('Unresolvable');
    break;
end

fig = gcf;

% Select the best
if (orient ==1),
    crossplt = sum(imgf)/length(xrange);
    xvalue = [1:length(xrange)];
    betas = polyfit(xvalue,crossplt,min(10,length(crossplt)-2));
    fitplt = polyval(betas,xvalue);
    xcen = round(sum(crossplt.*xvalue)/sum(crossplt));
    xcen = [xcen-1:xcen+1];
    cen = xcen(find(fitplt(xcen)==max(fitplt(xcen))))
    cut = mean(imgf(:,xcen)); cut=medfilt1(cut,4);
    df2 = diff(cut,2);
    sortcut = unique(cut);
    upper75 = round(prctile(sortcut,75));
    keepers = find(cut >= upper75);
    lower = min(keepers) ; topper = max(keepers);
    yrange = lower:topper;
    crossplt = sum(imgf)/length(xrange);
    tmpfig = figure;
    plot(xvalue,crossplt,'b');
    [maxloc,minloc,dmaxloc,dminloc,fitplt,mult] = finder(crossplt,xvalue,cen);
    hold on;
    xtra = [1:length(fitplt)]/mult;
    plot(xcen,crossplt(xcen),'r*')
    plot(cen,crossplt(cen),'yO')
    plot(xtra,fitplt,'w:');
    figure(fig);
    cutarea = length(yrange)*length(xrange);
    orientlabel = 'Across LOF';
else
    crossplt = sum(imgf)/length(yrange);
    xvalue = 1:length(yrange);
    betas = polyfit(xvalue,crossplt,min(11,length(crossplt)-2));
    fitplt = polyval(betas,xvalue);
    ycen = round(sum(crossplt.*xvalue)/sum(crossplt))
    ycen = [ycen-1:ycen+1];
    cen = ycen( find(fitplt(ycen)==max(fitplt(ycen))))
    cut = mean(imgf(ycen,:)); cut = medfilt1(cut,4);
    df2 = diff(cut,2);

```

```

sortcut = unique(cut);
upper75 = round(prctile(sortcut,75));
keepers = find(cut >= upper75);
lower = min(keepers) ; topper = max(keepers);
xrange = lower:topper;
crossplt = sum(imgf)/length(yrange);
tmpfig = figure;
plot(xvalue,crossplt,'g');
[maxloc,minloc,dmaxloc,dminloc,fitplt,mult]=finder(crossplt,xvalue,cen);
hold on;
xtra = [1:length(fitplt)]/mult;
plot(ycen,crossplt(ycen),'r*')
plot(cen,crossplt(cen),'yO')
plot(xtra,fitplt,'w:');
figure(fig);
cutarea = length(yrange)*length(xrange);
orientlabel = 'In LOF';
end

xlabel(orientlabel)
hold off;

fplt = fitplt;
xplt = crossplt;

subplot(1,2,2)
load wdgresul
crossplt = ([crossplt' ones([length(crossplt),1])*LOG_E_GL']);
fitplt = ([fitplt' ones([length(fitplt),1])*LOG_E_GL']);

plot(xvalue,10.^crossplt(xvalue),'y')
hold on;
plot(xtra,10.^fitplt,'w:');
plot(dmaxloc,10.^crossplt(dmaxloc),'r*');
plot(dminloc,10.^crossplt(dminloc),'b*');

%altitude =1666; % Pass 1, Average altitude in meters
%altitude = 1630; % Pass 2
%altitude = 1610; % Pass 3
altitude = 1608; % Pass 4
%altitude = 1613; % Pass 5
%altitude = 11648;

%%Which bar group??

barwidth0 = grpwidth/6;
maxloc = sort(maxloc);
minloc = sort(minloc);

if (length(maxloc)==3)&(length(minloc)==2),
    barwidth1 = abs(minloc(1)-maxloc(1));
    barwidth2 = abs(maxloc(2)-minloc(1));
    barwidth3 = abs(minloc(2)-maxloc(2));

```

```

barwidth4 = abs(maxloc(3)-minloc(2));
barwid = mean((1/mult)*[barwidth1 barwidth2 barwidth3 barwidth4])
barwidth = round(barwid)
stdwid = std((1/mult)*[barwidth1 barwidth2 barwidth3 barwidth4]);
else
  goon = menu('ERROR: Not Resolved','Continue?','RETURN');
  if (goon == 2), return; end
  barwidth = barwidth0;
  barwid = barwidth0;
end

barlength = cutarea/grpwidth;
barspace = zeros([1,barwidth]);
barhat = ones([1,barwidth]);

avgmaxht = (mean(crossplt(dmaxloc)));
avgminht = (mean(crossplt(dminloc)));

delta_e = abs(avgmaxht-avgminht);

C = 10^delta_e;
K2 = (C-1)/(C+1)

avgmaxexp = max(10^abs(avgmaxht),10^abs(avgminht));
avgminexp = min(10^abs(avgmaxht),10^abs(avgminht));
meanmod = abs(avgmaxexp-avgminexp)/(avgmaxexp+avgminexp);

[group,con,fwid] = findgrp(barwid,altitude)

if (con < 0.7),
  guess = menu(['Is this really GROUP #' num2str(group) ' ?'],'YES','NO');
  if (guess == 2),
    fixwid = menu('CHOOSE CORRECT WIDTH',num2str(group+3),num2str(group+2),...
      num2str(group+1),num2str(group-1),num2str(group-2),num2str(group-3));
    if (fixwid == 1),group=group+3;
      elseif (fixwid == 1),group=group+3;
        elseif (fixwid == 2),group=group+2;
          elseif (fixwid == 3),group=group+1;
            elseif (fixwid == 4),group=group-1;
              elseif (fixwid == 5),group=group-2;
                elseif (fixwid == 6),group=group-3;
    end
    fwid = (120E-2/(2^(1/6))^(3+group))/(altitude*5.737E-6/(3*2.54E-2));
  end
end

title(['Group # ' num2str(group)])
xlabel(['Width=' num2str(fwid)])
ylabel('Exposure');
bar = ones([1,barwidth]);
barmodel =ones([1,length(xvalue)])*avgminht;
model = [bar*avgminht bar*avgmaxht bar*avgminht bar*avgmaxht bar*avgminht bar*avgmaxht
bar*avgminht];

```

```

firstmid = mult*( barwid + barwid/2 )
firstpk = maxloc(1)

err=round(firstpk - firstmid);
if (err >= 1),
% model=[ones([1,round(err/mult)])*avgminht model(max(1,abs(err)):length(model))];
  model=model(abs(round(err/mult))+1:length(model));
else
  model = model(abs(round(err/mult))+1:length(model));
end
barmodel([1:length(model)]) = model;
plot(xvalue,10.^barmodel(xvalue),'w')

hold off
save datafit

filename = get(hdl,'UserData');
fid = fopen(outfile,'a');
fprintf(fid,'%s\t %s\t\n',filename,date);
params = ['group ', 'fwid ', 'barwid', 'orient ', 'barwidth ', 'contrast ', ...
'K2 ', 'stdel2x ', 'stdel2y ', 'vardel2x ', 'vardel2y ', 'confidence' ];

fprintf(fid,'%s\n',params);

format1 = ['%i\t %d\t %i\t %i\t %d\t %d\t'];
format2 = ['%d\t %g\t %g\t %g\t %g\t %g\n'];
params1 = [group;fwid;orient;barwidth;barwid;C];
params2 = [K2;stdx2;stdy2;vardx2;vardy2;con];
fprintf(fid,format1,params1);
fprintf(fid,format2,params2);

figure(tmpfig)
title([filename ' Group #', num2str(group),' ', orientlabel])
ylabel('Gray Level')
xlabel('Pixels')
drawnow;

elseif (m ==1),
%=====
imshow(imgf,map);
pixnum = prod(size(imgf));
title([filename ' Median Filtered'])
oldfig = gcf;
xsection = medfilt1(mean(imgf),4);
bins = round(2*log(prod(size(imgf))));
[xcounts, xlocate] = HIST(xsection,rem(bins,2)+bins);
sortcounts = sort(xcounts);
L = length(sortcounts);
loc1 = max(find(xcounts == sortcounts(L)));
loc2 = max(find(xcounts == sortcounts(L-1)));
loc3 = max(find(xcounts == sortcounts(L-2)));
loc4 = max(find(xcounts == sortcounts(L-3)));

```

```

max1loc = xlocate(max(loc1-1,1):min(loc1+1,L));
max2loc = xlocate(max(1,loc2-1):min(loc2+1,L));
if (any(max1loc==loc3)|any(max1loc==loc4)|any(max1loc==loc2)),
    max1loc = round(sum(xcounts(max1loc).*max1loc)/sum(xcounts(max1loc)));
else
    max1loc = loc1;
end
if (any(max2loc==loc3)|any(max2loc==loc4)|any(max2loc==loc1)),
    max2loc = round(sum(xcounts(max2loc).*max2loc)/sum(xcounts(max2loc)));
else
    max2loc = loc2;
end
save xhist xcounts xlocate xsection
load wdgresul
maxloc = max(max1loc,max2loc)
minloc = min(max1loc,max2loc)
%% Assume histogram is counted at the right edge of each bin, so the mid-value
%% must be calculated as the average of the selected bin and its left neighbor.
avgmaxht = mean(xlocate(maxloc-1:maxloc));
avgminht = mean(xlocate(minloc-1:minloc));

avgmaxht = (abs([avgmaxht 1]*LOG_E_GL'));
avgminht = (abs([avgminht 1]*LOG_E_GL'));

delta_e = abs(avgmaxht-avgminht);

C = 10^delta_e;
K2 = (C-1)/(C+1)
maxht = 10^avgmaxht;
minht = 10^avgminht;
meanmod = abs(maxht-minht)/(maxht+minht);

save imghist L max1loc max2loc avgmaxht avgminht
figure(oldfig);

filename = get(hdl,'UserData');
fid = fopen(outfile,'a');
fprintf(fid,'%s\t %s\t',filename,date);
params = ['BP ', ' K2 ', ' meanmod ', ' contrast ', ' max1loc ', ' max2loc '];
fprintf(fid,'%s\n',params);
format1 = [' %d\t %d\t %d\t %d\t %d\t\n'];
params1 = [K2; meanmod; C; max1loc; max2loc];
fprintf(fid,format1,params1);
close
end

return

```

---

```

function [maxloc,minloc,xloc,nloc,fitplt, L] = finder(dataplt,xval,cen)
% Finds Peaks and Valleys

```

```

%
% Programmer: Donna Keating
%
% Search routine written by Maj Michael Roggemann
% Modified by Donna Keating

betas = polyfit(xval,dataplt,min(10,length(dataplt)-2));
f = polyval(betas,xval);
L = 10;
x = [1:length(f)*L]/L;
cen = cen*L;
fitplt = polyval(betas,x);
fitplt(1:L)=ones([1,L])*fitplt(L+1); % Removes extrapolated data less than ONE (causes false min).

ln = length(fitplt);
x = [1:ln];

% Use prctile for initial values to avoid false edge maxima
%firstmax = prctile(fitplt((cen):(ln-1)),30);
firstmax = min(fitplt);
firstmin = prctile(fitplt,60);
%secondmax = prctile(fitplt((cen):(ln-1)),30);
secondmax =min(fitplt);
firstmaxflag = 0;
firstminflag = 0;
firstmaxloc = cen;

%find min and max going right

for j=(cen-1):(ln-1),

% CASE 1: The next element is larger, but max not yet found

if (fitplt(j) >= firstmax) & (firstmaxflag == 0),

    firstmax = fitplt(j);
    firstmaxloc = j;

    if (fitplt(j+1) <= fitplt(j)),

        firstmaxflag = 1;

    end;

end;

% Found first max, now need to find min!
if (firstmaxflag==1) & (firstminflag==0),

if (fitplt(j) <= firstmin ),
    firstmin = fitplt(j);
    firstminloc = j;
end;

```

```

if (fitplt(j+1)>=fitplt(j))&(fitplt(j-2)>=fitplt(j)),
    firstminflag = 1;

end;

end;

if (firstmaxflag==1) & (firstminflag==1) & (fitplt(j)>=secondmax),

    if (fitplt(j)>=fitplt(j-1))&(fitplt(j)>=fitplt(j+2)),
        secondmax = fitplt(j);
        secondmaxloc = j;
    elseif (j==(ln-1)) & (fitplt(j+1)>fitplt(j)),
        secondmax = fitplt(j+1);
        secondmaxloc = j+1 ;
    end;
end;

end;

%find min and max going left

thirdmax = prctile(fitplt,30);
secondmin = min(firstmax,secondmax);
thirdmaxflag = 0;
secondminflag = 0;

%find min and max going right

for j=firstmaxloc:-1:(L+1),

    if (thirdmaxflag == 0) & (secondminflag ==0),

        if (fitplt(j)<=secondmin),
            secondmin = fitplt(j);
            secondminloc = j;
        end;

        if (fitplt(j-1)>=fitplt(j))&(fitplt(j+2)>=fitplt(j)),
            secondminflag = 1;
        end;

    end;

    if (fitplt(j) >= thirdmax) & (thirdmaxflag == 0) & (secondminflag == 1),
        thirdmax = fitplt(j);
        thirdmaxloc = j;

        if (fitplt(j-1) <= fitplt(j)) & (fitplt(j+1) <= fitplt(j)),
            thirdmaxflag = 1;
        end;
    end;
end;

```

```

end;

%-----
maxloc=[firstmaxloc secondmaxloc thirdmaxloc];
minloc=[firstminloc secondminloc];

% Convert from fitplt coordinates back to dataplt coords.
xloc = unique(maxloc)/L;
nloc = unique(minloc)/L;

for i=1:length(xloc),
    lox = floor(xloc(i));
    hix = ceil(xloc(i));
    xbounds = [lox:hix];
    if (dataplt(lox)>=dataplt(hix)),
        X = lox;
    else
        X = hix;
    end
    xloc(i) = X;
end

for i = 1:length(nloc),
    lox = floor(nloc(i));
    hix = ceil(nloc(i));
    xbounds = [lox:hix];
    if (dataplt(lox)<=dataplt(hix)),
        X = lox;
    else
        X = hix;
    end
    nloc(i) = X;
end

save finder

```

---

```

%% Findgrp.m

```

```

function [group,confid,twid] = findgrp(barwidth,altitude)

```

```

%% ASSUME Sensor is the KS-87
%% I have pixels of bar width and ground meters of bar width --->> Which bar
%% Need ground width per pixel!!! Need ground pitch (how much ground distance in a
%% 5.737 um image plane distance???)
%% pitch:FL, as ground pitch:altitude

```

```

pitch = 5.737*10^(-6);

```

```

% meters
FL = 3*2.54*10^(-2);
%FL = 18*2.54*10^(-2);
% meters
groundpitch = (pitch/FL)*altitude;

% So, estimated width of the bar in question is groundpitch*pixelnumber!!!

gbarwidth = barwidth*groundpitch

% So in what known bargroup range does this fall????

prog= 2^(1/6);
% Bar dimension reduction factor.
biggest = 120*10^(-2);
% meters

if (gbarwidth >= biggest/(prog^4)),
    left = biggest-gbarwidth;
    right = gbarwidth-biggest/prog^4;
    if (left < right),
        group = 0;
        confid = 1 - left/right;
        twid = biggest/groundpitch;
        return;
    else
        group = 1;
        confid = 1 - right/(left);
        twid = (biggest/(prog^4))/groundpitch;
        return;
    end
end

for i = 1:12,
%-----
leftbar = biggest/prog^(3+i);
rightbar = biggest/prog^(3+i+1);
if (gbarwidth<=leftbar & gbarwidth>=rightbar)
    left = leftbar-gbarwidth;
    right = gbarwidth-rightbar;
    delta = left-right;
    if (left < right),
        group = i;
        confid = 1 - left/right;
        twid = leftbar/groundpitch;
        return;
    else
        group = i+1;
        confid = 1 - right/left;
        twid = rightbar/groundpitch;
        return;
    end
end
end

```

```
%-----  
end %for loop
```

---

```
%  
% expsmth.m, exponentially weighted smoothing  
%  
function result = expsmth(DATA)  
  
ALPHA = 0.2;  
  
f = zeros([length(DATA)+1,1]);  
result = zeros([length(DATA)+1,1]);  
  
f(1) = min(DATA);  
f(2) = DATA(1)*ALPHA + (1-ALPHA)*f(1);  
  
for i = 1:length(DATA),  
    f(i+2) = DATA(i)*ALPHA + (1-ALPHA)*f(i+1);  
end;  
  
result = f;
```

---

```
function y = prctile(x,p);  
%PRCTILE gives the percentiles of the sample in X.  
%    Y = PRCTILE(X,P) returns a value that is greater than P percent  
%    of the values in X. For example, if P = 50 Y is the median of X.  
%  
%    P may be either a scalar or a vector. For scalar P, Y is a row  
%    vector containing Pth percentile of each column of X. For vector P,  
%    the ith row of Y is the P(i) percentile of each column of X.  
  
%    Copyright (c) 1993 by The MathWorks, Inc.  
%    $Revision: 1.1 $ $Date: 1993/05/24 18:56:10 $  
  
[prows pcols] = size(p);  
if prows ~= 1 & pcols ~= 1
```

```

    error('P must be a scalar or a vector. ');
end

if any(p > 100) | any(p < 0)
    error('P must take values between 0 and 100');
end

xx = sort(x);
[m,n] = size(x);

if m==1 | n==1
    m = max(m,n);
    n = 1;
    q = 100*(0.5:m - 0.5)./m;
    xx = [min(x); xx(:); max(x)];
else
    q = 100*(0.5:m - 0.5)./m;
    xx = [min(x); xx; max(x)];
end

q = [0 q 100];

y = interp1(q,xx,p);

```



REPORT DOCUMENTATION PAGE			Form Approved OMB No. 0704-0188	
Public reporting burden for this collection of information is estimated to average 1 hour per response, including the time for reviewing instructions, searching existing data sources, gathering and maintaining the data needed, and completing and reviewing the collection of information. Send comments regarding this burden estimate or any other aspect of this collection of information, including suggestions for reducing this burden, to Washington Headquarters Services, Directorate for Information Operations and Reports, 1215 Jefferson Davis Highway, Suite 1204, Arlington, VA 22202-4302, and to the Office of Management and Budget, Paperwork Reduction Project (0704-0188), Washington, DC 20503.				
1. AGENCY USE ONLY (Leave blank)	2. REPORT DATE MARCH 1997	3. REPORT TYPE AND DATES COVERED Master's Thesis		
4. TITLE AND SUBTITLE Automatic Digital Processing for Calibration Data of Open Skies Treaty Sensors			5. FUNDING NUMBERS	
6. AUTHOR(S) Donna D.B. Keating, Captain, USAF				
7. PERFORMING ORGANIZATION NAME(S) AND ADDRESS(ES) Air Force Institute of Technology, 2750 P Street Wright-Patterson Air Force Base, OH			8. PERFORMING ORGANIZATION REPORT NUMBER AFIT/GOR/ENP/97M-01	
9. SPONSORING/MONITORING AGENCY NAME(S) AND ADDRESS(ES) NAIC/DXHX (AIA), Open Skies Media Processing Facility			10. SPONSORING/MONITORING AGENCY REPORT NUMBER	
11. SUPPLEMENTARY NOTES				
12a. DISTRIBUTION/AVAILABILITY STATEMENT Approved for public release; distribution unlimited.			12b. DISTRIBUTION CODE	
13. ABSTRACT (Maximum 200 words) <p>The Open Skies Treaty provides guidelines allowing participants to fly in air space over other participants' countries to monitor strategic military placement and development. The treaty restricts the ground size of the smallest detail recorded by these aerial imaging systems to any size larger than 30 cm. This restriction is enforced by placing a lower limit on the altitude at which a participating aircraft can fly and it is computed as the value of <math>H_{min}</math>. Current techniques rely on human photographic interpreters to select the value of <math>H_{min}</math> for every calibration pass and is very resource intensive. The Open Skies participants are investigating machine based techniques to supplement the traditional human role in an effort to increase the objectiveness of the measurement.</p> <p>This thesis presents a software tool called, ADiM, a man-in-the-loop, algorithm which manipulates image statistics to identify the orientation and width of individual target bar groups from digitized images of aerial photographs of Open Skies Treaty calibration triple bar target. ADiM <math>H_{min}</math> results achieved an 88.6 percent correlation with the Open Skies Media Processing Facility's <math>H_{min}</math> computations.</p>				
14. SUBJECT TERMS Image Statistics; Digital Image Calibration; Automated Calibration; Bar Target Calibration; Airborne Optical System Calibration			15. NUMBER OF PAGES 125	
			16. PRICE CODE	
17. SECURITY CLASSIFICATION OF REPORT Unclassified	18. SECURITY CLASSIFICATION OF THIS PAGE Unclassified	19. SECURITY CLASSIFICATION OF ABSTRACT Unclassified	20. LIMITATION OF ABSTRACT UL	

## GENERAL INSTRUCTIONS FOR COMPLETING SF 298

The Report Documentation Page (RDP) is used in announcing and cataloging reports. It is important that this information be consistent with the rest of the report, particularly the cover and title page. Instructions for filling in each block of the form follow. It is important to *stay within the lines* to meet *optical scanning requirements*.

**Block 1. Agency Use Only (Leave blank).**

**Block 2. Report Date.** Full publication date including day, month, and year, if available (e.g. 1 Jan 88). Must cite at least the year.

**Block 3. Type of Report and Dates Covered.** State whether report is interim, final, etc. If applicable, enter inclusive report dates (e.g. 10 Jun 87 - 30 Jun 88).

**Block 4. Title and Subtitle.** A title is taken from the part of the report that provides the most meaningful and complete information. When a report is prepared in more than one volume, repeat the primary title, add volume number, and include subtitle for the specific volume. On classified documents enter the title classification in parentheses.

**Block 5. Funding Numbers.** To include contract and grant numbers; may include program element number(s), project number(s), task number(s), and work unit number(s). Use the following labels:

<b>C</b> - Contract	<b>PR</b> - Project
<b>G</b> - Grant	<b>TA</b> - Task
<b>PE</b> - Program Element	<b>WU</b> - Work Unit Accession No.

**Block 6. Author(s).** Name(s) of person(s) responsible for writing the report, performing the research, or credited with the content of the report. If editor or compiler, this should follow the name(s).

**Block 7. Performing Organization Name(s) and Address(es).** Self-explanatory.

**Block 8. Performing Organization Report Number.** Enter the unique alphanumeric report number(s) assigned by the organization performing the report.

**Block 9. Sponsoring/Monitoring Agency Name(s) and Address(es).** Self-explanatory.

**Block 10. Sponsoring/Monitoring Agency Report Number.** (If known)

**Block 11. Supplementary Notes.** Enter information not included elsewhere such as: Prepared in cooperation with...; Trans. of...; To be published in.... When a report is revised, include a statement whether the new report supersedes or supplements the older report.

**Block 12a. Distribution/Availability Statement.** Denotes public availability or limitations. Cite any availability to the public. Enter additional limitations or special markings in all capitals (e.g. NOFORN, REL, ITAR).

**DOD** - See DoDD 5230.24, "Distribution Statements on Technical Documents."

**DOE** - See authorities.

**NASA** - See Handbook NHB 2200.2.

**NTIS** - Leave blank.

**Block 12b. Distribution Code.**

**DOD** - Leave blank.

**DOE** - Enter DOE distribution categories from the Standard Distribution for Unclassified Scientific and Technical Reports.

**NASA** - Leave blank.

**NTIS** - Leave blank.

**Block 13. Abstract.** Include a brief (*Maximum 200 words*) factual summary of the most significant information contained in the report.

**Block 14. Subject Terms.** Keywords or phrases identifying major subjects in the report.

**Block 15. Number of Pages.** Enter the total number of pages.

**Block 16. Price Code.** Enter appropriate price code (*NTIS only*).

**Blocks 17. - 19. Security Classifications.** Self-explanatory. Enter U.S. Security Classification in accordance with U.S. Security Regulations (i.e., UNCLASSIFIED). If form contains classified information, stamp classification on the top and bottom of the page.

**Block 20. Limitation of Abstract.** This block must be completed to assign a limitation to the abstract. Enter either UL (unlimited) or SAR (same as report). An entry in this block is necessary if the abstract is to be limited. If blank, the abstract is assumed to be unlimited.